UNIVERSITÀ DELLA CALABRIA

Dipartimento di Farmacia e Scienze della Salute e della Nutrizione

Dottorato di Ricerca in Medicina Traslazionale

XXX CICLO

TITOLO TESI

ADVANCED MATERIALS FOR PHARMACEUTICAL AND BIOMEDICAL PURPOSES

Settore Scientifico Disciplinare CHIM-09

Coordinatore: Ch.mo Prof. Sebastiano Andò

Firma _____

Supervisore/Tutor: Dott.ssa Roberta Cassano

Firma _____

Dottorando: Dott.ssa Silvia Mellace

Firma _____

UNIVERSITÀ DELLA CALABRIA

Department of Pharmacy, Health and Nutritional Sciences

Ph.D. program in Translational Medicine

XXX Cycle

CHIM/09

Advanced Materials for Pharmaceutical and Biomedical Purposes

Coordinator:

Prof. Sebastiano ANDÒ

Supervisor:

Dott.ssa Roberta CASSANO

Candidate:

Dott.ssa Silvia MELLACE

Academic Year: 2016/2017

Author's e-mail: mellace.silvia@gmail.com

Author's address:
Department of Pharmacy, Health and Nutritional Sciences
University of Calabria
Edificio Polifunzionale
87036 Arcavacata di Rende, Cosenza, Italy.

ph.: +39 0984 493227
ph.: +39 0961 915533
cell.: +39 3299320290

The one who follows the crowd will usually go no further than the crowd. Those who walk alone are likely to find themselves in places no one has ever been before.

(Albert Einstein)

Table of contents

Preface

General Introduction, Aims and Organization of this Thesis

1. General Introduction

The XX century has witnessed more than doubling in global life expectancy thanks to the historical evolution of clinical medicine, therapeutics and pharmacy. In this context, design and synthesis of advanced materials may influence the future of drug delivery systems, that are of vital importance for healthcare and medicine. Materials innovation and nanotechnology have synergistically helped the advancement of drug delivery. Novelty in material chemistry allows the generation of biodegradable, biocompatible, environment-responsive, and targeted delivery systems (1). Nanotechnology permits control over size, shape and multi-functionality of particulate drug delivery systems. Since the first FDA approval of drug delivery systems (DDS), several DDS are commercially available to treat varied diseases from cancer to fungal infection and to muscular degeneration (2). In improving therapeutic efficacy, DDS has benefited tens of millions of patients by relieving suffering and prolonging life (3). Innovations in materials chemistry have initially fuelled the development of DDS, creating carriers that are several implementations from numerous point of view, these carriers may protect a drug from degradation, enhance drug absorption, modify drug tissue distribution profile, and/or improve intracellular penetration and distribution. The comprehension that size and shape of nanoparticles (NPs) can help pilot biological carriers has stimulated the application of nanofabrication technologies to develop more effective particulate DDS. For example, the size of NPs determines their biodistribution. While particles smaller than 20nm will be cleared from circulation via reticuloendothelial system (RES) within a few hours when injected intravenously, larger ones will be trapped in the liver and the spleen within minutes (4, 5). Moreover, innovations in design and fabrication of materials could help to alter and optimize the pharmacokinetics of therapeutic agents (6). Since the size of polymer-drug conjugates could be controlled by adjusting the molecular weight of the polymer, it could be optimized to maximize the benefits of enhanced permeability effect at leaky tumour vasculature (7). Furthermore,

conjugating drugs to a polymeric carrier can enhance solubility of hydrophobic drugs, extend drug circulation *in vivo* and enhance uptake by addition of targeting motifs to the polymer (8). They possess low toxicity and potentially favourable pharmacokinetics in the circulation. For these reasons among numerous biomaterials based on inorganic or organic matter, polymers are considered to be widely used in formulation of drug delivery systems for controlled and targeted drug delivery. In particular, the use of natural polymers such as polysaccharides (9) as drug carriers has a long history of significant clinical benefits (10). DDS were also found useful to improve the performance of imaging techniques applied for the *in vivo* diagnosis of tumours and other diseases (11). Additionally, the applications of nanotechnology in the food sector to improve the nutritional value, shelf-life and traceability of food products has the potential to subvert agriculture and food systems. In fact, the nanoscale level of foods can affect the safety, efficiency, bioavailability, and nutritional value properties of food, as well as the molecular synthesis of new products and ingredients. The development of new functional materials in food production are only new emergent, but it is already predicted to grow rapidly in the coming years (12). In summary, intensive efforts for the last three decades enabled the development of functional devices, most of which belong to lipids, peptides and other polymers. There is great potential in the combination of bioactive macromolecules with polymers, either covalently through conjugation or non-covalently using hydrogels or higher-order self-assembled structures, to address challenging in biomedical problems. Currently, the areas of drug delivery and nanomedicine is rapidly expanding. A prerequisite for further development is the design and synthesis of novel materials that are biocompatible and biologically active, are biodegradable with a controlled degradation rate, and have tenable mechanical properties. In conclusion, novel materials synthesis, introduction of environmental-sensitive polymers, successful adoption of natural polymers as carrier and improved understanding of the structure-function relationship have together transformed DDS development.

2. Aims of this Thesis

The present thesis was realized in the Pharmaceutical Technology group, Department of Pharmacy, Health and Nutritionals Sciences (University of Calabria) and deals about the development of advanced materials for biomedical and pharmaceutical purposes. Moreover, part of the PhD was focused on the application of *in vitro* and *in silico* methods for the effective and efficient prediction of human pharmacokinetics following transdermal administration of dissolvable microneedles array. This last work was carried out during a stimulating and productive scientific visiting period at the School of Pharmacy of the UCC (University College of Cork, Ireland), under the supervision of Dr. Sonja Vucen.

3. Organization of this thesis

Due to the multitude of independent projects, the present thesis is divided into three self-contained sections. The first section, named "Microspheres and Hydrogels for Active Molecules Release", is itself divided into three self-explained parts. The first part of this section concerns the preparation of a gallate hydrogel for oral administration of phloretin, a flavonoid of natural origin, with proved antioxidant activity. The results suggest a possible use of this hydrogel for intestinal release of phloretin for the maintenance of an appropriate blood glucose level in the diabetic patient. The second part of this first section concerns the preparation and characterization of microspheres based on a mixture of three natural triterpene saponins (saikosaponina a, songarosaponina D, buddlejasaponina IV) useful as a carrier for the specific release of gemcitabine to lung cells. The aim of the third part of this first section was the synthesis and characterization of swellable liquid crystalline microspheres for a specific release of 5-fluorouracil to cancer cells. The second section named "Chemical Modification of Fatty Acids for the Implementation of Drug Delivery Systems", is itself divided into two self-explained parts. Both are aimed to develop modified lipids for the preparation of new solid lipid nanoparticles. Particularly, in the first part α-linolenic acid was successfully derivatized with α-tocopherol, the results indicated that these lipid nanoparticles could provide the delivery and the protection of unstable molecules, such as α-

linolenic acid, and could be a good agent in the treatment of melanoma. Cyclosporin A, in the second part of this second section, was efficiently encapsulated in trehalose oleate SLNs. Results indicate the possibility of using the nanoparticles prepared for topical treatment of psoriasis, indeed, the risk of side effects due to systemic absorption of cyclosporin A is reduced whereas the drug concentration at injury level is increased. The third section named "Natural and Synthetic Polymers for the Preparation of Biomedical Materials" is itself divided into two self-explained parts, both addressed to the preparation of innovative materials for topical approach. The first part was aimed at the preparation of a functional gauze linking coagulant substances, chitosan and hydroquinone useful as a topical haemostatic agent for the treatment of bleeding wounds. The gauze showed the ability to short the blood clotting time and to induce the adhesion and activation of platelets. The second part of this third session contains all the experiments performed during my scientific visiting period at UCC School of Pharmacy. The work aimed to fabricate and characterize ketoprofen loaded dissolvable microneedle arrays using *in vitro* and *in silico* methods. The presented delivery strategy demonstrates potential for enhanced delivery of ketoprofen. *In silico* results showed that the simulation was in agreement with the *in vitro* experimental results. Overall, dissolving microneedles may be useful as a method for patients to self-administer drugs without the pain or hazards of hypodermic needles.

References

1. Zhang Y, Chan HF, Leong KW. Advanced materials and processing for drug delivery: the past and the future. Advanced drug delivery reviews. 2013;65(1):104-20.
2. Allen TM, Cullis PR. Drug delivery systems: entering the mainstream. Science. 2004;303(5665):1818-22.
3. Verma RK, Garg S. Drug delivery technologies and future directions. Pharmaceutical Technology. 2001;25(2):1-14.
4. Schipper ML, Iyer G, Koh AL, Cheng Z, Ebenstein Y, Aharoni A, et al. Particle size, surface coating, and PEGylation influence the biodistribution of quantum dots in living mice. Small. 2009;5(1):126-34.
5. Carrstensen H, Mueller RH, Müller B. Particle size, surface hydrophobicity and interaction with serum of parenteral fat emulsions and model drug carriers as parameters related to RES uptake. Clinical nutrition. 1992;11(5):289-97.
6. Jain RA. The manufacturing techniques of various drug loaded biodegradable poly (lactide-co-glycolide)(PLGA) devices. Biomaterials. 2000;21(23):2475-90.
7. Li C, Wallace S. Polymer-drug conjugates: recent development in clinical oncology. Advanced drug delivery reviews. 2008;60(8):886-98.
8. Vasconcelos T, Sarmento B, Costa P. Solid dispersions as strategy to improve oral bioavailability of poor water soluble drugs. Drug discovery today. 2007;12(23):1068-75.
9. Liu Z, Jiao Y, Wang Y, Zhou C, Zhang Z. Polysaccharides-based nanoparticles as drug delivery systems. Advanced drug delivery reviews. 2008;60(15):1650-62.
10. Felt O, Buri P, Gurny R. Chitosan: a unique polysaccharide for drug delivery. Drug development and industrial pharmacy. 1998;24(11):979-93.
11. Sun C, Lee JS, Zhang M. Magnetic nanoparticles in MR imaging and drug delivery. Advanced drug delivery reviews. 2008;60(11):1252-65.

12. Cassano C, Mellace S, Trombino S. Nano- and Micro-Technologies for the Management of Food Ingredients. Book chapter, Ebook Bentham, (Accepted Manuscript).

Italian abstract:

L'innovazione nella chimica dei materiali e nella nanotecnologia hanno sinergicamente contribuito all'avanzamento e allo sviluppo dei Drug Delivery Systems (DDS) creando devices in grado di proteggere farmaci e sostanze biologicamente attive, aumentarne l'assorbimento, modificarne e migliorarne la penetrazione intracellulare e la distribuzione. Il presente lavoro ha avuto come obiettivo la progettazione, la preparazione e la caratterizzazione di materiali che potrebbero contribuire a trasformare e ottimizzare le performances di vari agenti terapeutici. In sintesi, sono stati preparati diversi dispositivi medici e DDS, utilizzando perlopiù polimeri, poiché esiste un grande potenziale nella combinazione di molecole bioattive con i polimeri, per affrontare sfide in campo farmaceutico e biomedico. Nella progettazione di questi nuovi materiali che sono biocompatibili e biologicamente attivi l'attenzione è stata anche focalizzata sull'applicazione di metodi *in vitro* e *in silico* per una previsione efficace ed efficiente dell'attività *in vivo.* In conclusione, la sintesi di nuovi materiali, l'adozione di polimeri naturali come carriers e una migliore comprensione del rapporto struttura-funzione hanno permesso lo sviluppo di DDS e devices con incoraggianti risultati sperimentali che suggeriscono un possibile utilizzo per una futura sperimentazione in ambito clinico.

SECTION 1

"HYDROGELS AND MICROSPHERES FOR ACTIVE MOLECULES RELEASE"

Part A: New gallic acid based hydrogel for phloretin intestinal release.

Part B: Novel microspheres based on triterpene saponins from the roots of *Physospermum verticillatum* (Waldst & Kit) (Apiaceae) for the improvement of gemcitabine release.

Part C: Liquid crystalline microspheres for 5-fluorouracil specific release.

PART A

"New Gallic Acid Based Hydrogel for Phloretin Intestinal Release" (1)

Abstract

The present work aims to realize a hydrogel based on gallic acid, a molecule with antioxidant and antidiabetic activity. The compound has in its structure two different functional groups, carboxyl and hydroxyl, susceptible to derivatization. Due to these characteristics, it was developed a hydrogel, potentially useful for oral administration of phloretin, a flavonoid of natural origin, found in apples and pears, with glucose transporter (GLUT) inhibitory activity. The obtained gallate hydrogel was characterized by Fourier Transform Infrared spectroscopy (FT-IR). Its equilibrium swelling degree (α %) and the phloretin release were evaluated in simulating gastric and intestinal fluids. The antioxidant activity in inhibiting lipid peroxidation, induced *in vitro* by a source of free radicals, was also assessed, after exposure of gallate hydrogel containing phloretin to gastrointestinal environmental conditions. The results showed that the gallate hydrogel could be successfully used in pharmaceutical field for phloretin intestinal release and suggest a possible use for the maintenance of an appropriate blood glucose level in the diabetic patient.

Keywords: *hydrogel, phloretin, gallic acid, intestinal release.*

1. Introduction

Diabetes mellitus is a group of metabolic diseases characterized by a congenital (type I insulin-dependent) or an acquired (type II non-insulin-dependent) inability to transport glucose from the blood to the cells. The chronic hyperglycemia, due to a deficiency of insulin secretion or insulin resistance (2), leads to glucose toxicity and is associated with long-term damage, dysfunction, and failure of various organs, especially the eyes, kidneys, nerves, heart, and blood vessels (3-5). Consequently it is necessary, in particular, in diabetic patient, the maintenance of an appropriate blood glucose level in postprandial state (6). Carbohydrates in the diet are hydrolyzed by digestive enzymes and then cleaved into monosaccharides, these can be absorbed from the small intestine via influx hexose transporters (7, 8). There are two type of transporter: Na^+-dependent glucose transporter (SGLT1), located at the brush border membrane (BBM), that mediates the uptake of glucose into the cell against its concentration gradient. The other type of transporter GLUT2, transports sugars across the basolateral membrane to the blood (9). Literature data suggest that GLUT2 can also be found onto the BBM in the presence of glucose in the lumen (10) and can contribute at the glucose absorption process (11). Thus, these glucose transporters might be an attractive therapeutic target for diabetes (12).

In this work, was developed a hydrogel for intestinal release of phloretin. A hydrogel is a three-dimensional, water-swollen structure composed of hydrophilic polymers. This network attains physical integrity and is made insoluble due to the presence of chemical and/or physical crosslinks (13-15). In addition, it is offers excellent potential as oral therapeutic systems due to intrinsic biocompatibility, diversity of both natural and synthetic material options and tunable properties. In particular, stimuli-responsive hydrogels exploit physiological changes along the intestinal tract to achieve site-specific and controlled release of protein, peptide and chemotherapeutic molecules for local and systemic treatment applications (16). In this context, was obtained a hydrogel based on gallic acid, a polyphenolic compound commonly distributed in plant-derived foods, such as cereals, legumes, nuts, vegetables, fruits, and in beverages such as green or black tea, wine, fruit juice, beer and etc (17-19). Literature data proved antidiabetic and antioxidant properties of gallic acid (20). So the polyphenolic compound

was chosen for hydrogel development, both for its properties and its chemical structure: in fact, it possesses two different functional groups, carboxyl and hydroxyl, susceptible to derivatization and so able to provide polymerizable derivatives (20). The compound entrapped in our gallate hydrogel is the phloretin (Figure 1).

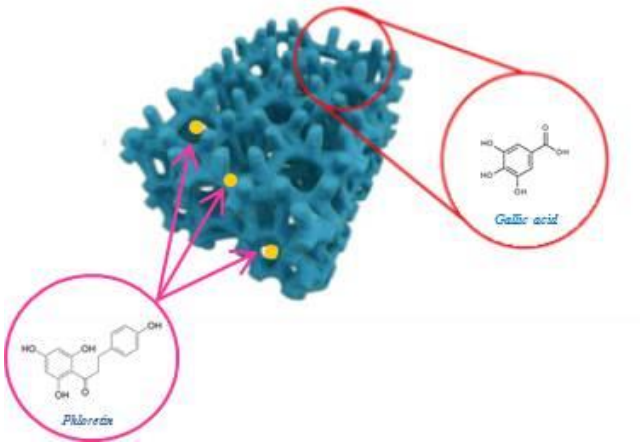

Figure 1: *Graphical representation of the gallic acid based hydrogel loaded with phloretin.*

This is a dihydrochalcone flavonoid, found in apples and other fruits, that displays also a potent antioxidant activity in peroxynitrite scavenging and the inhibition of lipid peroxidation (21). It is known to inhibit the protein kinase C (22-24) and human leukemia cell growth (25) . Literature data suggest that phloretin decreases the glucose absorption impeding its intestinal transport mediated by GLUT2 (26, 27). On the other hand, the phloretin, as well as other flavonoids, can be easily modified by environmental factors such as temperature, pH and light (28). These compounds, in fact, are poorly adsorbed in the intestine because are, probably, degraded by intestinal microorganism and/or enzymes, producing different metabolites. For these reasons flavonoids, when administered through delivery systems, show an improved stability and absorption profile and, consequently, their activity becomes enhanced, more detectable and prolonged (28). Therefore, our gallate hydrogel has been formulated

specifically to facilitate the phloretin intestinal release, protect it from chemical degradation in gastrointestinal tract and enhancing its bioavailability (29). The obtained hydrogel was characterized by Fourier Transform Infrared spectroscopy (FT-IR). Its equilibrium swelling degree (α%) was also evaluated in simulating gastric and intestinal fluids. The phloretin release from hydrogel was carried out in the same condition of swelling studies. The antioxidant activity in inhibiting lipid peroxidation, in rat-liver microsomal membranes, induced *in vitro* by a source of free radicals, such as *tert*-butyl hydroperoxide (*t*-BOOH), was assessed after exposure of gallate hydrogel, containing phloretin, to gastrointestinal environmental conditions.

2. Materials and Methods

2.1 Chemicals

Acetone, hydrochloric acid, chloroform, diethyl ether, ethanol, isopropanol, methanol, n-hexane, tetrahydrofuran (THF), allyl alcohol and sodium sulfate were purchased from Carlo Erba Reagents (Milan, Italy). Gallic acid (MW = 170.12), phloretin (MW = 274.27), acrylic acid (MW = 72.06, d = 1051 g / ml), dicyclohexylcarbodiimide (DCC), N,N-dimethylaminopyridine (DMAP), potassium tert-butoxide, N,N-dimethylacrylamide (DMAA), ammonium persulfate ($(NH_4)_2S_2O_8$), N,N'-methylene-bis-acrylamide, sorbitan trioleate (Span85), polyoxymethylene sorbitan trioleate (Tween 85), N,N,N',N'-tetramethyl-ethylenediamine (TMEDA), tert-butylhydroperoxide (*t*-BOOH), trichloroacetic acid (TCA) acid, 2-thiobarbituric acid (TBA), butylated hydroxytoluene (BHT) were purchased from Sigma-Aldrich (Sigma Chemical Co, St Louis, MO, USA).

2.2 Instrument

The FT-IR spectra were performed on KBr pellets using a spectrometer Perkin Elmer 1720, in the range 4000-400 cm^{-1} (16 scans). The ^{1}H-NMR spectra were obtained by the use of a spectrophotometer Burker VM30; the chemical shifts were expressed as δ and referring to the solvent. The UV-VIS spectra have been realized by means of JASCO-530 UV-

spectrophotometer. Samples were freeze-dried using a freeze-drying "Micro Modulyo Edwards apparatus".

2.3 Acrylation of 3,4,5-trihydroxybenzoic acid with 2-propenoic acid

Acrylic acid (0.14 ml, $2 \cdot 10^{-3}$ mole) was dissolved in dry THF. Then DCC (0.42 g, 2×10^{-3} mol) and DMAP (0.05 g, 4×10^{-4} mol) were added and the reaction mixture was kept under stirring at 50 °C for 1h. After that, gallic acid (1g, 5.8×10^{-3} moles) was added to the solution. The reaction was kept under magnetic stirring at 50 °C for other 72 h and monitored by thin layer chromatography (TLC/silica gel, eluent mixture: chloroform-methanol 7:3). The dicyclohexylurea (DCU), formed during the reaction, was eliminated by filtration. The solvent reaction was removed by evaporation at reduced pressure. The obtained product, with a gelatinous consistency and yellow color, was purified through silica gel column chromatography (eluent: chloroform). The purified product has been characterized by FT-IR, and ^{1}H-NMR.

2.4 Hydrogel based on diacrylate gallic acid preparation

In a two-neck flask fitted with a reflux condenser, magnetic stirring, thoroughly flamed and maintained under nitrogen bubbling, the acrylated derivative of 3,4,5-trihydroxybenzoic acid was solubilized in an aqueous solution of NH_3/urea. Subsequently, DMAA (0.035 g, 0.037 ml, 3.5×10^{-4} mol) and ($(NH_4)_2S_2O_8$) (0.8 g, 3.5×10^{-3} moles) were added. The reaction mixture was heated to 60 °C and left under magnetic stirring until the formation of the hydrogel. The obtained hydrogel was subsequently washed with diethyl ether in a porous filter, dried under vacuum and characterized by FT-IR (30).

2.5 Phloretin incorporation into the performed hydrogel

The hydrogel was loaded with phloretin using a drug solution water/ethanol 8/2. At first it was left under constant stirring at 37 ° C in a water bath for 72 h. The solution was than filtrated and analyzed by UV-VIS (λ = 288nm). The drug loading efficiency (LE%) of hydrogel was calculated by the following equation (Eq. 1):

$$LE\% = \frac{Mi-M0}{Mi} \times 100 \qquad \text{(Eq.1)}$$

were Mi and M0 are respectively the amount of the drug in solution before and after impregnation. The loading efficiency was measured spectrophotometrically.

2.6 Antioxidant activity evaluation

The ability of the prepared hydrogel, loaded and not with phloretin, to protect against lipid peroxidation induced by *tert*-BOOH, was examined in rat liver microsomal membranes during 120 min of incubation and after hydrogel exposure to gastrointestinal environmental conditions. Aliquots of both phloretin-loaded and not loaded hydrogel were added to the microsomal suspension. The suspension was then incubated at 37°C in a shaking bath in the dark. After incubation, the thiobarbituric acid–malondialdehyde complex (TBA–MDA) formation was monitored by the use of UV–Vis spectrophotometry at 535 nm (31). The experiment was repeated in triplicate (n= 3).

2.7 Hydrogel swelling studies

The swelling behavior of the hydrogel, was assessed in accordance with a procedure reported in literature (31), in order to check its hydrophilic affinity. This study was performed at two different pHs, which simulated the typical conditions of the gastro-intestinal tract. In particular aliquots of dried hydrogel of 0.05 g were placed in glass filters (⌀10mm, porosity, G3), previously weighed, and immersed in beakers containing buffer solutions of the two different pHs (1.2 to mimic the acid environment of the stomach and phosphate buffer at 7.4 to mimic the small intestine ones). At predetermined time intervals (1h, 2h, 3h, 6h, 12h, 24h), the water excess has been removed from the filters by percolation at atmospheric pressure. Subsequently, the filters were placed in a properly sized centrifuge test tube by fixing them with the help of a bored silicone stopper, then centrifuged at 8000 rpm for 5 minutes and weighed. This operation was repeated at each time point. The

weights, measured at each time intervals, were averaged and used to give the water content percent by the following equation:

$$\alpha(\%) = \frac{(Ws - Wd)}{Ws} \times 100 \qquad \text{(Eq. 2)}$$

Where Ws and Wd are weights of swollen and dried hydrogels, respectively. The swelling was evaluated for the first two hours at pH 1.2 and then from the third hour onwards the pH was adjusted to 7.4. This was done to simulate the natural transit time in the gastro-intestinal tract.

2.8 Drug release studies

Dried and loaded hydrogel (0.031 g) was placed in the of swelling media. The test tubes were put in a water bath at 37 °C under stirring. At predetermined time intervals (1h, 2h, 3h, 6h, 12h, 24h), the samples were centrifuged, the supernatant were removed and the medium was replaced with fresh solution to maintain the same total volume throughout the study. The phloretin concentration in the different solutions was monitored by the use of UV-Vis spectrophotometry at 288 nm. As well as for swelling studies, the release was evaluated at pH 1.2 only for the first two hours, while the release at 7.4 was performed by the third hour onwards. The experiment was repeated in triplicate (n=3). Data were calculated in terms of drug release percentage.

2.9 Statistical analysis

All data present the mean values ±SD ($n \geq 3$) and were analysed using GraphPad version 5 for Windows (GraphPad Software Inc, La Jolla, CA, USA). The significance of the difference between groups was evaluated by Student's *t*-test or one-way analysis of variance, as appropriate according to the number of groups analysed. Mean differences with $P \leq 0.05$ were considered statistically significant.

3. Results and Discussions

Many literature data, concerning polymers as drug delivery systems, show an increasing interest respect of biocompatible and site-specific materials exploiting the possibility of combine the controlled release of the drug with it protection from possible degradation causes like light, pH temperature etc. This work fits in this context and had as its purpose the design and synthesis of a gallate hydrogel useful for phloretin intestinal release and maintenance of an appropriate blood glucose level in the diabetic patient. The starting material is gallic acid, organic acid widely present in the plant kingdom, which presents in its structure a carboxyl group and three hydroxyl groups, all susceptible to derivatization and therefore able to provide various polymerizable derivatives. Therefore, through an acrylation reaction has been possible to obtain a diacrylate derivative of gallic acid which was used for the preparation of a hydrogel.

3.1 Acrylation of 3,4,5-trihydroxybenzoic acid with 2-propenoic acid

Objective of this reaction has been to synthesize the diacrylate derivative of gallic acid. This reaction provides for the use of DCC (dicyclohexylcarbodiimide) condensing agent, that reacting with the carbonyl group of acrylic acid, allowed the formation of an adduct which subsequently underwent nucleophilic attack by the hydroxyl groups of gallic acid. The DMAP (N,N-dimethylaminopyridine), has also been used as nucleophilic activator because, deprotonating the hydroxyl group of gallic acid, permitted the alcoholate formation that reacted with the electrophile carbonyl of acrylic acid. In addition, the DMAP, acting as a base, preventing the pH lowering (Scheme 1). The dicyclohexylurea (DCU) that was formed during the reaction was eliminated by treating the product with hot methanol and filtering it. The product was dried under reduced pressure, purified by column chromatography and characterized by FT-IR and ^{1}H-NMR. FT-IR (KBr) ν (cm^{-1}): 3324 (-OH), 3261 (-OH), 3034 (-CH), 1780 (-C = O), 1739 (-C = O), 1710 (- C = O), 1626 (-C = C), 1261 (-CO), 985 (-CH), 905 (-CH). M / Z: 205 (100%), 277 (4%). ^{1}H-NMR (CD_3OD) δ (ppm): 5.916 (2H, dd), 6.378 (2H, dd), 6.675 (2H, dd), 7.651 (2H, d). Yield 70%.

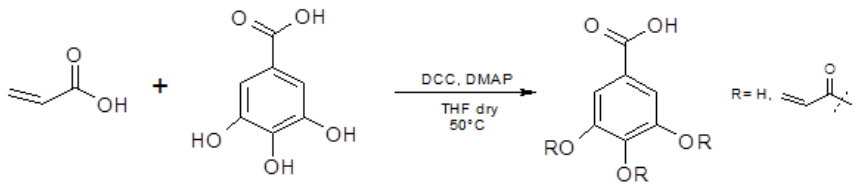

Scheme 1: *Graphical representation of gallic acid acrylation-reaction.*

3.2 Preparation of the hydrogel based on gallic acid diacrylate

The gallic acid diacrylated was dissolved in an aqueous solution of NH_3/urea. The comonomer N,N-dimethylacrylamide and the radical initiator ammonium persulfate were added. The obtained solution was kept under stirring and warm up until the formation of the hydrogel. This latter, washed with distilled water, frozen and freeze-dried and has been thoroughly characterized by FT-IR that showed the complete disappearance of the bands typical of the acrylic group at 985 cm^{-1} and 905 cm^{-1} and the appearance of a new band of stretching carbonyl at 1640 cm^{-1}.

3.3 Hydrogel impregnation with phloretin

The hydrogel was loaded with phloretin using a drug solution water/ethanol 8/2. The solution was analyzed, after filtration, by UV-VIS (λ = 288nm, ε = 3201.4 mol • dm^{-1} • cm^{-1}). Experiment was repeated in triplicate and results showed that the loading efficiency was 80% ± 1,2.

3.4 Antioxidant activity evaluation

The ability of the gallate hydrogel, loaded and not loaded with phloretin, to inhibit lipid peroxidation induced by the *t*-BOOH, a source of free radicals, was examined in microsomal membranes of rat liver over a period of 120 minutes of incubation. Both hydrogels were previously exposed for two hours to intestinal environmental conditions (pH 7.4) to verify the preservation of the antioxidant activity of gallic acid-based hydrogel. Results revealed (Figure 2) that the hydrogels antioxidant activity was preserved in the time.

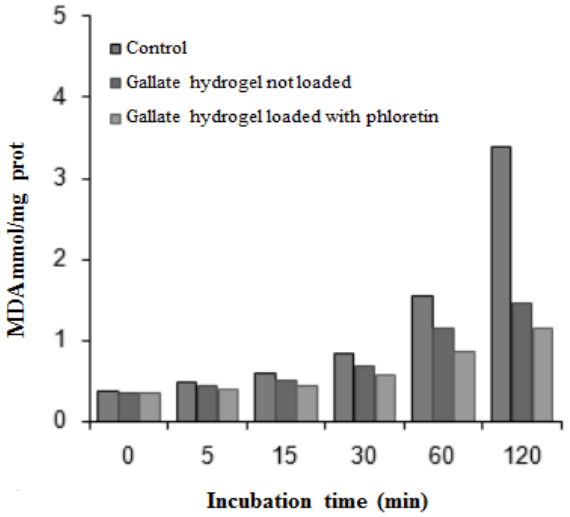

Figure 2: *Comparative graphs of malondialdehyde formation (MDA) vs time (min)in the control vs loaded and not gallate hydrogel. Means value ± SD, n = 3.*

3.5 Swelling studies

The swelling behavior of the gallate hydrogel has been evaluated at to two different pHs (1.2 and 7.4) and at predetermined time intervals (1h, 2h, 3h, 6h, 12h, 24h). Each experiment was carried out in triplicate and the results were in agreement within ± 4% standard error. The values of swelling degree (α%) for the prepared material at pHs 1.2 and 7.4 and different time intervals are reported in Table 1.

Table 1: *Swelling behavior of the gallate hydrogel at pHs 1.2 and 7.4.*

Time (h)	α% pH 1.2	α% pH 7.4
1	*67%*	-
2	*118%*	-
3	-	*540%*
6	-	*779%*
12	-	*938%*
24	-	*1060%*

The obtained data showed the actual ability of this hydrogel for phloretin intestinal specific release.

3.6 Hydrogel release studies

The release studies of phoretin were conducted on fixed aliquots of hydrogel at two different pH (1.2, and 7.4), which mimic the conditions of the gastro-intestinal tract, and at different time intervals (1h, 2h, 3h, 6h, 12h, 24h) through the use of a water bath at 37 ° C and under stirring. The results of release tests revealed that the hydrogel effectively released the drug at higher percentages at pH 7.4 (Figure 3).

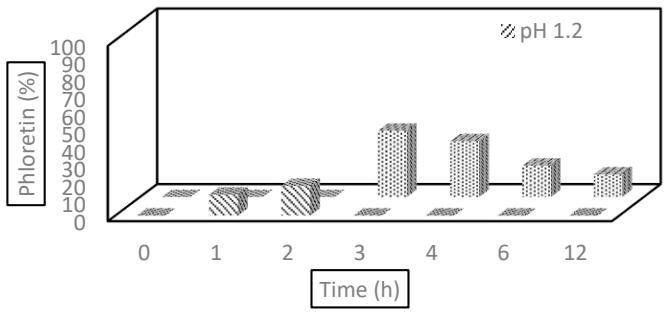

Figure 3: *Graphic representation of phloretin release from gallate hydrogel, plotting time (h) vs percentage of drug released, at two different pHs. Means value ± SD, n = 3.*

Therefore, these data allow to assume an oral administration of the gallate hydrogel and the use of this material as a vehicle of phloretin in the intestine.

4. Conclusions

The aim of this work was the inclusion of phloretin, a natural dihydrochalcone flavonoid with multiple properties including antidiabetic and antioxidant, in a hydrogel based on gallic acid formulated specifically to facilitate the phloretin intestinal release and protect it from chemical

degradation in gastrointestinal tract, enhancing its bioavailability. The swelling degree of the hydrogel not containing the phloretin, was carried out at two different pHs and predetermined time intervals. In particular, acidic solutions of HCl at pH 1.2 to mimic the pH of the stomach and 7.4 to mimic the pH of the small intestine, have been used. The obtained results revealed that the gallate hydrogel swells more at pH 7.4. Furthermore, the hydrogel was subjected to release studies in the same conditions of swelling tests. The results have shown the ability of hydrogel to release the phloretin at pH 7.4. Finally, the hydrogel was also submitted to evaluation of the antioxidant activity. The obtained data show that the hydrogel based on gallic acid could be used for the controlled release of phloretin through the gastro-intestinal tract, suggesting also a possible use in the treatment of diabetes.

References

1. Trombino S, Cassano R, Mellace S, Picci N. New Gallic Acid Based Hydrogel for Phloretin Intestinal Release, IJPRD, 2015;7(5):1-9.
2. Ikumi Y, Kida T, Sakuma S, Yamashita S, Akashi M. Polymer–phloridzin conjugates as an anti-diabetic drug that Inhibits glucose absorption through the Na+/glucose cotransporter (SGLT1) in the small intestine. Journal of controlled release. 2008;125(1):42-9.
3. Schwartz MW. Diabetes complications: why is glucose potentially toxic? Science. 1996;272(5262):699.
4. Bonadonna RC. Alterations of glucose metabolism in type 2 diabetes mellitus. An overview. Reviews in endocrine & metabolic disorders. 2004;5(2):89-97.
5. Mertes G. Safety and efficacy of acarbose in the treatment of type 2 diabetes: data from a 5-year surveillance study. Diabetes research and clinical practice. 2001;52(3):193-204.
6. Hediger MA, Coady MJ, Ikeda TS, Wright EM. Expression cloning and cDNA sequencing of the Na+/glucose co-transporter. Nature. 1987;330(6146):379-81.
7. Wood IS, Trayhurn P. Glucose transporters (GLUT and SGLT): expanded families of sugar transport proteins. British Journal of Nutrition. 2003;89(1):3-9.
8. Drozdowski LA, Thomson AB. Intestinal sugar transport. World journal of gastroenterology: WJG. 2006;12(11):1657.
9. Kellett GL, Helliwell PA. The diffusive component of intestinal glucose absorption is mediated by the glucose-induced recruitment of GLUT2 to the brush-border membrane. Biochemical Journal. 2000;350(1):155-62.
10. Kellett GL, Brot-Laroche E, Mace OJ, Leturque A. Sugar absorption in the intestine: the role of GLUT2. Annu Rev Nutr. 2008;28:35-54.
11. Goto T, Horita M, Nagai H, Nagatomo A, Nishida N, Matsuura Y, et al. Tiliroside, a glycosidic flavonoid, inhibits carbohydrate digestion and glucose absorption in the gastrointestinal tract. Molecular nutrition & food research. 2012;56(3):435-45.

12. Peppas NA, Wood KM, Blanchette JO. Hydrogels for oral delivery of therapeutic proteins. Expert Opinion on Biological Therapy. 2004;4(6):881-7.
13. Kim B, Peppas NA. Poly (ethylene glycol)-containing hydrogels for oral protein delivery applications. Biomedical Microdevices. 2003;5(4):333-41.
14. Ichikawa H, Peppas NA. Novel complexation hydrogels for oral peptide delivery: In vitro evaluation of their cytocompatibility and insulin-transport enhancing effects using Caco-2 cell monolayers. Journal of Biomedical Materials Research Part A. 2003;67(2):609-17.
15. Sharpe LA, Daily AM, Horava SD, Peppas NA. Therapeutic applications of hydrogels in oral drug delivery. Expert opinion on drug delivery. 2014;11(6):901-15.
16. Polyfenols BL. Chemistry, dietary sources, metabolism and nutritional significanve. Nutr Rev. 1998;56:317-33.
17. King A, Young G. Characteristics and occurrence of phenolic phytochemicals. Journal of the American Dietetic Association. 1999;99(2):213-8.
18. Trombino S, Cassano R. Preparation And In Vitro Activities Evaluation Of Gallic Acid-Based Microspheres For Phloretin Transdermal Delivery. Int. J Pharm. Res. Dev.2014; 6:1-11.
19. Al-Salih R. Clinical experimental evidence: synergistic effect of gallic acid and tannic acid as antidiabetic and antioxidant agents. Med J. 2010;4:109-19.
20. Rezk BM, Haenen GR, van der Vijgh WJ, Bast A. The antioxidant activity of phloretin: the disclosure of a new antioxidant pharmacophore in flavonoids. Biochemical and biophysical research communications. 2002;295(1):9-13.
21. Wu CH, Ho YS, Tsai CY, Wang YJ, Tseng H, Wei PL, et al. In vitro and in vivo study of phloretin-induced apoptosis in human liver cancer cells involving inhibition of type II glucose transporter. International journal of cancer. 2009;124(9):2210-9.
22. He X, Liu RH. Triterpenoids isolated from apple peels have potent antiproliferative activity and may be partially responsible for apple's

anticancer activity. Journal of agricultural and food chemistry. 2007;55(11):4366-70.
23. Yoon H, Liu RH. Effect of selected phytochemicals and apple extracts on NF-κB activation in human breast cancer MCF-7 cells. Journal of agricultural and food chemistry. 2007;55(8):3167-73.
24. Devi MA, Das N. In vitro effects of natural plant polyphenols on the proliferation of normal and abnormal human lymphocytes and their secretions of interleukin-2. Cancer letters. 1993;69(3):191-6.
25. Baldea LAN, Martineau LC, Benhaddou-Andaloussi A, Arnason JT, Lévy É, Haddad PS. Inhibition of intestinal glucose absorption by anti-diabetic medicinal plants derived from the James Bay Cree traditional pharmacopeia. Journal of ethnopharmacology. 2010;132(2):473-82.
26. Newey H, Parsons B, Smyth D. The site of action of phlorrhizin in inhibiting intestinal absorption of glucose. The Journal of physiology. 1959;148(1):83-92.
27. Bilia AR, Isacchi B, Righeschi C, Guccione C, Bergonzi MC. Flavonoids loaded in nanocarriers: an opportunity to increase oral bioavailability and bioefficacy. Food and Nutrition Sciences. 2014;5(13):1212.
28. Bartoli GM, Giannattasio B, Palozza P, Cittadini A. Superoxide dismutase depletion and lipid peroxidation in rat liver microsomal membranes: correlation with liver carcinogenesis. Biochimica et Biophysica Acta (BBA)-General Subjects. 1988;966(2):214-21.
29. Karakaya S. Bioavailability of phenolic compounds. Critical reviews in food science and nutrition. 2004;44(6):453-64.
30. Cassano R, Trombino S, Muzzalupo R, Tavano L, Picci N. A novel dextran hydrogel linking trans-ferulic acid for the stabilization and transdermal delivery of vitamin E. European Journal of Pharmaceutics and Biopharmaceutics. 2009;72(1):232-8.
31. Trombino S, Cassano R, Bloise E, Muzzalupo R, Tavano L, Picci N. Synthesis and antioxidant activity evaluation of a novel cellulose hydrogel containing trans-ferulic acid. Carbohydrate polymers. 2009;75(1):184-8.

PART B

"Novel Microspheres Based on Triterpene Saponins from the roots of *Physospermum Verticillatum* (Waldst & Kit) (Apiaceae) for the Improvement of Gemcitabine Release" (1)

Abstract

Objectives The present work concerns the preparation and characterization of microspheres based on a mixture of triterpene saponins, from *Physospermum verticillatum* (Waldst & Kit), as a carrier for the specific release of gemcitabine.

Methods Triterpene saponins were derivatized with acrylic acid. The obtained polymerizable product was characterized by Fourier Transform Infrared to confirm the ester linkage. Then, spherical microparticles were prepared by suspension radical copolymerization and impregnated with gemcitabine.

Key findings Microspheres exhibited a mean diameter of 2.7 µ. The swelling studies showed that particles swell most at pH 6.2, typical of the tumor pathology, then at pH 7.4, miming physiological conditions. The microspheres were loaded with gemcitabine (LE 72.2%). Their release profile showed an initial dot of around 24% and a further release for 24 h.

Conclusions This carrier could be potentially release the drug in a in the lung, as a function of different pHs between tumor cells and healthy, reducing the systemic drug toxicity, allowing the reduction of the doses number, increasing the drug half-life, and eliminating the problems related to the fast clearance of gemcitabine administration.

Keywords: *Triterpene saponins, microspheres, lung cancer, gemcitabine, release.*

1. Introduction

Over the last years the interest towards pulmonary drug delivery systems, suitable for cancer therapy, is increasing. Lung cancer is one of the most frequently occurring malignancies and the leading cause of death worldwide (2-4). The systemic drug administration has hardly successful for the treatment of this pathology because only a partial amount of the drug reaches the lungs, even when used at high dose. In addition, the majority of these agents acts on normal cells, inhibiting their growth, weakening the patient that undergoes the antitumor therapy causing, in some cases, even the death (5). Therefore, the novel therapeutic strategies aim to improve the delivery of drugs that play a fundamental role in the treatment of lung cancer reducing also their toxicity (5). For this reason, there is an extensive interest in encapsulating the drugs in carrier systems micrometer and nanometer-sized. In particular, liposomes, polymer conjugates, polymeric micelles, microparticles, and nanoparticles have been investigated to selectively deliver various bioactive substances at the tumor site (6-9). Gemcitabine (GEM) is one of this kind of drugs.

It is a difluoro analogue of deoxycytidine (dFdC) and an antineoplastic drug belonging to the class of anti-metabolites that find indications in the treatment of large cell lung cancer, non-squamous cell lung cancer, metastatic pancreatic cancer, ovarian cancer and bladder cancer (10). This drug has a short plasma half-life of about 15 minutes (11), and a slower clearance in women and in the elderly. Peak levels reach 20-60 μM doses of 1000 mg/m^2 administered intravenously over 30 minutes (12). Furthermore, it is converted into its inactive and soluble metabolites and cleared rapidly out of body through renal excretion. The dosage should be controlled and appropriately modified in patients with kidney and liver diseases. The main toxic effect of gemcitabine is the myelo-suppression (13).

Therefore, novel therapeutic strategies aiming to improve the pharmacokinetic, reduce the toxicity and obtain a better bio-distribution, are now needed (14). In this context, the microparticles could be used as carrier to achieve an efficient release of the chemotherapeutic drugs in the lung cancer therapy. Over the main method of microparticles preparation is the emulsion polymerization (15), that occurs with radical mechanism. Through this procedure microparticles based on triterpene saponins were

prepared and characterized. The saponins are a group of naturally occurring plant glycosides, reported in more than 100 families of plants. Several natural saponins have found to possess significant anticancer properties against colon, liver, gastric, ovarian, breast, thyroid, and lung epithelial cancer cells (16-19). These phytochemicals are able to induce cell cycle arrest, apoptosis and inhibit angiogenesis or tumor cell metastasis by influencing the dynamics or lateral organization of mammalian cellular membranes, by inhibiting proteins involved in the cell cycle (cyclins or cyclin-dependent kinases) and by other important cancer promoting pathways (20-22). In particular, the saponins are able to interact with cholesterol present in the cell membranes on both normal and cancer cells causing membrane damage. However, these compounds bind more efficiently to cancer cells containing more cholesterol than normal ones, but that is not enough to give adequate therapeutic index to be of any clinical value (23).

A rich source of saponins is the Apiaceae family (24-26). In this paper the interest was focused on triterpene saponins isolated from the roots of *Physospermum verticillatum* (Waldst & Kit) (Apiaceae), namely saikosaponin a, buddlejasaponin IV and songarosaponin D. In our previous study, these compounds have been tested *in vitro* for their potential antiproliferative activity against different human tumor cell lines. A remarkable activity was detected against COR-L23 (large cell lung carcinoma) cells with IC_{50} values in the range 0.4-0.6 μM (16). The interest in these compounds is related also to their ability to exerted significant inhibition of nitric oxide (NO) production in LPS induced RAW 264.7 macrophages. Recently, special attention is giving to combinations of saponins and other anticancer drugs (e. g. docetaxel, cisplatin, doxorubicin, paclitaxel, etc.) as efficient treatment against cancer cell line (27, 28). The improved therapeutic success of saponin-anticancer drug combination is related to the potentiation of cancer growth inhibition and the possibility to by-pass drug resistance (16, 19). In view of their potential value and of the considerations reported above, a mixture of saikosaponin a (**1**), buddlejasaponin IV (**2**) and songarosaponin D (**3**) was used to prepare and investigate the feasibility of microspheres loaded with gemcitabine to obtain synergic effects (Figure 1).

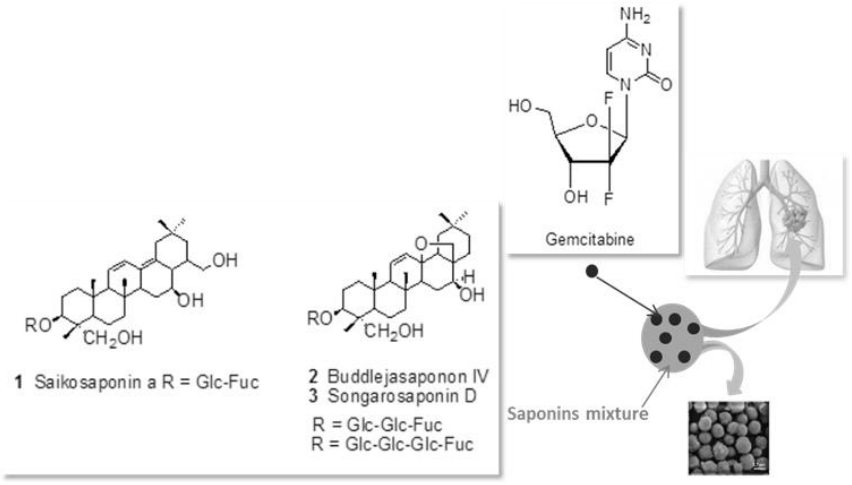

Figure 1: *Representative scheme of gemcitabine loaded microparticles triterpene saponins based.*

The formation of microspheres could enhance the saponins selectivity towards cancer cells and reduce their toxicity, increasing their therapeutic index. In fact, it is known that saponins can cause side effects because of their hydrophobic-lytic properties resulting in trapping at the site of administration, causing cell and tissue destruction with local and systemic adverse reactions and a low therapeutic index.

2. Materials and Methods

2.1 Chemicals

Acetone, chloroform, dichloromethane, ethanol, methanol, isopropanol, n-hexane, acetonitrile, tetrahydrofuran (THF) were obtained from Carlo Erba

Reagents (Milan, Italy). *n*-Hexane, chloroform and tetrahydrofuran were purified by standard procedures. Acrylic acid, dicyclohexylcarbodimide (DCC), dimethylaminopyridine (DMAP), *N*,*N*-dimethylacrylamide, sorbitan trioleate (Span 85), polyoxymethylene sorbitan (Tween 85), *N*,*N*,*N*',*N*'-tetramethylethylenediamine (TMEDA), ammonium persulfate (APS) and gemcitabine hydrochloride were purchased from Sigma-Aldrich (Sigma Chemical Co., St. Louis, MO, USA).

2.2 Plant materials

The roots of *Physospermum verticillatum* (Waldst & Kit) (Apiaceae) were collected in Calabria (Southern Italy) and authenticated by dr. D. Puntillo, Natural History Museum of Calabria and Botanical Garden, University of Calabria (Italy). A voucher specimen (No. CLU 21188) was deposited in the Botany Department Herbarium at the University of Calabria, Italy.

2.3 Extraction procedure

The triterpene saponins mixture was obtained by extraction from the roots of *P. verticillatum* as previously reported (21). Briefly, the roots (650 g) were subjected to maceration with methanol (5 × 72 h). The total extract (87.8 g) was suspended in distilled water and partitioned successively with ethyl acetate and water-saturated *n*-butanol. An *n*-butanol fraction of 52.5 g was obtained. 5 g of this was chromatographed on a silica gel column (0.040-0.063 mm) eluted with $CHCl_3$/MeOH/H_2O gradient and fractions of 10 ml were collected. After monitoring by thin layer chromatography (TLC), fractions were combined into six main parts (1-5). The fifth one (3.5 g) was subjected to flash column chromatography over silica gel by using $CHCl_3$/MeOH/H_2O mixture as eluent to afford a mixture (2.7 g) of saikosaponin a, buddlejasaponin IV and songarosaponin D (*ratio* of 2.1:1.8:1).

2.4 Measurements

The FT-IR spectra were carried out using a spectrometer FT-IR Jasco 4200 (Jasco Analytical Instrument, Japan) and KBr diskes. The structures of the synthesized compounds were confirmed by GC-MS Hewlett Packard 5972 (Hewlett-Packard Company, CA) instrument. The UV-Vis spectra were

performed using UV-Vis spectrophotometer V-530 JASCO (Jasco Analytical Instrument, Japan). Dimensional analysis of the microparticles was made by light scattering using a Brookhaven 90 Plus Particle Size Analyzer (Brookhaven Instruments Corporation, USA) by measuring the autocorrelation function at 90° scattering angle. The polydispersity index (PI), which indicates the measure of the distribution of nanoparticle populations, was also determined. Six separate measurements were made in order to obtain the average. Data were fitted by the method of inverse ‘‘Laplace transformation’’ and Contin. Samples were lyophilized using a ‘‘Freezing-drying’’ Micro module apparatus, Edwards (Crawley, West Sussex, UK). Photomicrografies of microparticles were obtained using a scanning electron microscope JEOL JSMT 300 A (JSMT, Jeol Ltd., Tokyo, Japan); the surface of the samples was made conductive by deposition of a gold layer in a vacuum chamber.

2.5 Esterification of triterpene saponins with acrylic acid

The reaction was conducted in accordance with the procedure of Steglich esterification (29). In a three-necked flask fitted with reflux condenser and magnetic stirrer, accurately flamed and maintained in an inert atmosphere, 19.75 μl (0.288 mmol) of acrylic acid were dissolved in 25 ml of dry tetrahydrofuran. After dissolution was added 0.040 g of DCC (0.192 mmol), 0.0012 g of DMAP (0.0096 mmol). After 30 minutes 0.15 g of saponins mixture (0.192 mmol) were added. The reaction mixture was kept cold, in a cold water bath, under stirring for 72 hours and monitored by TLC (silica gel, eluent mixture *n*-hexane/chloroform 9:1). At the end of the reaction the solvent was removed at reduced pressure. The dicyclohexylurea (DCU) was removed using methanol. The product was then dried with a mechanical pump and subsequently purified by column chromatography on silica gel using as eluent n-hexane/chloroform 8:2. The product was characterized by FT-IR.

2.6 Preparation of microspheres based on triterpene saponins

Microspheres based on were produced by radical polymerization technique. Briefly, in a cylindrical reactor of glass (100-150 ml) equipped with mechanical stirrer, dropping funnel and a screw cap with puncture-proof

rubber septum, was flamed in a current of nitrogen, and after cooling was placed in a bath thermostatically controlled at 40 ° C. Then, the required amounts of *n*-hexane (20 ml) and chloroform (18 ml), distillates, constituting the dispersant phase, were introduced in the reactor. The polymerization reaction was conducted according to the procedure reported in the literature (30). The dispersing phase was kept in a mechanical shaker for 30 minutes. A quantity of 0.15 g of ester (0.593 mmol) was suitably dissolved in 4 ml of distilled water, sonicated for a few minutes to facilitate the dissolution process. In the environmental reaction were added, under nitrogen stream, the solution containing the ester, 122.2 µl of *N*, *N*-dimethylacrylamide (1.186 mmol) and 0.80 g of ammonium persulfate ($(NH_4)_2S_2O_8$) (3.5 mmol) which acts as a radical initiator. The density of the organic phase was adjusted with the addition of one of the two solvents to obtain an aqueous phase in equilibrium with the organic phase. Then was added under nitrogen stream 150 µl of sorbitan trioleate (Span 85), after 10 minutes 150 µl of polyoxyethylene sorbitan trioleate (Tween 85) and after additional 10 minutes 150 µl of tetramethylenediamine (TMEDA). The system was kept under stirring for 3h and the temperature of 40 ° C. The content of the reactor was then filtered and washed in succession with 100 ml of isopropanol, 100 ml of ethanol and 100 ml of acetone. The filtrate was than analysed and characterizated.

2.7 Microspheres characterization

The obtained samples were characterized by FT-IR spectrophotometry, scanning electron microscopy (SEM) and measurement of the swelling degree in aqueous solutions at different pH values (6.2 and 7.4).

2.7.1 Dimensional analysis

The size of the microparticles was determined by light scattering using a particle size analyzer 90 Plus, at 25 °C. It was also determined the polydispersity index (PI), indicating the extent of the distribution of the microparticle population (31). The microparticles were also observed by means of (SEM).

2.7.2 Swelling studies

The affinity of the hydrophilic microparticles towards the aqueous environment was determined by their swelling degree (% WR). Aliquots notes of dry material (20 mg) were placed in glass filters (porosity G2/3) previously wetted, centrifuged (5 min at 2000 rpm), and then weighed.
Subsequently, the filters were put in contact with a solution of phosphate buffer (Na_2HPO_4) at pH 6.2 (to mimic the conditions typical of the lungs tumor) and at pH 7.4 (to simulate the physiological environment) at the temperatures of 37 °C until reaching swelling equilibrium. At predetermined intervals time (1h, 2h, 3h, 12h, 18h, 24h) the excess of water was removed from the filters by means of percolation at atmospheric pressure. Three replicates were used for each pH value. Subsequently, the filters were centrifuged at 2000 g/min for 5 min. Finally, after centrifugation, the filters are weighed. The weights recorded to the time listed above were averaged and used to give the equilibrium swelling degree by the following equation:

$$WR(\%) = \frac{(Ws - Wd)}{Ws} \times 100 \qquad \text{(Eq. 1)}$$

where Ws and Wd are the weights of the swollen and dried microspheres respectively (30).

2.8 Impregnation of the microspheres with gemcitabine

The preformed matrix (about 50 mg) was placed in contact with a solution of known concentration of drug obtained by dissolving 5 mg of gemcitabine in 20 ml of distilled water. The impregnation was carried out under stirring at room temperature for 3 days, during which the solution of drug was absorbed by the matrix with consequent swelling (15). Finally, the solvent was removed by filtration and the microparticles were dried to constant weight. The analysis of filtrated water through spectrophotometer UV-Vis allowed to calculate the drug loading percentage (LE%) through the next equation:

$$LE\% = \frac{Mi-M0}{Mi} \times 100 \qquad \text{(Eq. 2)}$$

where Mi represents the drug concentration in the solution before loading and M0 the drug concentration in the solution after loading respectively.

2.9 *In vitro* release studies of gemcitabine from microparticles

Dried and loaded microparticles (10 mg) were dispersed in 6ml of swelling media with pH 6.2 or 7.4 (32). The test tubes were put in a water bath at 37 °C under stirring. At predetermined time intervals (1h, 2h, 3h, 6h, 12h, 24h), the samples were centrifuged, 5 ml of supernatant were removed and the medium was replaced with fresh solution to maintain the same total volume throughout the study. The gemcitabine concentration in the different solutions was monitored by the use of UV-Vis spectrophotometry at 275 nm. Each *in vitro* release study was performed in triplicate and under sink conditions. The release was calculated in terms of percentage of drug released.

2.10 Statistical analysis

Data are represented as the mean value ± standard deviation (S.D.) of three independent experiments. Differences within and between groups were evaluated by nonparametric ANOVA tests (Krushal-Wallis) completed by and with a multicomparison Dunn test using GraphPad softwere. A *P* value of <0.05 was considered significant.

3. Results and discussion

The microspheres are prepared using a triterpene saponins mixture containing saikosaponin a, songarosaponin D and buddlejasaponin IV, with a known antineoplastic activity (33). From the chemical point of view these saponins have a triterpene aglycone linked to several sugar moieties. Moreover, in the structure are present numerous hydroxyl groups, which have been exploited in the acrylation reaction to obtain the corresponding acrylic ester. The most reactive OH groups are the primary ones; in saikosaponin a are three primary -OH groups, four in songarosaponin D and

three in buddlejasaponin IV. Their esterification with acrylic acid furnished a derivatized saponins mixture, with numerous polymerizable moieties, that was used to prepare multifunctional microspheres, through radical polymerization. These particles were characterized and analyzed by means of common analyses methods. In particular, were effected studies to verify the microparticles swelling degree at the typical pHs of healthy and cancer cells.

3.1 Esterification of triterpene saponins with acrylic acid

The first step involves the esterification of the hydroxyl groups of saponins with acrylic acid through esterification of Steglich (29). This reaction allows obtaining an ester with practically unitary yields (Figure 2).

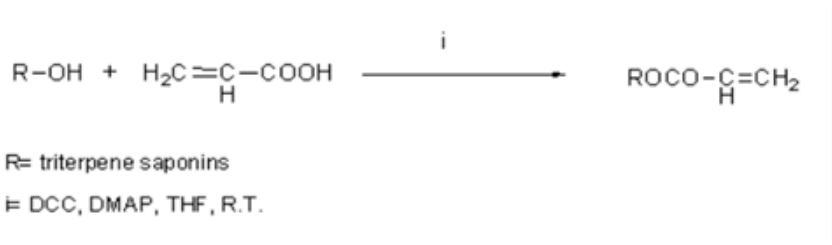

Figure 2: *Synthetic route of triterpene saponins derivatization with acrylic acid.*

Respect to Fischer esterification this procedure provides the advantage of not using a protic acid as catalyst and avoids the formation of water molecules, making easier the purification operations of the final product. The obtained product was dried, purified by column chromatography and characterized by FT-IR. FT-IR (KBr), ν (cm^{-1}): 3422, 2963, 2920, 1764, 1752, 980, 905.

3.2 Preparation of microspheres

The preparation of the microspheres was carried out using the technique of emulsion polymerization in reverse phase. This technique consists in the addition of a monomer solution (dispersed phase) in an excess of organic

solvent immiscible with water (dispersing phase). Under stirring small droplets of the dispersed phase are formed, that in order to reduce their interfacial free energy assume a spherical shape (15). The radical polymerization provides a mechanism for growing chain that begins with the generation of primary radicals after the splitting of a suitable initiator. These radicals are then reacted with acrylic functions present on the side chain of the product and determine the progressive crosslinking. The main advantage of the radical polymerization in inverse suspension is that in microparticles made with the above process the cross-linking takes place by means of covalent bonds between carbon atoms (34); this confers to the system more stability than systems in which the connection is with weak interactions and/or easily hydrolysable bonds. The size, defined as the average of particle diameter, which are generally obtained with this technique of polymerization, are included in the wide range of 1 mm-10 mM although 30-300 pM constitutes the most common range. The particle sizes are determined by many parameters such as the nature and the ratio of the substances used as well as reactor's characteristics, like the speed and type of agitation, the shape and size. Some generalizations were made and it is possible to affirm that the average diameter of the particles is directly proportional to the interfacial tension between the two liquid phases and the volume fraction of the disperse phase, while it is inversely proportional to the speed of agitation, the density of the monomers droplets and the size of the blades of agitation (35).

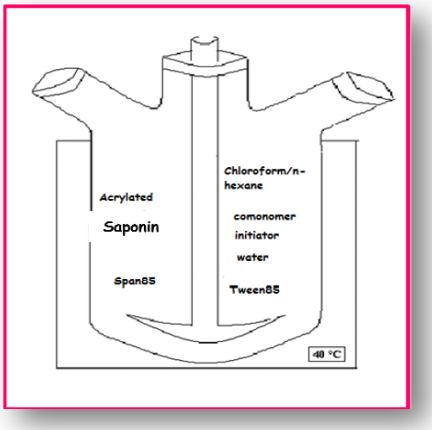

Figure 3: *Instrumentation for radical polymerization.*

3.3 Characterization of microspheres

The obtained microspheres were characterized by dimensional and morphological analyses and FT-IR spectrometry. The analysis by means of light scattering confirmed the presence of microparticles with a good polydispersity (0.190 with margin of error of ± 0.02) and an average diameter of about 2.7 µm ± 0.01. Moreover, the scanning electron microscopy (SEM) analysis of the dry microparticles highlighting and confirmed the spherical shape and the micrometric dimensions (Figure 4).

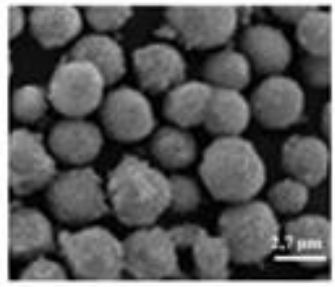

Figure 4: *Photomicrograph of microparticles triterpene saponins based*.

It was also carried out the FT-IR analysis which confirmed the presence of a new band at 1653 cm^{-1} attributable to the carbonyl group of the amide that originated the microparticellar matrix.

3.4 Studies of swelling

To assess the affinity of the microparticles to the aqueous media their swelling degree (α %), at two different pH (6.2 and 7.4) and at different time intervals (1h, 2h, 3h, 12h, 18h, 24h) was evaluated. In the Table 1 are shown the different values of α% to the two different pHs and time intervals. The results obtained indicate that the microspheres prepared may be used to release anticancer drug in a slow and specific way at pH 6.2, typical of the lung tumor. In fact, when the pH is 6.2, the water content is larger than that found in 7.4 at any time tested. This behaviour could be attributable to the electrostatic repulsions between the polymer chains due to higher groups

dissociated at pH 6.2. The groups responsible for this behaviour are those acids of the co-monomer *N, N*-dimethylacrylamide.

Table 1: *Swelling degree (α %) at two different pH (6.2 and 7.4) and at different time intervals (1h, 2h, 3h, 12h, 18h, 24h). The degree of swelling is expressed as the percentage of water in the microparticlesat any time during swelling. Data are the mean ± SD of three separate experiments. Differences within and between groups were evaluated by nonparametric ANOVA tests (Krushal-Walllis) completed with a multicomparison Dunn test. P>0.05.*

		Time (h)					
	pH	**1**	**2**	**3**	**12**	**18**	**24**
α %	6.2	120±4.2 ***	133±5.2 ***	145±5.8 ***	326±6.2 ***	360±6.8 ***	373±6.9 ***
	7.4	71±2.3	75±2.8	75±2.9	92±3.5	100±4.0	111±4.2

3.5 Impregnation of the microspheres with gemcitabine

The promising results obtained analysing the structural properties and evaluating the capability of swelling in aqueous medium at different pH values, have suggested a possible use of the polymeric matrix, based on a triterpene saponins mixture as systems for the delivery of active principles. Due to the chemical nature of the drug and the matrix a portion of the active substance interact with the core of the microspheres and another one with the surface. During the impregnation, the polymer synthesized increases in volume, but retains its three-dimensional structure without breaking up because it is insoluble in water. The percentage of active principle (LE%) and therefore the efficiency of loading of the microspheres was found to be 72.2%.

3.6 *In vitro* gemcitabine release studies from hydrogel

The release studies of gemcitabine from the microparticles were conducted miming the pulmonary pH in the pathological (6.2) and physiological (7.4) conditions, respectively, at different time intervals (1h, 2h, 3h, 12h, 18h, 24h) through the use of a water bath at 37 ° C and under stirring. Drug release profile was determined by spectrophotometric analyses and expressed as the

percentage of drug delivered, respect to the effectively entrapped total dose, as a function of time. Data showed that gemcitabine release at pH 6.2 is significantly higher than pH 7.4 at each time tested (Figure 5). The total amount of drug released in 24 h, at this pH in the dissolution medium, was about 72%. It is possible to observe an initial massive release after 1 h due mainly to the desorption of drug trapped on the surface. After 12 h the percent of released drug remains substantial showing that loaded microspheres could be useful to transport gemcitabine to the lung thus reducing its systemic toxicity.

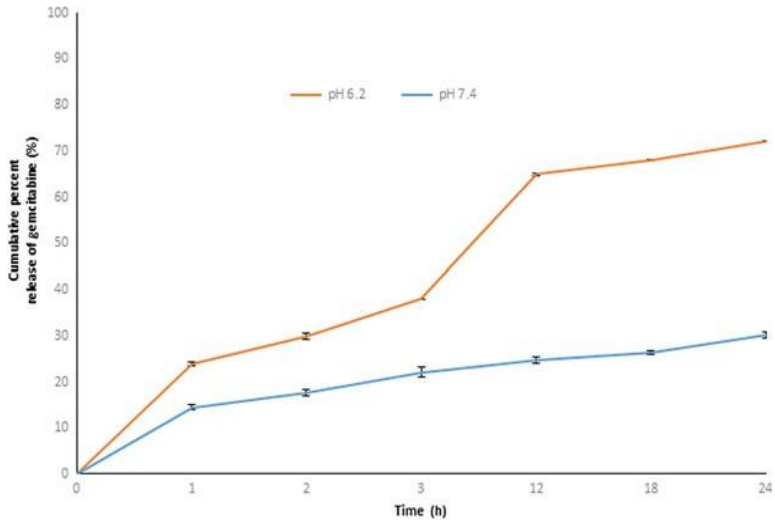

Figure 5: *Graph of gemcitabine release from saponins-based microspheres. Data are the mean ± SD of three separate experiments. Differences within and between groups were evaluated by nonparametric ANOVA tests (Krushal-Walllis) completed with a multicomparison Dunn test. P>0.05.*

4. Conclusions

The aim of the present work was the preparation and characterization of microspheres based on a mixture of three natural triterpene saponins

(saikosaponina a, songarosaponina D, buddlejasaponina IV) useful as a carrier for the specific release of gemcitabine to lung cells. The results obtained revealed that the microspheres swell most at pH 6.2 indicating that the obtained carrier could potentially release the drug in a specific manner reducing the systemic toxicity of both triterpene saponins and gemcitabine allowing to reduce the number of doses, to increase the half-life of the drug, thus eliminating the problems related to the rapid clearance of administration of gemcitabine. The results obtained revealed that the microspheres swell most at pH 6.2 indicating that the obtained carrier could potentially release the drug in a specific manner reducing the systemic toxicity of both triterpene saponins and gemcitabine allowing to reduce the number of doses, to increase the half-life of the drug, thus eliminating the problems related to the rapid clearance of administration of gemcitabine. *In vivo* studies, useful to verify these last aspects and also the safety of these systems, are in progress and they will object of a new work.

References

1. Trombino S, Cassano R, Mellace S, Picci N, Loizzo MR, Menichini F, et al. Novel microspheres based on triterpene saponins from the roots of Physospermum verticillatum (Waldst & Kit)(Apiaceae) for the improvement of gemcitabine release. Journal of Pharmacy and Pharmacology. 2016;68(2):275-81.

2. Roa WH, Azarmi S, Al-Hallak MK, Finlay WH, Magliocco AM, Löbenberg R. Inhalable nanoparticles, a non-invasive approach to treat lung cancer in a mouse model. Journal of controlled release. 2011;150(1):49-55.

3. Garbuzenko OB, Saad M, Pozharov VP, Reuhl KR, Mainelis G, Minko T. Inhibition of lung tumor growth by complex pulmonary delivery of drugs with oligonucleotides as suppressors of cellular resistance. Proceedings of the National Academy of Sciences. 2010;107(23):10737-42.

4. Goel A, Baboota S, Sahni JK, Ali J. Exploring targeted pulmonary delivery for treatment of lung cancer. International journal of pharmaceutical investigation. 2013;3(1):8.

5. Tseng C-L, Wu SY-H, Wang W-H, Peng C-L, Lin F-H, Lin C-C, et al. Targeting efficiency and biodistribution of biotinylated-EGF-conjugated gelatin nanoparticles administered via aerosol delivery in nude mice with lung cancer. Biomaterials. 2008;29(20):3014-22.

6. Liu J, Liu J, Chu L, Wang Y, Duan Y, Feng L, et al. Novel peptide–dendrimer conjugates as drug carriers for targeting nonsmall cell lung cancer. International journal of nanomedicine. 2011;6:59.

7. Brannon-Peppas L, Blanchette JO. Nanoparticle and targeted systems for cancer therapy. Advanced drug delivery reviews. 2012;64:206-12.

8. Reddy LH, Couvreur P. Novel approaches to deliver gemcitabine to cancers. Current pharmaceutical design. 2008;14(11):1124-37.

9. Anabousi S, Bakowsky U, Schneider M, Huwer H, Lehr C-M, Ehrhardt C. In vitro assessment of transferrin-conjugated liposomes as drug delivery systems for inhalation therapy of lung cancer. European journal of pharmaceutical sciences. 2006;29(5):367-74.

10. Burris 3rd H, Moore MJ, Andersen J, Green MR, Rothenberg ML, Modiano MR, et al. Improvements in survival and clinical benefit with gemcitabine as first-line therapy for patients with advanced pancreas cancer: a randomized trial. Journal of clinical oncology. 1997;15(6):2403-13.
11. Immordino ML, Brusa P, Rocco F, Arpicco S, Ceruti M, Cattel L. Preparation, characterization, cytotoxicity and pharmacokinetics of liposomes containing lipophilic gemcitabine prodrugs. Journal of Controlled Release. 2004;100(3):331-46.
12. Abbruzzese JL, Grunewald R, Weeks E, Gravel D, Adams T, Nowak B, et al. A phase I clinical, plasma, and cellular pharmacology study of gemcitabine. Journal of Clinical Oncology. 1991;9(3):491-8.
13. Starlinger P, Brugger P, Schauer D, Sommerfeldt S, Tamandl D, Kuehrer I, et al. Myelosuppression of thrombocytes and monocytes is associated with a lack of synergy between chemotherapy and anti-VEGF treatment. Neoplasia. 2011;13(5):419-27.
14. Walton DJ LJ. Polymers2001.
15. Iemma F, Spizzirri UG, Puoci F, Muzzalupo R, Trombino S, Cassano R, et al. pH-Sensitive hydrogels based on bovine serum albumin for oral drug delivery. International journal of pharmaceutics. 2006;312(1):151-7.
16. Kuroda M, Mimaki Y, Sashida Y, Kitahara M, Yamazaki M, Yui S. Securiosides A and B, novel acylated triterpene bisdesmosides with selective cytotoxic activity against M-CSF-stimulated macrophages. Bioorganic & medicinal chemistry letters. 2001;11(3):371-4.
17. Gaidi G, Miyamoto T, Laurens V, Lacaille-Dubois M-A. New Acylated Triterpene Saponins from Silene f ortunei that Modulate Lymphocyte Proliferation. Journal of natural products. 2002;65(11):1568-72.
18. Liu R, Ma S, Yu S, Pei Y, Zhang S, Chen X, et al. Cytotoxic oleanane triterpene saponins from Albizia chinensis. Journal of natural products. 2009;72(4):632-9.
19. Tundis R, Bonesi M, Deguin B, Loizzo MR, Menichini F, Conforti F, et al. Cytotoxic activity and inhibitory effect on nitric oxide production of triterpene saponins from the roots of Physospermum verticillatum (Waldst & Kit)(Apiaceae). Bioorganic & medicinal chemistry. 2009;17(13):4542-7.

20. Man S, Gao W, Zhang Y, Huang L, Liu C. Chemical study and medical application of saponins as anti-cancer agents. Fitoterapia. 2010;81(7):703-14.
21. Ali R, Mirza Z, ASHRAF GM, Kamal MA, Ansari SA, Damanhouri GA, et al. New anticancer agents: recent developments in tumor therapy. Anticancer research. 2012;32(7):2999-3005.
22. Lorent JH, Quetin-Leclercq J, Mingeot-Leclercq M-P. The amphiphilic nature of saponins and their effects on artificial and biological membranes and potential consequences for red blood and cancer cells. Organic & biomolecular chemistry. 2014;12(44):8803-22.
23. Hu K, Berenjian S, Larsson R, Gullbo J, Nygren P, Lövgren T, et al. Nanoparticulate Quillaja saponin induces apoptosis in human leukemia cell lines with a high therapeutic index. International journal of nanomedicine. 2010;5:51.
24. Navarro P, Giner RM, Recio MC, Máñez S, Cerdá-Nicolás M, Ríos J-L. In vivo anti-inflammatory activity of saponins from Bupleurum rotundifolium. Life Sciences. 2001;68(10):1199-206.
25. Ebata N, Nakajima K, Hayashi K, Okada M, Maruno M. Saponins from the root of Bupleurum falcatum. Phytochemistry. 1996;41(3):895-901.
26. Calabria LM, Piacente S, Kapusta I, Dharmawardhane SF, Segarra FM, Pessiki PJ, et al. Triterpene saponins from Silphium radula. Phytochemistry. 2008;69(4):961-72.
27. Du J-R, Long F-Y, Chen C. Research Progress on Natural Triterpenoid Saponins in the Chemoprevention and Chemotherapy of Cancer. The Enzymes. 2014;36:95-130.
28. Gaidi G, Correia M, Chauffert B, Beltramo J-L, Wagner H, Lacaille-Dubois M-A. Saponins-mediated potentiation of cisplatin accumulation and cytotoxicity in human colon cancer cells. Planta medica. 2002;68(01):70-2.
29. Hrdina R, Müller CE, Schreiner PR. Kinetic resolution of trans-cycloalkane-1, 2-diols via Steglich esterification. Chemical Communications. 2010;46(15):2689-90.
30. Cassano R, Trombino S, Ferrarelli T, Bilia AR, Bergonzi MC, Russo A, et al. Preparation, characterization and in vitro activities evaluation of curcumin based microspheres for azathioprine oral delivery. Reactive and Functional Polymers. 2012;72(7):446-50.

31. Koppel DE. Analysis of macromolecular polydispersity in intensity correlation spectroscopy: the method of cumulants. The Journal of Chemical Physics. 1972;57(11):4814-20.
32. Trombino S, Ferrarelli T, Pellegrino M, Ricchio E, Mauro L, Ando S, et al. Anticancer activity of a hydrogel containing folic acid towards MCF-7 and MDA-MB-231 cells. Anticancer research. 2013;33(11):4847-54.
33. Podolak I, Galanty A, Sobolewska D. Saponins as cytotoxic agents: a review. Phytochemistry Reviews. 2010;9(3):425-74.
34. Omidian H, Zohuriaan-Mehr M, Bouhendi H. Polymerization of sodium acrylate in inverse-suspension stabilized by sorbitan fatty esters. European Polymer Journal. 2003;39(5):1013-8.
35. Scully D. Scale-up in suspension polymerization. Journal of Applied Polymer Science. 1976;20(8):2299-303.

PART C

"Liquid crystalline microspheres for 5-fluorouracil specific release"(1)

Abstract

The aim of this study was the synthesis and characterization of swellable microspheres based on fenoprofen and poloxamer. Morphology, average diameter and thermal behaviour of obtained microparticles were studied by scanning electron microscopy, dynamic light scattering, and differential scanning calorimetry. The swelling degree was evaluated at different time intervals and at two pH values. The results revealed that the microspheres swelled better at a pH 6.2, typical of tumour pathologies, than at 7.4, physiological one. Then, microspheres were impregnated with 5-fluorouracil with the aim to increase its bioavailability and reduce its toxicity. The percentage of cumulative amount of 5-fluorouracil released from microparticles was calculated at pH 6.2. Surprisingly, calorimetry and optical microscopy showed the preservation of fenoprofen liquid crystallinity in the obtained microparticles with a transition temperature close to those of typical tumour-sites. The liquid crystallinity of microparticles could be exploited to modulate the release of 5-fluorouracil to tumor site.

Keywords: *Fenoprofen, poloxamer, 5-fluoruracil, microspheres, liquid crystals, thermosensitive hydrogels*.

1. Introduction

Cancer is one of the most overwhelming diseases of modern society, with an annual frequency of more than 10 million cases (2). The usual anticancer treatments, e.g. irradiation and chemotherapy, generally cause significant side effects mainly due to toxicity towards normal cells and tissues (3). In this regard, there has been a flurry of activity towards the development of novel site-specific and stimuli responsive drug delivery systems (DDS) for cancer therapy, in order to maximize the anticancer drug efficacy and avoid their cytotoxic limitations (4, 5). These DDS can deliver chemo-drugs selectively to the tumour area, thanks to various chemical and physical stimuli (6-8). Hydrogels are crosslinked polymer systems able to retain large amounts of water by swelling. The presence of crosslinking in the polymer matrix makes them insoluble in water. Hydrogel microparticles are micrometre-sized particles that have found many applications in daily life as catalysts, sensors, lubricants, actuators, waste adsorbers, advanced materials, regenerative tissues, imaging tools, fillers, cosmetics, pharmaceuticals, and as DDS (9). Stimulus-responsive gels offer the opportunity to develop smart drug delivery systems thanks to their ability to swell/shrink in response to external stimuli, such as pH, temperature, ionic strength, external electric/magnetic fields, solvent quality, and enzymes (10-12). The swelling or shrinking of a microgel is caused by the globule-to-coil or vice versa transition of polymer chains between two neighbouring crosslinking points inside the gel network. For example, the pH-sensitive hydrogels are widely used for administering active drugs irritating to the gastric mucosa by using formulations in a shrunk state at low pH and in a swollen state at high pH values. Recently, liquid crystalline materials have attracted significant attention for their potential use as DDS with improved properties such as physicochemical stability, drug loading, sustained release patterns, and a reduction in drug leakage (13); in addition to their well-known technological applications (14, 15). 5-fluorouracil (5-FU) is an anticancer agent, analogue of pyrimidine bases, belonging to the family of anti-metabolites. It is widely used alone or in combination with other drugs in the treatment of various malignancies, including cancers of the gastrointestinal tract, breast, ovary, head and neck area (16). However, 5-FU is characterized by poor bioavailability and high toxicity (17). Several

modalities of drug administration have been investigated to improve 5-FU bioavailability and to reduce the related toxicity (18, 19). Although some progress has been achieved, these approaches have issues of poor drug loading, drug leakage, burst release patterns, and poor physicochemical stability that are unaddressed. Fenoprofen is an analgesic, anti-inflammatory and antipyretic nonsteroidal drug that exhibits liquid crystalline properties. Literature data suggest that both fenoprofen sodium and calcium salts can form stable thermotropic mesophases in dehydrated conditions (20-22). In this mesomorphic state, the director of fenoprofen molecules can align along the direction of an applied external field due to their particular electrical nature (23). Poloxamers are non-ionic copolymers (triblock) composed of a central hydrophobic chain of polyoxypropylene flanked by two chains of hydrophilic polyoxymethylene (24). Poloxamers are commonly used polymers in many pharmaceutical applications for their thermogelling properties. In fact, they can be used to increase the water solubility of hydrophobic substances or the miscibility of substances with different hydrophobicity. In addition, they have been evaluated as drug delivery systems and found able to enhance the action of chemotherapeutic drugs. They preferentially target cancer cells, due to differences present in their membranes, and are able to inhibit multi-drug resistant (MDR) proteins, which are responsible for the drug efflux from the cells. Therefore, it is possible to increase the susceptibility of cancer cells to chemotherapeutic agents (25-27). Furthermore, literature data report that poloxamers can be utilized for controlled drug delivery applications. A designed composition in polymers and poloxamers could lead to the development of DDS with enhanced properties. This paper deals with the synthesis and characterization of swellable microspheres based on fenoprofen and poloxamer for the controlled and targeted release of 5-FU (Figure 1).

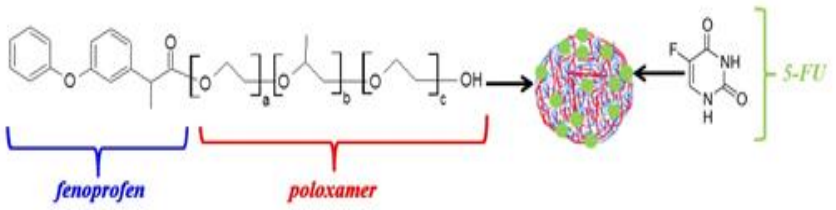

Figure 1: *Representation of microspheres based on fenoprofen and poloxamer*

The obtained microparticles were characterized by scanning electron microscopy, dynamic light scattering, and differential scanning calorimetry. Their swelling degree was evaluated at two different pHs, simulating the environment typical of tumour sites and the physiological conditions, respectively. Then, they were loaded with 5-FU and drug release studies were performed at pH 6.2.

Surprisingly, differential scanning calorimetry and polarizing optical microscopy showed the preservation of fenoprofen liquid crystallinity in the obtained microparticles with a transition temperature close to those of typical tumour-sites. The liquid crystallinity of synthesized microparticles could be exploited to modulate the release of 5-fluorouracil by the application of an external stimulus such as a magnetic field and/or temperature.

2. Materials and methods

2.1 Materials

The solvents such as acetone, chloroform, dichloromethane, ethanol, methanol, isopropanol, *n*-hexane, acetonitrile, tetrahydrofuran (THF) and sulfuric acid (H_2SO_4) were obtained from Carlo Erba Reagents (Milan, Italy). The *n*-hexane and chloroform were distilled before their use. Furthermore, the calcium salt of fenoprofen (MW = 522.60 g / mol),

Synperonic P105® (MW = 6500 g / mol), acryloyl chloride, triethylamine, sorbitan trioleate (Span 85), polyoxyethylene sorbitan (Tween 85), N,N,N',N'-tetramethylethylenediamine (TMEDA), N,N'-methylene-bisacrylamide (MBA), ammonium persulfate (APS), dicyclohexylcarbodimide (DCC), dimethylaminopyridine (DMAP), sodium hydroxide, and 5-fluorouracil were purchased from Sigma-Aldrich (Sigma Chemical Co., St. Louis, MO, USA).

2.2 Measurements

FT-IR spectra were measured by a Jasco 4200 IR spectrophotometer using KBr disks in the range of 4000-400 cm^{-1} (number of scan 16). ^{1}H-MNR spectra were recorded on a Bruker VM-300 ACP NMR spectrometer; the chemical shifts were expressed as δ-values (ppm) and referred to the solvent. The UV-Vis spectra were carried out using a JASCO UV-530 spectrophotometer. The samples were lyophilized by using a freezing-drying equipment (Micro modulyo, Edwards). Scanning electron microscopy (SEM) analysis of microspheres was performed with a JEOL JSMT 300 A microscope; the surface of the samples was made conductive by deposition of a thin gold layer in a vacuum chamber. The liquid crystalline properties of compounds were investigated by a polarizing optical microscope, POM (Laborlux 12 POL, Leitz, equipped with a heating stage, PR 600, Linkam) and differential scanning calorimetry. The transition temperatures were evaluated with a differential scanning calorimeter (DSC-200, Netzsch and DSC-141, Setaram) operating under nitrogen atmosphere at a heating rate of 10 °C min^{-1}. The mass of samples (around 4.0 mg) was placed in aluminium crucibles with pierced lids. Liquid crystalline phases were identified through the comparison of the texture changes around the transition temperatures with reference textures (28).

2.3 Fenoprofen preparation

The acid form of fenoprofen was obtained from the corresponding salt. Briefly, 1 g of fenoprofen calcium salt was solubilized in 400 ml of distilled water and heated to 100 °C under magnetic stirring (200 rpm) for 1 h. Then, H_2SO_4 was added to promote the precipitation of fenoprofen acid, which was recovered by filtration, through porous glass filters with porosity grade

4, dried with a mechanical vacuum pump and then characterized by FT-IR and ^{1}H-NMR.

2.4 Esterification of poloxamer with fenoprofen

In a three-neck flask fitted with a reflux condenser, a dripping funnel and a magnetic stirrer, thoroughly flamed and maintained under nitrogen bubbling, 0.100 g of fenoprofen acid (0.412 mmol) were dissolved in 50 ml of dry chloroform. Then, DCC ($8.5\cdot10^{-2}$ g, 0.412 mmol) and DMAP ($2.5\cdot10^{-3}$ g, $2.06.10^{-2}$ mmol) were added and, after 15 minutes, poloxamer (1.34 g, 0.206 mmol) was dispersed in the reaction mixture. It was kept cold, in a cold-water bath, stirred for 12 hours and continuously monitored by thin layer chromatography (TLC) (silica gel, eluent mixture chloroform/n-hexane 3/7). Finally, the solvent was removed at reduced pressure. The raw product was washed with methanol to remove the dicyclohexylurea (generated as a reaction by-product), dried with a mechanical vacuum pump and, then, purified by column chromatography (silica gel, eluent mixture chloroform/*n*-hexane 3/7) to yield **1**. The final compound was characterized by FT-IR and ^{1}H-NMR.

2.5 Derivatization of the hydroxyl group of 1 with acryloyl chloride

In a three-necked flask fitted with a reflux condenser, a dripping funnel and a magnetic stirrer, accurately flamed and maintained under nitrogen bubbling, $7{,}8\cdot10^{-2}$ g of **1** (0.01 mmol) were dissolved in dry chloroform (50 ml) and added of dry triethylamine (2.3 µl, 0.0173 mmol) and, after 30 minutes, acryloyl chloride (1.4 µl, $1.73\cdot10^{-2}$ mmol). The reaction was conducted at room temperature under mild stirring for 72 hours and constantly monitored by TLC (silica gel, eluent mixture chloroform/n-hexane 3/7). The acrylate **2** was purified by column chromatography (silica gel, eluent mixture chloroform/*n*-hexane 3/7), dried and characterized by FT-IR and ^{1}H-NMR.

2.6 Microspheres preparation

Microspheres based on **2** were obtained by radical copolymerization. Briefly, a cylindrical glass reactor (150 ml), equipped with a mechanical stirrer and dripping funnel, a screw cap with puncture-proof rubber septum,

was flamed under nitrogen flow, and after cooling was immersed in a thermostatically controlled bath at 40 °C. Then, 20 ml of *n*-hexane and 18 ml of chloroform were poured into the reactor as dispersing phase. After 30 min of N_2 bubbling, this mixture was treated with distilled water (4 ml) containing **2** (0.24 g, 0.0354 mmol), N, N'-methylenbisacrylamide (MBA) (co-monomer) (3.10^{-3} g, $1.77 \cdot 10^{-2}$ mmol) and ammonium persulfate ($(NH_4)_2S_2O_8$) (0.8 g, 3.5 mmol), which acts as a radical initiator. Whilst stirring at 1000 rpm and at regular intervals (10 min), the mixture was treated with 150 µl of sorbitan trioleate (Span 85), 150 µl of polyoxyethylene sorbitan trioleate (Tween 85) and, finally, 150 µl of tetramethylenediamine (TMEDA) (29). The obtained microspheres were filtered, washed with 100 ml portions of isopropanol, ethanol and acetone to eliminate the Span 85 and Tween 85 surfactants and unreacted reagents, and dried overnight under vacuum at 40 °C. Their characterization was performed by POM, dynamic light scattering (DLS, Brookhaven Instruments, 90 PLUS), DSC and FT-IR.

2.7 Swelling studies

The swelling behaviour was investigated in order to check the hydrophilic affinity of microparticles. 25 mg of dried material were placed in two different glass filters (porosity G3, previously wet, centrifuged for 5 minutes at 2000 g / min, and weighed) immersed in two beakers containing the swelling media (phosphate buffer pH 6.2, simulating the conditions typical of tumour pathology and phosphate buffer pH 7.4, miming physiological environment) at the temperature of 37 °C. At predetermined time intervals (1h, 3h, 6h, 24h, and 32h), the excess of water was removed from both filters by percolation at atmospheric pressure. Subsequently, the filters were centrifuged at 3500 rpm for 15 minutes and weighed to give the equilibrium swelling degree, α (%), by equation 1.

The equilibrium swelling degree, α (%), is a measure of how much water is retained by hydrogels and can be expressed as:

$$\alpha(\%) = \frac{W_s - W_d}{W_d} 100 \qquad (1)$$

where W_s and W_d were the weights of swollen and dried microspheres, respectively (30).

2.8 Microspheres loading with 5-FU

50 mg of microspheres were placed in a drug solution with a known concentration of 5-fluorouracil (5 mg in 20 ml of distilled water). After 3 days under slow stirring at 37 °C, the microspheres were filtered and dried to constant weight at reduced pressure in presence of P_2O_5. The loading efficiency percentage (LE%) of all samples was determined by spectrophotometric analysis of filtered solvent, according to the following equation 2 (31):

$$LE\% = \frac{Mi - M0}{Mi} \times 100 \quad (2)$$

where M_0 was the concentration of drug in the solution before loading, M_i was the drug concentration in the solution after loading.

2.9 Release studies

10 mg of dried microspheres were dispersed in 1.5 ml of swelling media (phosphate buffer pH 6.2, simulating pathological conditions). The test tubes were shaken in a horizontal-shaking bath at 37 °C and a rate of 100 rpm. At fixed time intervals, the samples were centrifuged at 3500 rpm for 15 min and 1.5 ml of supernatant was replaced with 1.5 ml of fresh solution. The 5-fluoruracil concentration was determined by UV spectrophotometry at 265 nm. The experiment was repeated in triplicate. The release was evaluated as cumulative drug release percentage over a time interval of 32 h (32).

2.10 Statistical analysis

Each datum point represents the mean ± SD of three different experiments. Data were analysed by Student's t-test using the Graph Pad Prism 4 software program. $P < 0.05$ was considered as statistically significant.

3. Results and Discussion

3.1 Synthesis of acrylate 2

Fenoprofen was purchased in its calcium salt form. In order to obtain the corresponding acid, it was solubilized in hot, slightly alkaline, distilled water. After the complete solubilisation of fenoprofen, sulfuric acid was added to favour the acid precipitation. The desired product was then recovered by filtration, dried at reduced pressure and subsequently characterized by FT-IR and ^{1}H-NMR. FT-IR (KBr) ν (cm^{-1}): 3258 (OH), 3065 (CH), 3030 (CH), 2930 (CH), 2848 (CH), 1705 (C=O). ^{1}H-NMR ($CDCl_3$) δ (ppm): 10.5, 7.376, 7.376, 7.322, 7.287, 7.142, 6.999, 6.999, 6.922, 6.575, 3.889, 1.325. The purified fenoprofen acid was successfully esterified through its carboxyl group with the poloxamer Synperonic P105® to give **1** (82% yield, Scheme 1) that was purified by column chromatography and characterized by FT-IR and ^{1}H-NMR. FT-IR (KBr) ν (cm^{-1}): 3447 (OH), 3070 (CH), 3035 (CH), 2977 (CH), 2930 (CH), 2879(CH), 1750 (C=O).^{1}H-NMR (CD_3CN) δ (ppm): 7.376, 7.376, 7.311, 7.288, 7.142, 6.999, 6.999, 6.923, 6.575, 4.474- 3.539, 1.324-1.129. The product **1** was finally reacted with acryloyl chloride to obtain the polymerizable derivative **2** (Figure 2), that was purified by chromatography and then characterized by FT-IR spectrometry and ^{1}H-NMR. FT-IR (KBr) ν (cm^{-1}): 3447 (OH), 3070 (CH), 3035 (CH), 2966 (CH), 2920 (CH), 2854 (CH), 1758 (C=O), 1734 (C=O), 980, 905 (C=C). ^{1}H-NMR (CD_3CN) δ (ppm): 7.374, 7.374, 7.311, 7.288, 7.142, 7.0, 6.923, 6.861, 6.575, 6.328, 6.020, 4.474-3.297, 1.924-1.115. **2** was used to prepare multi-sensitive microspheres as reported in literature (33).

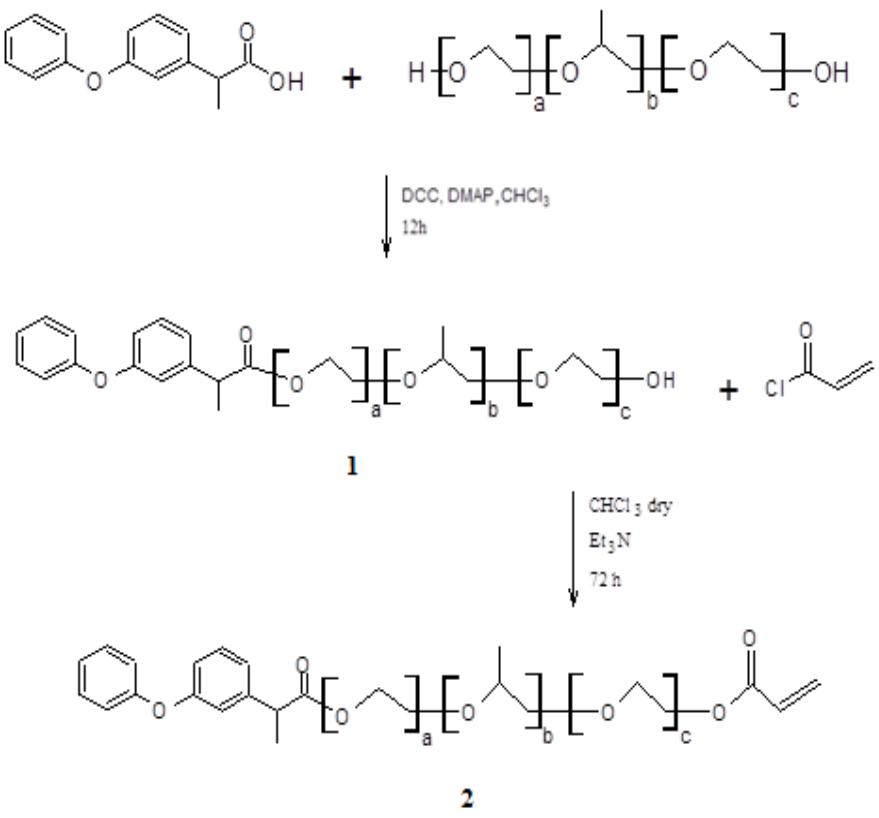

Figure 2 and Scheme 1: *Synthetic route to compound **2**.*

3.2 Microspheres characterization

The obtained microparticles were characterized by FT-IR, DLS, POM, SEM and DSC.

FT-IR spectra showed the appearance of a new band awardable to C=O stretching of co-monomer amidic group (1650 cm^{-1}) and the disappearance of the characteristic bands of the acrylic group double bond (C=C) at 980 cm^{-1} and 905 cm^{-1}. DLS analysis confirmed the presence of micron-sized particles with a rather good polydispersity (0.30 ± 0.04) and an average diameter of 3.00±0.02μm.

At the optical microscope (T=25 °C), dry particles appeared grouped into large clusters of microparticles (Figure 3). After water immersion, the dimensions of clusters decreased while individual microspheres swelled.
The morphological characterization by SEM confirmed that the samples were formed by micron-sized particles, generally grouped in large clusters (Figure 3). The shape aspect is rather irregular and could be due to the particular sample preparation method for SEM analysis, softness and adhesion properties of synthesized microparticles.

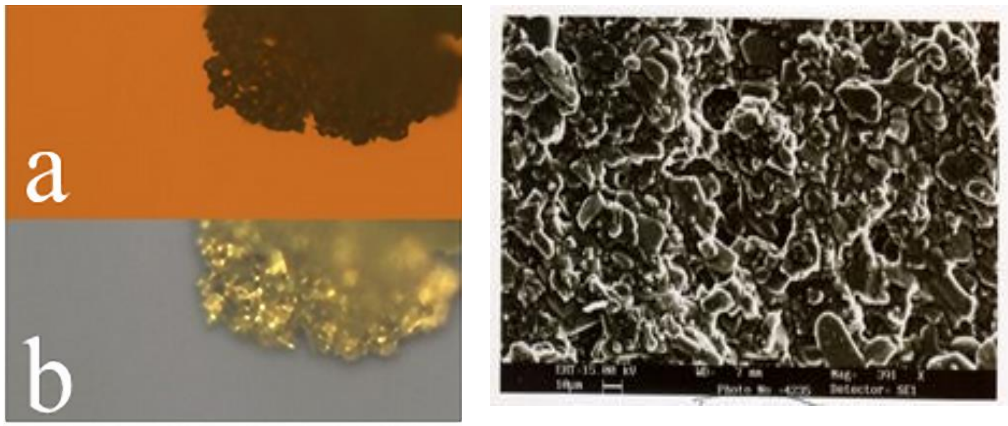

Figure 3: *POM pictures of microspheres at 25 °C between: a) parallel polarizers, b) crossed polarizers (left image); SEM picture of microspheres (magnification of 391 x) (right image).*

DSC analysis was carried out in the range 25 °C - 180 °C (under a nitrogen flow rate of 25 ml min^{-1} and a heating rate of 10 °C min^{-1}) in order to evaluate the transition temperatures (Figure 4). Microparticle thermograms are characterized by two broad peaks at around 43 °C (endothermic) and 147 °C (exothermic). POM observations confirmed that the endothermic peak originated from a crystal-nematic phase transition, while the exothermic peak was very likely a thermal decomposition of short oligomers (polymerization fragments that remained entrapped in the microsphere

networks) rather than the thermal decomposition of microspheres. These oligomers are able to reduce the thermal stability of microspheres hiding the presence of the nematic-isotropic transition of microspheres.
Interestingly, the thermogram of precursor fenoprofen acid showed three transition temperatures (at around 123 °C, 223 °C and 261 °C; Figure 4) that were attributed to the crystal-smectic, smectic-nematic, and nematic-isotropic phase transition by POM observation of mesophase textures.

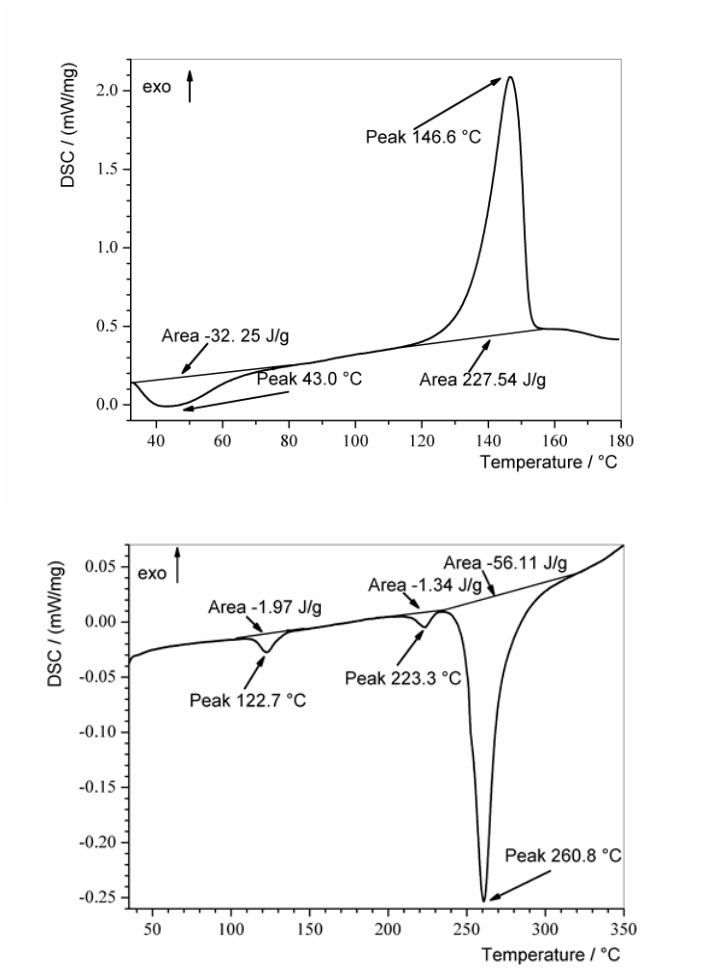

Figure 4: *Thermogram of microspheres based on fenoprofen and poloxamer. Scanning rate was 10 °C min^{-1} (top image). Thermogram of fenoprofen acid. Scanning rate was 10 °C min^{-1} (bottom image).*

3.3 Swelling studies

Microspheres swelling studies (34) were conducted at two different pHs (6.2 and 7.4) and at different time intervals (1h, 3h, 6h, 24h, and 32h) Table 1.

Table 1: *Swelling degree, α%, at two different pH (6.2 and 7.4) and at different time intervals (1h, 3h, 6h, 24h, and 32h). Data are the mean ± SD of three separate experiments.*

	pH	**Time (h)**				
		1	***3***	***6***	***24***	***32***
α%	***6.2***	0	31	338	485	487
	7.4	0	30	31	31	54

The obtained results indicated that microspheres are able to release 5-FU in a slow and specific way at pH 6.2, which is a pH value typical of tumour sites. In fact, the swelling degree at pH 6.2 was greater than that found at pH 7.4. It is possible to explain this behaviour because of electrostatic repulsion between polymeric chains due to the increase of dissociated groups at pH 6.2. This repulsive force would push the network chain segments apart and thus attract more water into the hydrogels, with a consequent higher swelling ratio.

3.4 Microspheres loading with 5-FU

In order to estimate the microparticles ability to encapsulate drugs, their loading efficiency was determined by spectrophotometric analysis after a soaking procedure with 5-FU. Data showed that 5-FU was efficiently loaded in the matrices (LE% = 90.6) because of the strong interactions between the polymeric matrix and the anticancer drug.

3.5 Release studies

The release studies were conducted only at pH 6.2 and at different time intervals (1h, 3h, 6h, 24h, and 32h). The choice to evaluate the drug release only at this pH value was justified by the lower swelling values of microparticles at pH 7.4 (see Table 1). 5-FU release profile was determined by spectrophotometric analysis and expressed as the percent of drug delivered over the effectively entrapped dose, as a function of time. Figure 5 show the 5-FU cumulative release at pH 6.2.

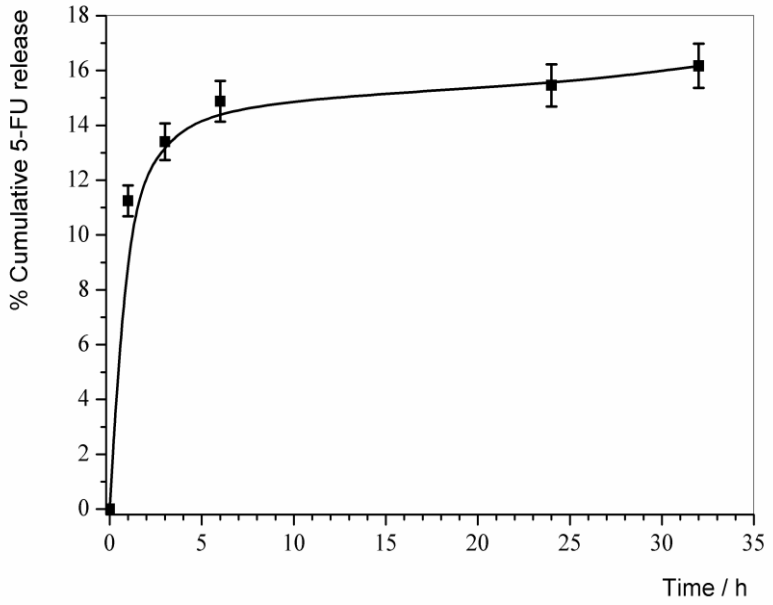

Figure 5 *5-FU release from microspheres based on fenoprofen and poloxamer. Data are the mean ± SD of three different experiments. Solid line is just a guide to the eye.*

From Figure 5, it is possible to distinguish two different stages in the release rate of 5-FU from microspheres due to the particular drug placement. In fact, 5-FU molecules adsorbed at the outer surfaces of microspheres were quickly released. This burst effect must not be considered a negative circumstance, as a fast release rate of anticancer drugs can show positive effects in tumour treatment (35). The release of drug molecules (up to 18%) loaded into the

volume of microspheres followed the burst effect. This release process was mainly governed by a diffusion mechanism, also promoted by the small dimensions of microparticles, which allowed drug molecules to easily spread out from hydrogel network.

It is very difficult to compare the properties of microparticles based on fenoprofen and poloxamer with those of other DDS, being the used components quite different. If this comparison is limited to systems loaded with 5-FU, there are in literature several papers dealing with the synthesis and characterization of microparticles able to release percentages of 5-FU (e.g. (36)) higher than that found with microparticles based on fenoprofen and poloxamer (around 18%). The 5-FU release and swelling behaviour of these particles were evaluated at 37 °C. We can hypothesize that the 5-FU release from these microparticles decreased due to the higher viscosity and lower swelling degree that microspheres containing the poloxamer Synperonic P105® showed at 37°C, the temperature at which the swelling and release studies were carried out (37). In the next future, these swelling and release properties will be compared with the behaviour of hydrogels based on acrylated fenoprofen without poloxamer.

However, it is important to highlight that microspheres based on fenoprofen and poloxamer are expected to be multi-sensitive liquid crystalline DDS, which represents a real benefit. In fact, the presence of a liquid crystal phase in microparticle thermograms could allow a multisensitive drug release driven by either temperature or a magnetic field. The alignment of liquid crystal director, either perpendicular or parallel to the applied magnetic field, could favour a further targeted release of drugs to specific sites. In addition, being the transition temperature (around 43 °C) close to the temperature of tumoral areas, the microparticles based on fenoprofen and poloxamer could allow a specific thermally driven drug release.

4. Conclusions

Microspheres, based on fenoprofen and poloxamer, were successfully obtained and characterized as carrier of 5-FU. Microparticles had an average diameter of 3 μm and showed a swelling degree larger in pathological conditions (pH 6.2) than in physiological condition (pH 7.4). Then they were

efficiently loaded with 5-FU and tested for a site-specific release to cancer cells. Thanks to the properties of the two precursors, it is expected that microspheres could show a beneficial effect against tumour tissues. In fact, poloxamers are able to inhibit the production of ATP in multi-resistant tumour cells and increases the sensitivity of these cells to drug treatment. Moreover, fenoprofen can attenuate the inflammatory process typical of the tumour sites. Furthermore, the presence of a liquid crystal phase in microparticles could allow a multisensitive drug release driven by either temperature and/or a magnetic field. The magnetically and thermally driven 5-FU release from microspheres will be examined in a future work.

References

1. Cassano R, Nicoletta FP, Mellace S, Grande F, Picci N, Trombino S. Liquid crystalline microspheres for 5-fluorouracil specific release. Journal of Drug Delivery Science and Technology. 2017;41:482-7.
2. Peer D, Karp JM, Hong S, Farokhzad OC, Margalit R, Langer R. Nanocarriers as an emerging platform for cancer therapy. Nature nanotechnology. 2007;2(12):751-60.
3. Vasir JK, Tambwekar K, Garg S. Bioadhesive microspheres as a controlled drug delivery system. International journal of pharmaceutics. 2003;255(1):13-32.
4. Sinha V, Kumria R. Polysaccharides in colon-specific drug delivery. International journal of pharmaceutics. 2001;224(1):19-38.
5. Mathiowitz E. Encyclopedia of controlled drug delivery: Wiley; 1999.
6. Qiu Y, Park K. Environment-sensitive hydrogels for drug delivery. Advanced drug delivery reviews. 2001;53(3):321-39.
7. Mauro N, Campora S, Scialabba C, Adamo G, Licciardi M, Ghersi G, et al. Self-organized environment-sensitive inulin–doxorubicin conjugate with a selective cytotoxic effect towards cancer cells. RSC Advances. 2015;5(41):32421-30.
8. Mauro N, Campora S, Adamo G, Scialabba C, Ghersi G, Giammona G. Polyaminoacid–doxorubicin prodrug micelles as highly selective therapeutics for targeted cancer therapy. RSC Advances. 2016;6(81):77256-66.
9. Peppas NA, Hilt JZ, Khademhosseini A, Langer R. Hydrogels in biology and medicine: from molecular principles to bionanotechnology. Advanced materials. 2006;18(11):1345-60.
10. Liechty WB, Kryscio DR, Slaughter BV, Peppas NA. Polymers for drug delivery systems. Annual review of chemical and biomolecular engineering. 2010;1:149-73.
11. Nicoletta FP, Cupelli D, Formoso P, De Filpo G, Colella V, Gugliuzza A. Light responsive polymer membranes: a review. Membranes. 2012;2(1):134-97.
12. Cassano R, Trombino S. Drug delivery systems: Smart polymeric materials. Advanced Polymers in Medicine: Springer; 2015. p. 341-70.

13. Müller-Goymann C. Physicochemical characterization of colloidal drug delivery systems such as reverse micelles, vesicles, liquid crystals and nanoparticles for topical administration. European Journal of Pharmaceutics and Biopharmaceutics. 2004;58(2):343-56.
14. Cassano R, Dąbrowski R, Dziaduszek J, Picci N, Chidichimo G, De Filpo G, et al. The synthesis of new liquid–crystalline mesogens containing bicyclohexane units. Tetrahedron letters. 2007;48(8):1447-50.
15. Cupelli D, Nicoletta FP, De Filpo G, Formoso P, Chidichimo G. Reverse mode operation polymer dispersed liquid crystal with a positive dielectric anisotropy liquid crystal. Journal of Polymer Science Part B: Polymer Physics. 2011;49(4):257-62.
16. Longley DB, Johnston PG. 5-Fluorouracil. Apoptosis, cell signaling, and human diseases: Springer; 2007. p. 263-78.
17. Ezzeldin HH, Diasio RB. Predicting fluorouracil toxicity: can we finally do it? : American Society of Clinical Oncology; 2008.
18. Pitarresi G, Pierro P, Giammona G, Muzzalupo R, Trombino S, Picci N. Beads of acryloylated polyaminoacidic matrices containing 5-fluorouracil for drug delivery. Drug delivery. 2002;9(2):97-104.
19. Muzzalupo R, Tavano L, Cassano R, Trombino S, Cilea A, Picci N. Colon-specific devices based on methacrylic functionalized Tween monomer networks: Swelling studies and in vitro drug release. European Polymer Journal. 2010;46(2):209-16.
20. Rades T, MÜLLER-GOYMAN C. Melting behaviour and thermotropic mesomorphism of fenoprofen salts. European journal of pharmaceutics and biopharmaceutics. 1994;40(5):277-82.
21. Rades T, Padmadisastra Y, Mueller-Goymann C. Thermal behaviour and solubility of fenoprofen calcium. Pharmazie. 1996;51(11):846-51.
22. Omray L. Liquid crystals as novel vesicular delivery system: a review. Curr Trends Technol Sci. 2013;2(5):347-53.
23. De Filpo G, Siprova S, Chidichimo G, Mashin AI, Nicoletta FP, Cupelli D. Alignment of single-walled carbon nanotubes in polymer dispersed liquid crystals. Liquid Crystals. 2012;39(3):359-64.
24. Ludwig A. The use of mucoadhesive polymers in ocular drug delivery. Advanced drug delivery reviews. 2005;57(11):1595-639.

25. Batrakova EV, Kabanov AV. Pluronic block copolymers: evolution of drug delivery concept from inert nanocarriers to biological response modifiers. Journal of Controlled Release. 2008;130(2):98-106.
26. Albertini B, Passerini N, Di Sabatino M, Monti D, Burgalassi S, Chetoni P, et al. Poloxamer 407 microspheres for orotransmucosal drug delivery. Part I: Formulation, manufacturing and characterization. International journal of pharmaceutics. 2010;399(1):71-9.
27. Devi DR, Sandhya P, Hari BV. Poloxamer: a novel functional molecule for drug delivery and gene therapy. J Pharm Sci Res. 2013;5(8):159-65.
28. Dierking I. Textures of liquid crystals: John Wiley & Sons; 2003.
29. Freiberg S, Zhu X. Polymer microspheres for controlled drug release. International journal of pharmaceutics. 2004;282(1):1-18.
30. Trombino S, Cassano R, Cilea A, Ferrarelli T, Muzzalupo R, Picci N. Synthesis of pro-prodrugs l-lysine based for 5-aminosalicylic acid and 6-mercaptopurine colon specific release. International journal of pharmaceutics. 2011;420(2):290-6.
31. Iemma F, Spizzirri UG, Puoci F, Muzzalupo R, Trombino S, Cassano R, et al. pH-Sensitive hydrogels based on bovine serum albumin for oral drug delivery. International journal of pharmaceutics. 2006;312(1):151-7.
32. van Dijk-Wolthuis W, Franssen O, Talsma H, Van Steenbergen M, Kettenes-Van Den Bosch J, Hennink W. Synthesis, characterization, and polymerization of glycidyl methacrylate derivatized dextran. Macromolecules. 1995;28(18):6317-22.
33. Cassano R, Trombino S, Ferrarelli T, Mauro MV, Giraldi C, Manconi M, et al. Respirable rifampicin-based microspheres containing isoniazid for tuberculosis treatment. Journal of Biomedical Materials Research Part A. 2012;100(2):536-42.
34. Cassano R, Trombino S, Muzzalupo R, Tavano L, Picci N. A novel dextran hydrogel linking trans-ferulic acid for the stabilization and transdermal delivery of vitamin E. European Journal of Pharmaceutics and Biopharmaceutics. 2009;72(1):232-8.
35. Chen Y, Willmott N, Anderson J, Florence A. Comparison of albumin and casein microspheres as a carrier for doxorubicin. Journal of pharmacy and pharmacology. 1987;39(12):978-85.

36. Ganguly K, Aminabhavi TM, Kulkarni AR. Colon targeting of 5-fluorouracil using polyethylene glycol cross-linked chitosan microspheres enteric coated with cellulose acetate phthalate. Industrial & Engineering Chemistry Research. 2011;50(21):11797-807.
37. Chiappetta DA, Sosnik A. Poly (ethylene oxide)–poly (propylene oxide) block copolymer micelles as drug delivery agents: improved hydrosolubility, stability and bioavailability of drugs. European Journal of Pharmaceutics and Biopharmaceutics. 2007;66(3):303-17.

SECTION 2

"CHEMICAL MODIFICATION OF FATTY ACIDS FOR THE IMPLEMENTATION OF DRUG DELIVERY SYSTEMS"

Part A: α-Tocopheryl linolenate solid lipid nanoparticles for the encapsulation, protection, and release of omega-3 polyunsaturated fatty acid: *in vitro* anti-melanoma activity evaluation.

Part B: Solid Lipid Nanoparticles for Cyclosporin A Topic Release.

PART A

"α -Tocopheryl Linolenate Solid Lipid Nanoparticles for the encapsulation, protection and release of Omega-3 Polyunsaturated Fatty Acid: *In Vitro* Anti-Melanoma Activity Evaluation"(1)

Abstract

The main target of this study was the preparation, characterization and antioxidant activity evaluation of α-tocopheryl linolenate based solid lipid nanoparticles (SLNs-TL), able to incorporate omega-3 α-linolenic acid, useful for the treatment of melanoma, a type of skin cancer. In particular, α-linolenic acid was successfully derivatized with α-tocopherol and the obtained compound was characterized by Fourier transform infrared (FT-IR) and by ^{1}H-NMR to confirm the ester linkage. Both the empty SLNs-TL that SLNs-TL-LIN, containing omega-3-linolenic acid, were prepared through the technique of the microemulsion. The nanoparticles were characterized for entrapment efficiency, size and shape. Their antioxidant activity was investigated in rat liver microsomal membranes in inhibiting the lipid peroxidation induced by *tert*-butyl hydroperoxide (*tert*-BOOH), which endogenously produces alkoxyl radicals by Fenton reactions. The obtained results indicate that the α-tocopherol, linked by ester bond to α-linolenic acid, maintains an excellent antioxidant activity. The encapsulation efficiency was equal to 77% and the polydispersity index 0.198 indicating a good dimensional distribution. Furthermore, the nanoparticles were tested *in vitro* for their cytotoxic activity against human melanoma cancer cell line C32. Both empty SLNs-TL and loaded SLNs-TL-LIN showed a high biological activity, being more effective than α-linolenic acid and α-tocopherol. The results indicated that these nanoparticles could provide the

delivery and the protection of unstable molecules, such as α-linolenic acid, from degradation induced by mechanisms of oxidative stress.

***Keywords**: Omega-3, α-Tocopheryl linolenate, Solid lipid nanoparticles, Antioxidant, Melanoma, Antiproliferative.*

1. Introduction

Skin cancers have a higher incidence than all other cancers combined and are a major cause of morbidity worldwide. Laboratory data suggest that certain dietary constituents, notably omega-3 polyunsaturated fatty acids, could potentially protect against skin malignancy, although no large-scale review has been conducted in humans (2). Omega-3 polyunsaturated fatty acids are called essential because the body needs these substances but can't manufacture them, so we have to take them through diet. They have beneficial effects not only on the tumors skin but also on other cancers and on additional clinical disorders including edema (3), rheumatoid arthritis (4), and cardiovascular disease (5, 6). Hence the replacement of saturated fat with unsaturated fatty acids for the protection against metabolic diseases and disorders, omega-3 fatty acids have been widely accepted as one of the bases of healthy lifestyle and nutrition. However, despite this weight of evidence, during processing, distribution and handling, oils can easily oxidize, due to their high unsaturation degree. Oxidation leads to the formation of unpleasant tastes and odors. Consequently, the products' shelf life is decreased and free radicals are formed affecting negatively the organism. (7). Omega-3 encapsulation (8-15) represent is an alternative to protect fatty acids against lipid oxidation, thus increasing their shelf life (16). In addition, it also offers the possibility of their controlled release. In the last years Cassano et al. realized carriers for the topical delivery of sensitive substances. Particularly, with the aim to increase the stability of the vitamin E to the light, heat etc., trans-ferulic acid was covalently linked on the dextran backbone to realize a hydrogel, entrapping vitamin E. The carrier investigation revealed that vitamin E was preserved during the transport and

release (17). In addition, Trombino et al. developed and characterized stearyl ferulate based SLNs, as vehicle for both β-carotene and α-tocopherol, with the aim of increasing the photochemical stability of these substance. It was shown that ferulic acid exercised a synergistic effect with loaded antioxidants, and was able to protect and stabilize them from degradation (18). The obtained data demonstrated that the prepared antioxidant carriers could be interesting for transport and release of unstable active ingredients suggesting the possibility to prepare a new carrier loading linoleic acid, an oxidizable substance, having in the carrier structure the same substance. In the present study we prepared SLNs-TL-LIN based on tocopheryl linolenate and loading α-linolenic acid (Figure 1). In addition, the anti-proliferative effect of obtained formulations against human melanoma cells was also evaluated. Nanoparticles development constitutes an interesting new strategy in oncology. These carriers allow a new controlled and targeted way to deliver anticancer drugs and this results in high efficacy with low side effects (19). In fact, many studies deal with nanoparticle formulations in cancer treatment (20-23). This new approach appears particularly interesting in the treatment of skin cancer because, actually, conventional chemotherapy shows little effects against metastatic melanoma (24). Thus, the cytotoxic activity against C32 human melanoma cell line of both α- linolenic acid and α-tocopherol and prepared nanoparticles were tested and compared.

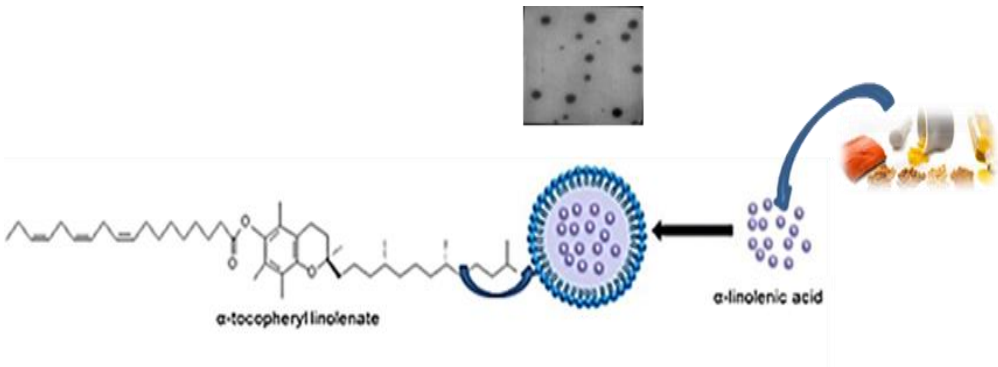

Figure 1: *Schematic representation of SLNs-TL-LIN.*

2. Materials and Methods

2.1. Chemicals

All solvents, analytical grade, were purchased from Carlo Erba Reagents (Milan, Italy): tetrahydrofuran (THF), chloroform ($CHCl_3$), n-hexane, ethyl acetate, isooctane and 1-butanol. α-linolenic acid (PM = 278.43 g / mol), α-tocopherol (PM = 430.72 g/mol), biliary salt of the taurodeossicolic acid, Tween 20, dicyclohexylcarbonymide (DCC), dimethylaminopyridine (DMAP), trichloroacetic acid (TCA), butylated hydroxytoluene (BHT), 2-thiobarbituric acid (TBA), tert-butyl hydroperoxide (*t*-BOOH), phosphate buffered saline (PBS), RPMI 1640 medium, fetal bovine serum, L-glutamine, penicillin/streptomycin, trypan blue, 3-(4,5-dimethylthiazol-2-yl)-2,5-diphenyltetrazolium bromide (MTT), were purchased from Sigma-Aldrich (Sigma Chemical Co.,St. Louis, MO, USA). Amelanotic melanoma cells C32 were purchased from ATCC no. CRL-1585, UK.

2.2. Measurements

FT-IR spectra were measured on a Jasco 4200 using KBr disks. ^{1}H-MNR spectra were acquired on Bruker VM-300 ACP; the chemical shifts are expressed in δ and referred to the solvent. The UV-Vis spectra were carried out using JASCO UV-530. Solid lipid nanoparticles were obtained by means homogenizer Model SL2, Silverson (Chesham Bucks, England) and washed using an Amicon TCF2A ultrafiltration system (Amicon Grace, Beverley, MA USA; membrane Amicon Diaflo YM 100). The samples were lyophilized using "Freezing-drying" Micro Modulyo, Edwards. Dimensional analysis of the nanoparticles prepared were carried out by means of light scattering using a Brookhaven 90 Plus Particle Size Analyzer (Brookhaven Instruments Corporation, New York, USA) at 25 °C by measuring the autocorrelation function at 90° scattering angle. The polydispersity index (PI), which indicates the measure of the distribution of nanoparticle populations, was also determined. Six separate measurements were made in order to obtain the average. Data were fitted by the method of inverse ‘‘Laplace transformation’’ and Contin. Absorbance values were measured using a microplate reader (GDV DV 990 B/V, Roma, Italy). Changes in cell morphology were visualized using an inverted microscope

(AE20 Motic; Motic Instruments, Inc., VWR, Milan, Italy). Images were captured on a VWR digital camera (Visi Cam 3.0 USB camera, Milan, Italy).

2.3. Synthesis of cis, cis, cis-9,12,15-octadecatrienoate of (2R) -2,5,7,8-tetramethyl-2-[(4R, 8R) - (4,8,12-trimetiltridecil)] -6-chromanol (TL)

In a three-necked flask, equipped with condenser, dropping funnel and magnetic stirrer, accurately flamed and maintained under an inert atmosphere, were placed 50 ml of dry THF to which are added 2 g of α-linolenic acid ($7.2 \cdot 10^{-3}$ moles), 1.5 g of DCC ($7.2 \cdot 10^{-3}$ moles) and 0.88 g of DMAP ($7.2 \cdot 10^{-3}$ moles). The solution was kept under stirring for 10 minutes at room temperature until complete dissolution of DMAP and DCC. Next, were slowly added 3.10 g of α-tocopherol ($7.2 \cdot 10^{-3}$ moles) dissolved in dry THF until obtaining a solution of light yellow color. The reaction was left under stirring in the dark at room temperature for 24 hours and monitored by TLC (Thin Layer Chromatography) on aluminum oxide plates using as eluent mixture $CHCl_3$: ethyl acetate in a ratio 1:1. At the end it was obtained a yellow solution with a white precipitate.

The product was subjected to filtration and the filtrate is stripped completely of the solvent at reduced pressure. It was obtained a dark brown-orange residue which was purified by chromatography column (eluent mixture n-hexane: $CHCl_3$, 8:2) and characterized by FT-IR spectroscopy and ^{1}H-NMR. We called the product obtained α-tocopheryl linolenate (TL).

2.4. Preparation of Solid Lipid Nanoparticles (SLNs)

SLNs were prepared by a microemulsion technique at moderate temperature according to Gasco (25) as shown in Table 1. Briefly, α-tocopheryl linolenate, in the presence or not of the active substance, the α-linolenic acid were melted at 70–75 °C. A warm water solution of sodium taurocholate, butanol and Tween 20 was then added to obtain an optically transparent system. The warm microemulsion was immediately dispersed in cold water (∼2 ◦C) under high-speed homogenation at 8000 rpm for 15min. The volume ratio of warm microemulsion to cold water was 1:20. The SLNs-TL and

SLNs-TL-LIN dispersions were washed two times using an Amicon TCF2A ultrafiltration system.

Table 1: *amount of all reagent used for SLNs preparation*

α-tocopheryl linolenate (g)	***tween 20 (ml)***	***1-butanol (ml)***	***biliary salt(g)***	***water(ml)***	***α-linolenic acid (g)***
0.41	0.21	0.09	0.11	0.85	0,04

The particles size was determined by dynamic light scattering at 25 °C by measuring the autocorrelation function at 90° scattering angle. Cells were filled with 100 µl of sample solution and diluted to 4 ml with filtered (0.22 µm) water. The polydispersity index (PI) indicating the measure of the nanoparticle population distribution (26) was also determined. Six separate measurements were made to derive the average. Data were fitted by the method of inverse "Laplace transformation" and Contin (27, 28).

2.5. Encapsulation efficiency determination

The encapsulation efficiency of SLNs was evaluated through a spectrophotometer UV-Vis. Briefly, the amount of unencapsulated substance in the SLNs was removed by centrifugation (at 8000 rpm for 30 min) and filtration. Subsequently the obtained samples were diluted in methanol (1:9) and analysed. The absorbance of the samples was measured using quartz cells with a thickness of 1 cm and operating at specific wavelengths of α-linolenic acid (λ = 268 nm).The encapsulation efficiency (EE) (%) is the percentage of active substance encapsulated in SLNs expressed referring to the initial drug amount used. This is calculated using the following equation:

$$EE\% = \frac{gf}{gi} \cdot 100 \qquad \text{(Eq. 1)}$$

where gi indicates the grams of α-linolenic acid initially used and gf the final amount effectively entrapped into nanoparticles.

2.6. SLNs antioxidant activity evaluation

To evaluate the antioxidant activity of the SLNs based on α-tocopheryllinolenate (TL-SLNs) loaded with α-linolenic acid, they were subjected to the test of malondialdehyde (MDA) using rat liver microsomal membranes. As control were used α-tocopherol, α-linolenic acid and TL-SLNs unloaded. The preparation of the microsomal suspension follows the procedure reported by Trombino et al. (18). Previously an aliquot of each sample was added to microsomal membranes to be tested and subsequently an amount of *t*-BOOH (*tert*-butylhydroperoxide) to reach a final concentration of 0.25 mM was also added. The microsomal suspension was then incubated at 37 ° C under stirring, in the dark for one hour. Subsequently, 1 ml of microsomal suspension was added to a solution consisting of 3 ml of trichloroacetic acid (TCA) at 0.5%, 0.5 ml of thiobarbituric acid (TBA) (two pieces of TBA to 0.4% in HCl 0.2 M and a part of distilled water) and 0,07 ml of butylated hydroxytoluene (BHT) 0.2% in 95% ethanol. The samples thus prepared were then incubated in a bath at 90 °C for 45 min and then centrifuged. After incubation, the TBA-MDA complex was detected by spectrophotometry UV-Visat 535 nm, because the formation of malondialdehyde is indicative of the lipid peroxidation process. The experiment was repeated in triplicate (n = 3).

2.7. Cell effect – MTT reduction assay

Melanoma cancer cells C32 were cultured in RPMI-1640 medium supplemented with 1% antibiotic solution (penicillin/streptomycin), 1% L-glutamine and 10% fetal bovine serum (FBS). Cells were incubated at 37°C under 5% CO_2. After cell count, performed using a standard trypan blue cell counting technique, cells were subcultured onto 96 well culture plates for 1 day to become nearly confluent. Cell concentration was 2 x 10^4 cells/ml. Different concentrations of samples were prepared from stock solutions by serial dilution in RPMI-1640 medium. One hundred µl/well of each concentration were added to obtain final dilutions ranging from 100 to 0.156 µg/ml. Treatments never exceeded 0.5% of the solvent (DMSO), the percentage that was used to treat control wells.

After 48 hours, cell viability was assessed by the 3-(4,5-dimethylthiazol-2-yl)-2,5-diphenyltetrazolium bromide (MTT) assay (29). Medium was removed and 0.5% (w/v) MTT in phosphate-buffered saline (100 µl) were added to each well. After further 4 h of incubation, DMSO (100 µl) was added to each well to dissolve the formazan crystals. Absorbance was measured at 570 nm. Each experiment was carried out in quadruplicate. Cytotoxicity was expressed as IC_{50}, which is the concentration giving 50% inhibition compared to the control (untreated cells).

2.8. Statistical analysis

Each datum represents the mean ± SD of three different experiments. Data were analyzed by Student's t test using the GraphPad Prism 4 software program. $P < 0.05$ was considered as statistically significant.

For the evaluation of the antiproliferative activity experiments were realized in quadruplicate. Data were expressed as means ± S.E. The raw data were fitted through nonlinear regression in order to obtain the IC_{50} values which indicate the dose needed to inhibit the 50% of cell viability. Data were checked for normality (D'Agostino-Pearson test) and tested for homogeneity of variances (Levene's test). The statistical significance of differences among group means were estimated by a one-way analysis of variance (ANOVA) followed by Bonferroni post hoc test ($P < 0.05$), using SigmaStat Software (Jantel Scientific Software, San Rafael, CA).

3. Results and Discussion

3.1. Synthesis of cis, cis, cis-9,12,15-octadecatrienoato of (2R) -2,5,7,8-tetramethyl-2-[(4R, 8R)-(4,8,12-trimetiltridecil)]-6-chromanol (TL).

The esterification reaction between the α-tocopherol and α-linolenic acid was conducted in order to obtain a new lipophilic and antioxidants compound that was used as lipid matrix in the formulation of a new type of SLN. This synthesis has allowed the derivatization of the alcoholic function of α-tocopherol to obtain a compound with a yield of 78% containing in its structure an Omega-3 (Scheme 1). This reaction was conducted in the dark due to the photosensitivity of the species involved. The product formation was confirmed by spectroscopy FT-IR e ^{1}H-NMR. FT-IR (KBr) ν (cm^-

[1]):3068, 3034 (-CH),1747 (-C=O), 996, 950 (HC=CH).[1]H-NMR (C_2D_6CO) δ (ppm):5.20-5.60 (m, 6H),2.87 (m, 4H), 2.55 (m, 4H), 2.20 (m, 4H), 2.0 (s, 3H), 2.05 (s, 3H), 2.1 (s, 3H), 1.55 (m, 4H), 0.80-1.50 (m, 47H).

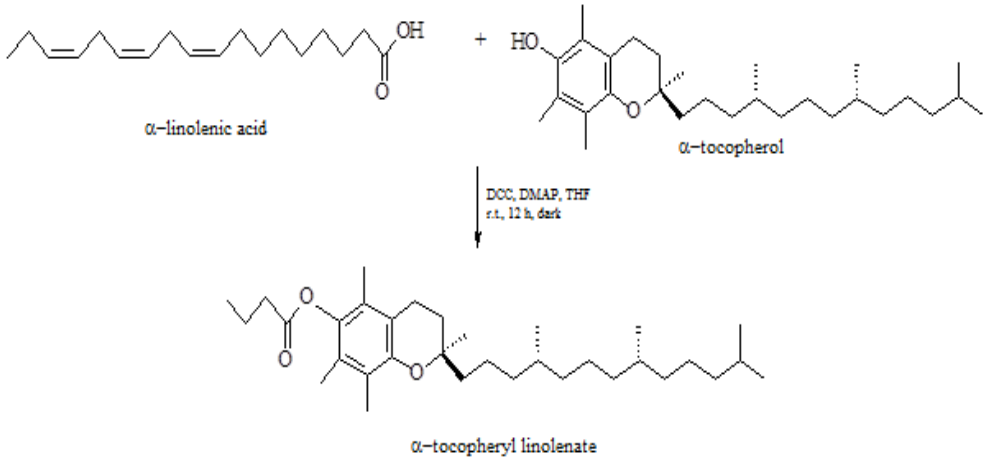

Scheme 1: *Schematic representation of α-tocopheryl linolenate synthetic route.*

3.2. Preparation and characterization of SLNs

The SLNs based on α-tocopheryl linolenate and loaded with α-linolenic acid were successfully prepared through the microemulsion technique. Dimensional analysis to the Light Scattering allowed to determine the average diameter of the nanoparticles synthesized and their polydispersity index (PI) as shown in Table 2.

Table 2: *Light scattering analysis*

Formulation	Mean particle size (nm)	Polydispersity Index (PI)
TL-SLNs	450.9 ±1.3	0.216±0.013
TL-SLN-LIN	181.0±1.8	0.198±0.021

It was noted a reduction in the diameter after loading α-linolenic acid. In particular, the diameter of TL-SLNs was about 450.9 nm, while TL-SLN-LIN was of 181.0 nm. The polydispersity index, as shown in Table 2, were lower than 0.220, these low values of PI are indicative of a good homogeneity in the distribution of particle sizes and the presence of only two families of nanoparticles. SLN dimensions were confirmed also through transmission electron microscopy (TEM). With this technique it is possible to observe that nanoparticles have a spherical shape (Figure 2).

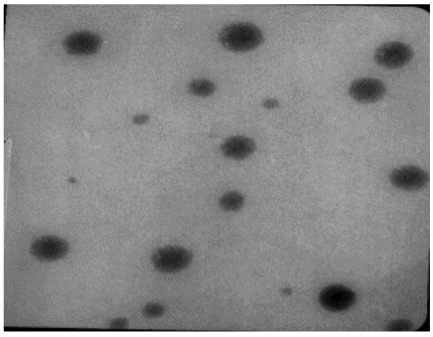

Figure 2: *TEM picture of TL-SLNs*

In addition, SLNs were characterized through UV-Vis spectrophotometer with the aim to evaluate the percentage of encapsulation of α-linolenic acid. The encapsulation efficiency (EE) was of 77 %. This value revealed that the acid is encapsulated in great amount due to its chemical affinity for the ester of which the nanoparticles are composed.

3.3. Evaluation of SLNs antioxidant activity

The ability of SLN prepared to inhibit lipid peroxidation induced by *t*-BOOH was examined in rat liver microsomal membranes, in an incubation period of 120 minutes. In particular, we evaluated the antioxidant activity of the following compounds: α-linolenic acid, α-tocopherol, the α-tocoferyl linolenate, the SLN loaded with the active ingredient and the SLN not loaded. Figure 3 shows that all samples tested preserve the antioxidant

activity of α-tocopherol and α-linolenic acid; more precisely, the SLN loaded with α-linolenic acid have antioxidant activity superior than nanoparticles not loaded due to the simultaneous presence of the linolenic acid in the matrix and inside. Also, the ester synthesized (α-tocopheryl linolenate) preserves the antioxidant activity of α-tocopherol and α-linolenic acid.

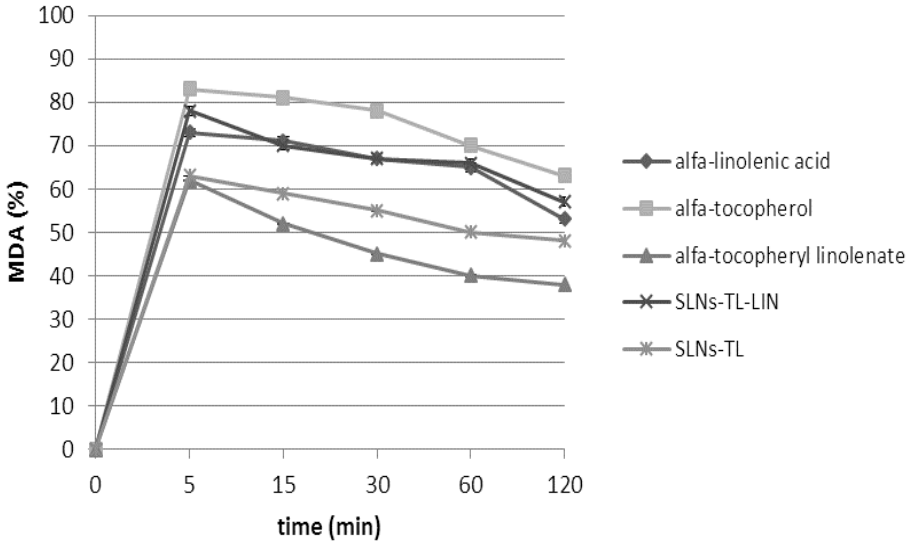

***Figure 3**: Graphic representation of % MDA inhibition of α-linolenic acid, α-tocopherol, α-tocoferyl linolenate, SLN loaded with the active ingredient and the SLN not loaded vs time. The results represent the mean standard error of six separate experiments done in triplicate.*

3.4. Evaluation of cytotoxic activity

Prepared nanoparticles were evaluated for their *in vitro* cytotoxic properties against C32 human melanoma cancer cell line, and compared to the effects exerted by α-linolenic acid and α-tocopherol. After 48 h of incubation, all reduced cell viability in a dose-dependent manner compared with control (0.5% DMSO treated control cells) (Figure 4).

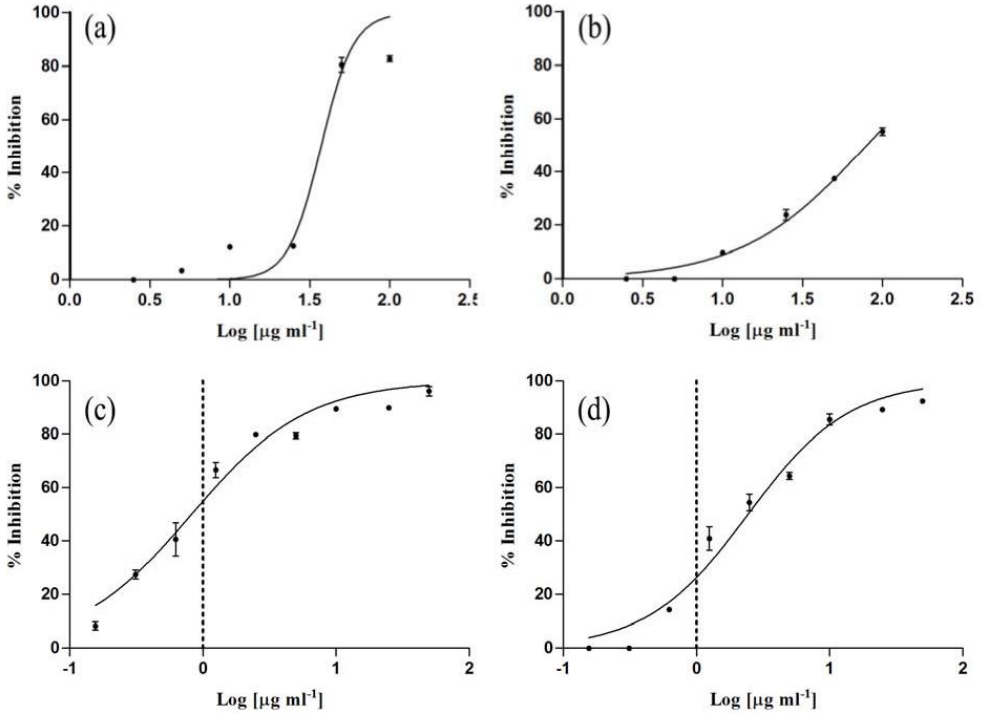

Figure 4: *Dose depending effect of α-linolenic acid (a), α-tocopherol (b), TL-SLNs (c) and TL-SLN-LIN (d) on C32 cell viability.*

In table 3 are reported the IC_{50} values referred to the different treatments. Interestingly, both empty TL-SLNs and TL-SLN-LIN pointed out a higher biological activity compared to the effects exerted by α-linolenic acid and α-tocopherol. In particular, the two formulations (empty nanoparticles and SLNs loaded with α-linolenic acid) pointed out IC_{50} values of 0.82 and 2.44 μg/ml, respectively. Statistical analyses (Bonferroni test) evidenced a significant difference between these excellent results and the cytotoxic activity on melanoma cell line C32 of the other two samples. Moreover, α-linolenic acid (IC_{50} = 37.26 μg/ml) was more effective than α-tocopherol (IC_{50} = 79.51 μg/ml) in inhibiting C32 cell viability, whereas no significant differences were observed between TL-SLNs and TL-SLN-LIN.

Changes in treated cells viability were visualized using an inverted microscope and captured on a VWR digital camera. As evidenced in Figure

5, each sample significantly affected cell viability. At the highest tested concentration (100 µg/ml), α-linolenic acid caused 82.81% of inhibition (Figure 5b), while an inhibition of 55.36% was observed after the incubation of cell cultures with the same concentration of α-tocopherol (Figure. 5c). Prepared α-tocopheryl linolenate based solid lipid nanoparticles induced an excellent inhibition of cell viability even at lower concentrations. At a concentration equal to 50 µg/ml, percent of inhibition of 96.17 and 92.42 were observed for empty TL-SLNs and TL-SLN-LIN, respectively. Figures 5d and 5e illustrate changes in treated cells viability induced by a concentration of 25 µg/ml of these active formulations, that were able to cause 89.96% and 89.33% of inhibition, respectively.

***Table 3**: Cytotoxic activity of α-tocopherol, α-linolenic acid, α-tocopheryl linolenate based solid lipid nanoparticles empty and loaded. Data are expressed as mean ± S. E. (n=4). Different indicate statistically significant differences at P < 0.05 (Bonferroni post hoc test).*

Sample	IC_{50} (µg/ml)
α-Linolenic acid	37.26±2.60 [b]
α-Tocopherol	79.51±2.15 [c]
TL-SLNs	0.82±0.08 [a]
TL-SLN-LIN	2.44±0.16 [a]

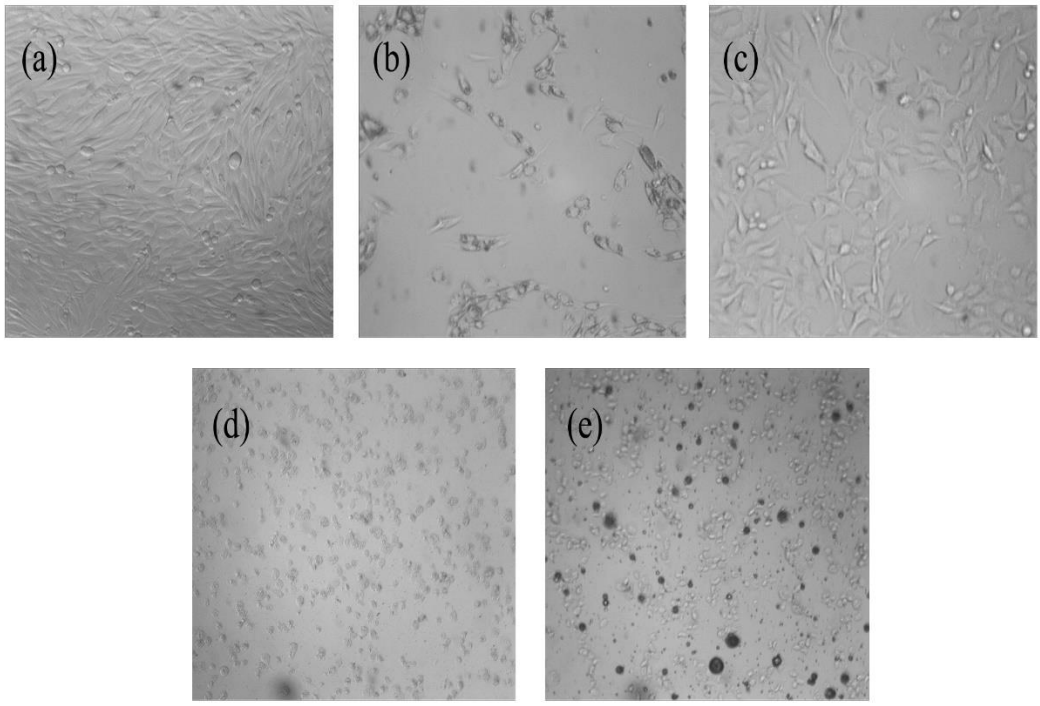

Figure 5: *Changes in cell viability induced on C32 cell line. a) control, cells in DMSO (0.5%, v/v), without sample; b) α-linolenic acid, 100 µg/ml; c) α-tocopherol, 100 µg/ml; d) TL-SLNs, 25 µg/ml; e) TL-SLN-LIN, 25 µg/ml.*

4.Conclusions

The aim of this work was the preparation of SLNs based on α -tocopheryl linolenate. The obtained results show that the new ester maintains an excellent antioxidant activity. For this reason, SLNs could provide the delivery and the protection of unstable molecules, such as α-linolenic acid, from degradation. In addition, a high encapsulation efficiency, suggests their possible use as valuable antioxidant systems. Moreover, prepared SLNs are more effective than both α-linolenic acid and α-tocopherol in inhibiting human melanoma cell viability *in vitro*. Preliminary obtained results suggest that these formulations could be good candidates for further *in vivo* studies to develop potential agents in the treatment of melanoma.

References

1. Cassano R, Mellace S, Marrelli M, Conforti F, Trombino S. α-Tocopheryl linolenate solid lipid nanoparticles for the encapsulation, protection, and release of the omega-3 polyunsaturated fatty acid: in vitro anti-melanoma activity evaluation. Colloids and Surfaces B: Biointerfaces. 2017;151:128-33.
2. Noel SE, Stoneham A, Olsen CM, Rhodes LE, Green AC. Consumption of omega-3 fatty acids and the risk of skin cancers: A systematic review and meta-analysis. International journal of cancer. 2014;135(1):149-56.
3. Yang R, Harris WS, Vernon K, Thomas AM, Qureshi N, Morrison DC, et al. Prefeeding with ω-3 fatty acids suppresses inflammation following hemorrhagic shock. Journal of Parenteral and Enteral Nutrition. 2010;34(5):496-502.
4. Rennie K, Hughes J, Lang R, Jebb S. Nutritional management of rheumatoid arthritis: a review of the evidence. Journal of Human Nutrition and Dietetics. 2003;16(2):97-109.
5. Hasler CM. Functional foods: their role in disease prevention and health promotion. FOOD TECHNOLOGY-CHAMPAIGN THEN CHICAGO-. 1998;52:63-147.
6. Zhao G, Etherton TD, Martin KR, West SG, Gillies PJ, Kris-Etherton PM. Dietary α-linolenic acid reduces inflammatory and lipid cardiovascular risk factors in hypercholesterolemic men and women. The Journal of nutrition. 2004;134(11):2991-7.
7. Ahn J-H, Kim Y-P, Seo E-M, Choi Y-K, Kim H-S. Antioxidant effect of natural plant extracts on the microencapsulated high oleic sunflower oil. Journal of Food Engineering. 2008;84(2):327-34.
8. Choi M-J, Ruktanonchai U, Min S-G, Chun J-Y, Soottitantawat A. Physical characteristics of fish oil encapsulated by β-cyclodextrin using an aggregation method or polycaprolactone using an emulsion–diffusion method. Food Chemistry. 2010;119(4):1694-703.
9. Katsuda MS, McClements D, Miglioranza LH, Decker EA. Physical and oxidative stability of fish oil-in-water emulsions stabilized with β-

lactoglobulin and pectin. Journal of agricultural and food chemistry. 2008;56(14):5926-31.
10. Kolanowski W, Jaworska D, Weißbrodt J, Kunz B. Sensory assessment of microencapsulated fish oil powder. Journal of the American Oil Chemists' Society. 2007;84(1):37-45.
11. Serfert Y, Drusch S, Schwarz K. Sensory odour profiling and lipid oxidation status of fish oil and microencapsulated fish oil. Food Chemistry. 2010;123(4):968-75.
12. Szente L, Szejtli J, Szemán J, Kató L. Fatty acid-cyclodextrin complexes: Properties and applications. Journal of Inclusion Phenomena and Macrocyclic Chemistry. 1993;16(4):339-54.
13. Torres-Giner S, Martinez-Abad A, Ocio MJ, Lagaron JM. Stabilization of a nutraceutical omega-3 fatty acid by encapsulation in ultrathin electrosprayed zein prolamine. Journal of food science. 2010;75(6).
14. Pereira DM, Valentão P, Andrade PB. Nano-and microdelivery systems for marine bioactive lipids. Marine drugs. 2014;12(12):6014-27.
15. Zimet P, Rosenberg D, Livney YD. Re-assembled casein micelles and casein nanoparticles as nano-vehicles for ω-3 polyunsaturated fatty acids. Food Hydrocolloids. 2011;25(5):1270-6.
16. Nadhi NS, Khanum F. Encapsulation of Omega-3-rich Oil and Anti-anxiolytic Properties of Flax Seed Oil.
17. Cassano R, Trombino S, Muzzalupo R, Tavano L, Picci N. A novel dextran hydrogel linking trans-ferulic acid for the stabilization and transdermal delivery of vitamin E. European Journal of Pharmaceutics and Biopharmaceutics. 2009;72(1):232-8.
18. Trombino S, Cassano R, Muzzalupo R, Pingitore A, Cione E, Picci N. Stearyl ferulate-based solid lipid nanoparticles for the encapsulation and stabilization of β-carotene and α-tocopherol. Colloids and Surfaces B: Biointerfaces. 2009;72(2):181-7.
19. Haley B, Frenkel E, editors. Nanoparticles for drug delivery in cancer treatment. Urologic Oncology: Seminars and original investigations; 2008: Elsevier.
20. Zheng D, Li X, Xu H, Lu X, Hu Y, Fan W. Study on docetaxel-loaded nanoparticles with high antitumor efficacy against malignant melanoma. Acta Biochim Biophys Sin. 2009;41(7):578-87.

21. Siddiqui IA, Bharali DJ, Nihal M, Adhami VM, Khan N, Chamcheu JC, et al. Excellent anti-proliferative and pro-apoptotic effects of (−)-epigallocatechin-3-gallate encapsulated in chitosan nanoparticles on human melanoma cell growth both in vitro and in vivo. Nanomedicine: Nanotechnology, Biology and Medicine. 2014;10(8):1619-26.
22. Qi L, Xu Z, Chen M. In vitro and in vivo suppression of hepatocellular carcinoma growth by chitosan nanoparticles. European journal of cancer. 2007;43(1):184-93.
23. Das RK, Kasoju N, Bora U. Encapsulation of curcumin in alginate-chitosan-pluronic composite nanoparticles for delivery to cancer cells. Nanomedicine: Nanotechnology, Biology and Medicine. 2010;6(1):153-60.
24. Zhao B, Yin J-J, Bilski PJ, Chignell CF, Roberts JE, He Y-Y. Enhanced photodynamic efficacy towards melanoma cells by encapsulation of Pc4 in silica nanoparticles. Toxicology and applied pharmacology. 2009;241(2):163-72.
25. Gasco M. Solid Lipid Nanospheres from Warm Micro-Emulsions: Improvements in SLN production for more efficient drug delivery. Pharmaceutical Technology Europe. 1997;9:52-8.
26. Koppel DE. Analysis of macromolecular polydispersity in intensity correlation spectroscopy: the method of cumulants. The Journal of Chemical Physics. 1972;57(11):4814-20.
27. Provencher SW. CONTIN: a general purpose constrained regularization program for inverting noisy linear algebraic and integral equations. Computer Physics Communications. 1982;27(3):229-42.
28. Provencher SW. A constrained regularization method for inverting data represented by linear algebraic or integral equations. Computer Physics Communications. 1982;27(3):213-27.
29. Marrelli M, Cristaldi B, Menichini F, Conforti F. Inhibitory effects of wild dietary plants on lipid peroxidation and on the proliferation of human cancer cells. Food and Chemical Toxicology. 2015;86:16-24.

PART B

"Solid Lipid Nanoparticles for Cyclosporin A Topic Release" (*)

Abstract

The aim of this work was to design solid lipid nanoparticles (SLNs) based on a new ester, oleate of trehalose for the psoriasis treatment. Trehalose was firstly esterified with oleic acid, this reaction was carried out in order to obtain a more lipophilic compound that could to be used as a lipid matrix in the formulation of a new type of SLNs carrying a potent immunosuppressant: cyclosporin A. The ester formation was confirmed by the analysis of the product obtained by the common spectroscopic techniques: FT-IR and ^{1}HNMR. Subsequently, trehalose ooleate SLNs were successfully prepared with and without cyclosporin A, using the microemulsion technique. Further characterizations were performed by differential scanning calorimetry (DSC). The drug release was then assessed from the SLNs through the Franz diffusion cells, using both dialysis membranes and rabbit ears skin. Additional investigations carried out using the confocal microscope and stripping tape test showed that cyclosporin A remains localized on the most superficial layers of the skin. These results indicate the possibility of using the nanoparticles prepared for topical treatment of psoriasis, indeed, the possibility of side effects due to systemic absorption of cyclosporin A is reduced whereas the drug concentration at injury level is increased.

Keywords*: Cyclosporine A, nanoparticle, topical, psoriasis, lipid.*

1. Introduction

The skin is a protective barrier involved in many important physiological functions such as fluid homeostasis, thermoregulation, immune surveillance, and provides a unique delivery pathway for therapeutic and active substances (1, 2). These functions are related to the skin's complex multiple layers with each layer associated with highly specified cells and structures. The permeation barrier properties of human skin are mostly attributed to the top layer of the epidermis, the stratum corneum (3). In fact, the specific content, composition and structure of the stratum corneum lipids selectively and effectively inhibit the penetration of chemicals (4, 5). At the moment, indeed, many skin diseases such as psoriasis are still waiting for treatment based on safer and more efficient cutaneous delivery of therapeutics across the stratum corneum barrier. Psoriasis is a chronic, autoimmune disease with a multifactorial pathogenesis associated with genetics, environmental and immune system factors (6-8). Cyclosporin A (CsA) is one of the most effective systemic drug available for the treatment of psoriasis (9, 10), nonetheless long term systemic administration of cyclosporin A produces harmful effects like nephrotoxicity, hypertension, hyperlipidaemia, hyperkalaemia, paraesthesia, granulomatous, hepatitis etc (11, 12). Topical treatment approaches targeting the drug to the basal layer of epidermis where psoriasis originates would be desirable. Unfortunately, topical penetration of cyclosporin A is not readily achieved due to its rigid cyclic structure, high molecular weight and barrier properties of stratum corneum (13, 14). An extensive research has been performed to overcome the stratum corneum barrier for the delivery of drugs across the skin using physical (iontophoresis, electrophoresis and sonophoresis) and chemical techniques (penetration enhancers) or combination of both (15). However, chemical enhancers induce irritation and physical methods cause damage and disruption of the skin barrier (16, 17). In this context novel nano carrier systems could make an important impact on clinical practice. Currently lipid-based nanoparticles gained much interest in this field. The achievements of SLN as topical drug carrier systems are due to several advantages these systems in fact could increasing the permeation of the drug while mitigating the damage to the skin barrier function (18). Recently many studies have been conducted to determine the potential of SLN as a topical

carrier but still few reports are available on this aspect in literature review (19-21). In the present study, our aim was to design and prepare nanoparticles based on a new ester oleate of trehalose for the topical administration of cyclosporin A. We selected trehalose because is an extensively used disaccharide in drug delivery due to its biocompatibility, bioprotector function and his stabilizing effect on bioactive substances (22). Also unsaturated free fatty acids, especially oleic acid, has shown a positive role in protecting substances from free radicals and has also showed the ability to modulate the inflammation process and to enhance reparative respons*e in vivo* (23, 24).

2. Materials and Methods

2.1 Chemicals

All solvents of analytical grade were purchased from Carlo Erba Reagents (Milan, Italy) and Fluka Chemika-Biochemika (Buchs, Switzerland): dichloromethane (DCM), chloroform, n-hexane, concentrated sulfuric acid (96% w/w), 1-butanol and methanol. Trehalose (PM 378.33 g/mol); oleic acid (PM 282.46 g/mol); dicyclohexylcarbodiimide, DCC, (PM 206.33 g / mol); dimethylaminopyridine, DMAP (PM 122.17 g/mol); Polyoxyethylene sorbitan monolaurate (Tween 20, PM 1227.54 g / mol, 1.1 g/mol); biliary acid biliary acid (PM 521.69 g/mol), Coumarin-6 were purchased from Sigma-Aldrich (Sigma Chemical Co., St. Louis, MO, USA). Cyclosporin A (PM 1202.61 g / mol) was purchased from Farmalabor srl (Milan, Italy). The cellulose acetate membrane 6-27/32" (MWCO: 12000-15000Da) was purchased by Medicell International LTD.

2.2 Instruments

The infrared spectra on potassium bromide (KBr) pellets were performed using a FT-IR Jasco 4200 spectrophotometer in the range 4000-400 cm^{-1}. UV-Vis spectra were carried out using UV/Vis JASCO V-530 spectrophotometer using quartz cells with a thickness of 1 cm. The ^{1}H-NMR analysis were performed using a Bruker VM 30 spectrometer; the chemical shifts are expressed in δ and related to the solvent. Dimensional analysis was

performed using a Brookhaven 90 Plus Particle Size Analyzer. The differential scanning calorimetry (DSC) was performed with DSC 200 PC NETZSCH at heating rate of 10 °C/min. The samples were freeze-dried by Micro Freeze-drying Modulyo, Edwards. Confocal analysis was carried out using Leica TC-SP2 Confocal System; Leica Microsystems Srl, Milan, Italy.

2.3 Esterification of the oleic acid with trehalose

In a three-necked flask fitted with a reflux condenser, dropping funnel and magnetic stirrer, accurately flamed and maintained under inert atmosphere, using nitrogen stream, were solubilized in DCM dry (240 ml) trehalose (1 g, 2,642 10^{-3} moles), DCC (1.091g, 5.286 10^{-3} moles), and DMAP (0.0323g, 2.64310^{-4} moles, 1:20 ratio with DCC moles). The solution was kept under stirring for 30 min at 0 °C and then at room temperature until complete dissolution of DMAP and DCC. Subsequently oleic acid (1.493g, 1.32 10^{-3} moles) was added, using the drop funnel. The reaction was left at room temperature under stirring for 3 hours and monitored by thin layer chromatography (TLC / silica gel, eluent mixture n-hexane-chloroform 1: 9). The solution was then filtered to remove dicyclohexylurea. The reaction solvent was removed by evaporation under reduced pressure. The product obtained, white and oily, trehalose oleate, was characterized by FT-IR and ^{1}H-NMR spectroscopies.

2.4 Preparation of Solid Lipid Nanoparticles (SLNs)

SLNs were prepared by a microemulsion technique at moderate temperature according to Gasco (25) as shown in Table 1. Briefly, the trehalose oleate, in the presence or not of the drug, cyclosporin A, were melted at 70–75 °C. A warm water solution of sodium taurocholate, butanol and Tween 20 was then added to obtain an optically transparent system. The warm microemulsion was immediately dispersed in cold water (∼2 ◦C) under high-speed homogenation at 8000 rpm for 15min. The volume ratio of warm microemulsion to cold water was 1:20. The empty and loaded SLNs dispersions were washed two times using an Amicon TCF2A ultrafiltration

system. Same method was employed for the preparation of coumarin-6 loaded SLNs.

Table 1: *amount of all reagent used for SLNs preparation*

Oleate of trehalose (g)	***tween 20 (g)***	***1-butanol (g)***	***biliary salt(g)***	***water(g)***	***Cyclosporin A (g)***
0,36	0,208	$5{,}02 \cdot 10^{-2}$	0,0884	0,611	0,0936

2.5. SLNs Characterisation

2.5.1. Particle Size

The particles size was determined by dynamic light scattering at 25 °C by measuring the autocorrelation function at 90° scattering angle. Cells were filled with 100 µl of sample solution and diluted to 4 ml with filtered (0.22 µm) water. The polydispersity index (PI) indicating the measure of the nanoparticle population distribution was also determined. Six separate measurements were made to derive the average. Data were fitted by the method of inverse "Laplace transformation" and Contin (26).

2.5.2 *Entrapment Efficiency determination*

The encapsulation efficiency of SLNs was evaluated through a spectrophotometer UV-Vis. Briefly, the amount of unencapsulated drug in the SLNs was removed by centrifugation (at 8000 rpm for 30 min) and filtration. Subsequently the obtained samples were diluted in methanol (1:9) and analyzed. The absorbance of the samples was measured using quartz cells with a thickness of 1 cm and operating at specific wavelengths of cyclosporin A (λ = 210 nm). The encapsulation efficiency (EE) (%) is the percentage of active substance encapsulated in SLNs expressed referring to the initial drug amount used. This is calculated using the following equation:

$$EE\% = \frac{gf}{gi} \cdot 100 \qquad \text{(Eq. 1)}$$

where gi indicates the grams of Cyclosporin A initially used and gf the final amount effectively entrapped into nanoparticles.

2.5.3. Differential Scanning Calorimetry (DSC) Analysis

DSC of drug loaded SLNs, blank SLNs and oleate of trehalose was carried out. Measurements were performed at heating rate of 5 °C/min from 0 to 200 °C. Scans of each component were carried out under a flux of nitrogen. Each sample was analyzed at least in triplicate.

2.6. Skin Permeation Experiments

2.6.1. In Vitro Skin Permeation Studies

The skin permeation studies were performed (n=6) using full thickness rabbit ears skin and cellulose acetate synthetic membranes for 24h. Vertical Franz diffusion cells having a diffusional surface area of about 0,85 cm^2 were mounted on the assembly with temperature maintained at 37 ± 0.5°C to mimic physiological conditions. Receptor medium (6.0 ml) was filled with NaCl solution 0.9% containing 20% ethanol to increase the solubility of cyclosporine A, under magnetic stirrer in order to maintain sink condition. After equilibration of the membranes (rabbit ears skin or dialysis membrane) SLNs suspension containing 0.005g of drug was placed in the donor compartment and covered with a laboratory film (Parafilm, Chicago) which prevented evaporation during the study. A solution of cyclosporin A (1%, w/w) in olive oil was used as the control formulation as reported in many previous studies (27-29). At specific time intervals, samples (1 ml) were withdrawn from receptor compartment and replaced with fresh receptor medium. Samples were analyzed by UV-Vis spectrophotometry for cumulative amount of drug permeated.

2.6.2. Quantification of Drug in Skin Using Tape Stripping

At the end of the permeation experiment, the excess formulation was removed from skin surface. The skin was washed 3 times with phosphate buffer (pH 7.4) and dried. Then the stratum cornuem (SC) was separated from dermal tissues (epidermis and dermis; E+D) using serial tape-stripping involving the removal of 15 strips using adhesive tape (Scotch 845 Book Tape, 3M). Previous studies have demonstrated that 15 strips are sufficient to separate the SC from the epidermis and dermis (29, 30). The cyclosporin

A in the adhesive tapes was extracted by vortexing adhesive tapes with acetonitrile for 2 min and the acetonitrile solution was then filtered with 0.45 µm membrane and analyzed by UV-Vis spectrophotometry. The remaining epidermis and dermis were cut in small pieces, vortex-mixed for 5 min in 1 ml acetonitrile, and sonicated for 40 min. The solution was filtrated using 0.45 µm membranes, and analyzed by UV-Vis spectrophotometry (31).

2.6.3. Localization of Nanoparticles in Skin (CLSM study)

Confocal Laser Scanning Microscopy (CLSM) was carried out to see the depth of penetration of the SLNs. To achieve this aim coumarin-6 dye loaded nanoparticles were prepared. Coumarin-6 (0.05%w/v) solution in propylene glycol was used as control. Propylene glycol was used to solubilize coumarin-6. The dye loaded SLNs were applied on the skin and kept for 24 h as in the permeation experiment. At the end of the experiment, the excess formulation was removed from the skin surface. The skin was washed 3 times with phosphate buffer (pH 7.4) and dried. Specimens were embedded in optimal cutting Temperature compound (Tissue-Tek, Sakura Finetek Europe, Alphen aan den Rijin, The Netherlands) and stored at -80°C until used. Cryostat-cut skin sections (16 mm thick) were mounted on slides and nuclei counterstained with Vectashield solution containing 1.5 mg/ml 4',6-diamidino-2-phenylindole (DAPI; Vector Laboratories, CA, USA). Images were acquired using a confocal microscope (Leica TC-SP2 Confocal System, Leica Microsystem Srl, Milan, Italy).

2.7. Statistical analysis

Data are expressed as mean (standard error of the mean of N replicates per experiment). Statistical analysis was carried out by Student's t test using the GraphPad Prism 4 software program. $P < 0.05$ was considered as statistically significant.

3. Results and Discussion

3.1. Esterification of trehalose with oleic acid

The esterification reaction between trehalose and oleic acid was conducted in order to obtain a compound lipophilic enough to be used as a lipid matrix

in the formulation of our SLNs carrying a potent immunosuppressant: cyclosporin A. This synthesis has allowed the derivatization of the alcoholic function of trehalose to obtain a compound with a yield of 86% containing in its structure an antioxidant, oleic acid (Scheme 1). This reaction was conducted in dry dichloromethane at room temperature (32).

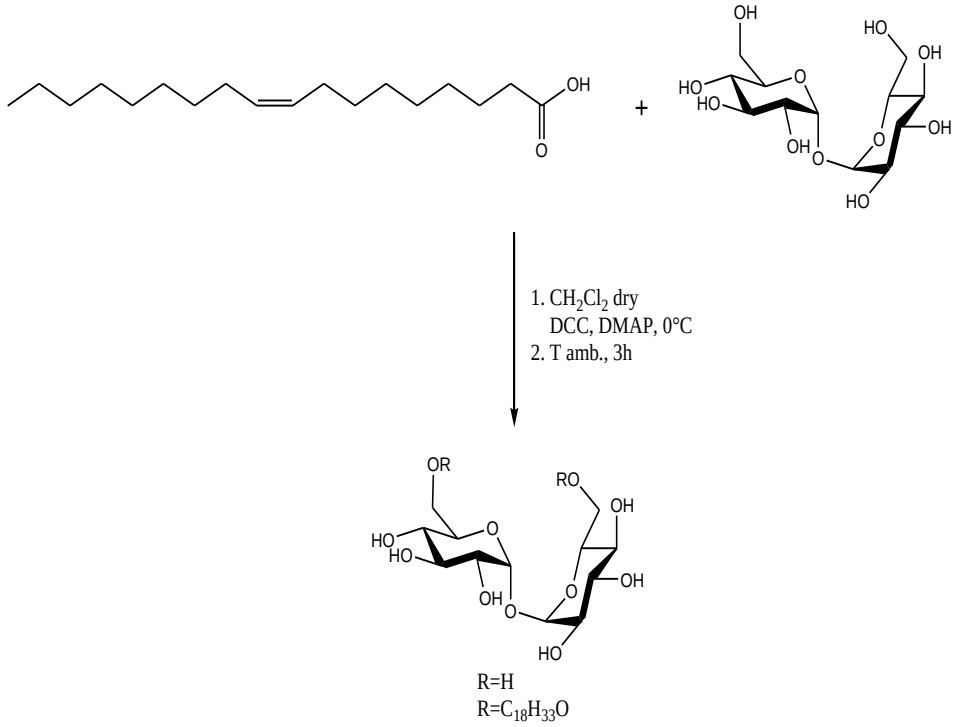

Scheme 1: *Schematic representation of oleate of trehalose synthetic route.*

The product formation was confirmed by spectroscopy FT-IR e ^{1}H-NMR. FT-IR (KBr) ν (cm-1): 3499, 3365, 3204, 2909, 2840, 1738, 1147.1HNMR (CD2Cl2) δ (ppm): 0.87 (3H), 1.20-1.45 (20H), 1.5-2.0 (6H), 2.26 (2H), 3.17-3.2 (4H), 3.45-3.85 (6H), 4.45-4.50 (4H), 5.37 (2H). In particular, the FT-IR spectrum of the ester (c) was compared with that of trehalose (b) and oleic acid (a) (Figure 1).

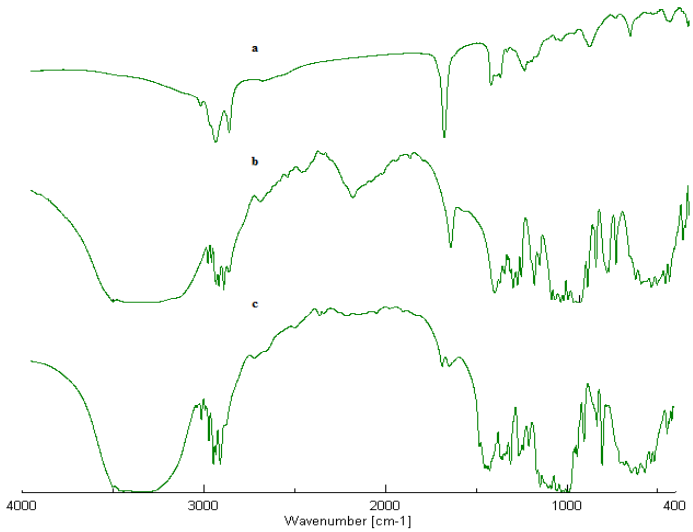

Figure 1: *FT-IR spectra of (a) oleic acid, (b) trehalose and (c) trehalose oleate.*

From the spectrum is it possible to observe the presence of a new band at 1738 cm^{-1} attributable to the stretching vibration of the C = O of the ester (Figure 1 curve c) and the presence at 3200 cm^{-1} and 3500 cm^{-1} of a vibration attributable to the stretching of the O-H of the trehalose glucosidic rings.

3.2. Preparation and characterization of SLNs

3.2.1. Size, Entrapment Efficiency and Size Distribution

The SLNs based on oleate of trehalose and loaded with cyclosporin A were prepared successfully through the microemulsion technique with high encapsulation efficiency that was found to be 92%. This is a satisfying result possibly due to the lipophilic features of cyclosporin A, that well suit the lipophilic nature of our nanoparticles. Light Scattering analysis allowed to determine the average diameter of the nanoparticles and their polydispersity index(PI) as shown in Table 2. These PI values are indicative of a good homogeneity in the distribution of particle size.

Table 2: *Light scattering analysis*

Formulation	Mean particle size (nm)	Polydispersity Index (PI)
empty SLNs	341,1±3,2	0,291±0,005
loaded SLNs	378,4±8,4	0,291±0,014

3.2.2. Differential Scanning Calorimetry (DSC) Analysis

Figure 2 shows the DSC thermograms of trealose oleate (curve a), empty (curve b) and drug loaded nanoparticles (curve c). Cyclosporin A in the pure form exhibits a melting peak at 139 °C indicating the crystalline nature of the drug. Cyclosporin A loaded into trehalose oleate nanoparticles shows a slight transition peak confirming its presence also on the surface of the SLNs. However, as underlined in the next section, this amount is negligible ($1 \cdot 10^{-7}$g vs. 0.043 g of cyclosporine actually loaded into the nanoparticles).

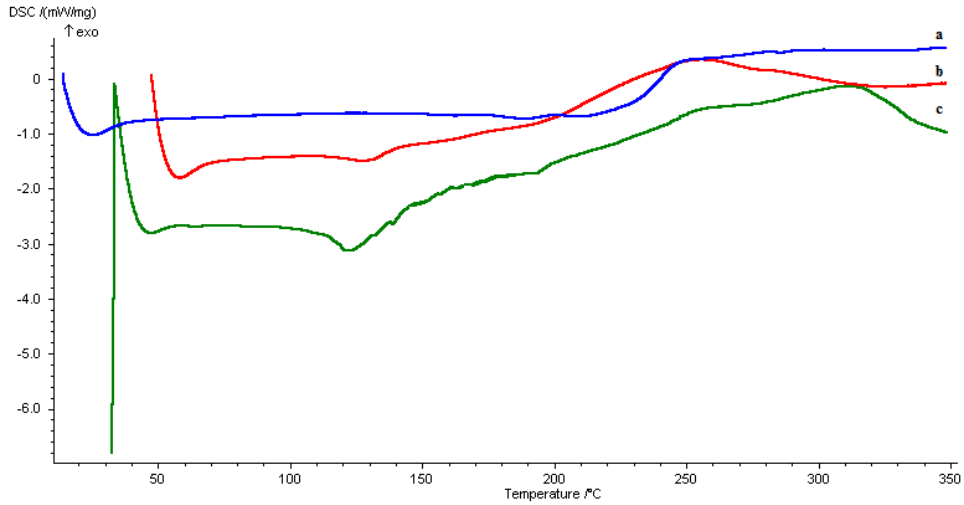

Figure 2: *DSC thermograms of trealose oleate (a), empty SLNs (b) and SLNs containing cyclosporin A (c).*

3.3. Skin Permeation Experiments

3.3.1 In Vitro Permeation Studies

As described in the Materials and Methods section, the release of the drug from solid nanoparticles has been evaluated by means of the Franz Diffusion Cells dialysis membrane and rabbit ears skin. Cyclosporin A is a substance characterized by a low absorbance range (around 200 nm) and this could cause interference by other skin components (33). Indeed, in the skin there are lipids, proteins and other constituents that in some cases absorb at the wavelength The presence of these components in the Franz cell receptor compartment is due to the ethanol present in the solution (0.9% NaCl / ethanol 8:2) used to solubilize SLNs, which causes greater mobility of phospholipids. (34). The use of ethanol is dictated by the cyclosporin A properties. In fact, this drug is practically insoluble in water whereas is soluble in 96% ethanol (35) . For this reason, it was chosen to use a 12000 Da cut-off dialysis membrane that allowed to read the adsorption of cyclosporin A present in the receptor compartment without any kind of possible interference. In particular, the active substance is present in the receptor compartment in the order of $1 \cdot 10^{-7}$ g after 30 min. This amount remains almost unchanged in the following time intervals (1h, 2h, 4h, 6h, 24h). This excluded the possibility of using SLNs for transdermal drug delivery and therefore the use for systemic absorption. The results are consistent with previous studies reported in the literature describing how particular drug delivery systems (microparticles and nanoparticles) increase the drug's permanence in the skin without transdermal delivery (5, 36, 37). This is desirable for topical treatment of skin disorders such as psoriasis as it reduces the possibility of side effects due to systemic absorption of cyclosporin A and increases drug concentration at the disease level.

3.3.2 Tape Stripping Test

Tape stripping method was used to determine drug content in skin layers: SC and dermal tissues (epidermis and dermis; E+D). Table **3** describes the drug content in receptor compartment, SC and dermal tissues (E+D) after *in vitro* skin permeation studies for 24h. The amount of drug detected in SC and dermal tissues from SLNs release was higher compared to control formulation, hence, SLNs significantly enhanced the penetration of drug in

SC as well as in dermal tissues (E+D). Previous reports suggest the ability of nanoparticulate delivery systems to increase the skin permeation. Labouta et al suggest that due to their particulate nature, permeation is dependent on the complex microstructure of the stratum corneum with its tortuous aqueous and lipidic channels (38). Barry at al propose several possible mechanisms. They speculate that the large surface area of nanoparticles may play an important role in dermal penetration facilitating the contact of the encapsulated molecules with the stratum corneum. Moreover, drug loaded nanoparticles are considered as a super saturated system but in drug solution, the saturation limit is quite below, so the supersaturated state facilitates the partitioning of drug into the SC (39).

Table 3: *Amount of Cyclosporin A permeated from the control and SLNs in the SC, Epidermis + Dermis and Receptor.*

Formulation	SC (µg/cm^2)	E+D (µg/cm^2)	Receptor (µg/cm^2)
Control	30±3,45	2,5±1,7	0,9±0,04
Cys A SLNs	150,89±4,0	13±2,6	0,1±0,02

3.2.2. CLSM Studies

Fluorescence microscopy imaging (CLSM) was used to visualize the distribution and penetration depth of our SLNs through the skin. It is clearly visible in Figure 3 that the SLNs were found to be concentrated into the superficial layer of the skin as compared to control formulation. This was a further confirmation of tape stripping test results. Therefore, it can be concluded that trehalose oleate solid lipid nanoparticles mainly followed transfollicular route for their penetration into the skin layers and the results are in accordance with the previous finding which used other nanoparticulate drug carriers for the topical delivery (40, 41). However, the mechanism by which such particulate formulations facilitate skin transport remains ambiguous and although more experiments are needed to help us completely understand the penetration mechanism, this study represents a step forward in the study of skin absorption. In fact, it is possible to foresee synthesized particles that have been designed specifically to target the skin.

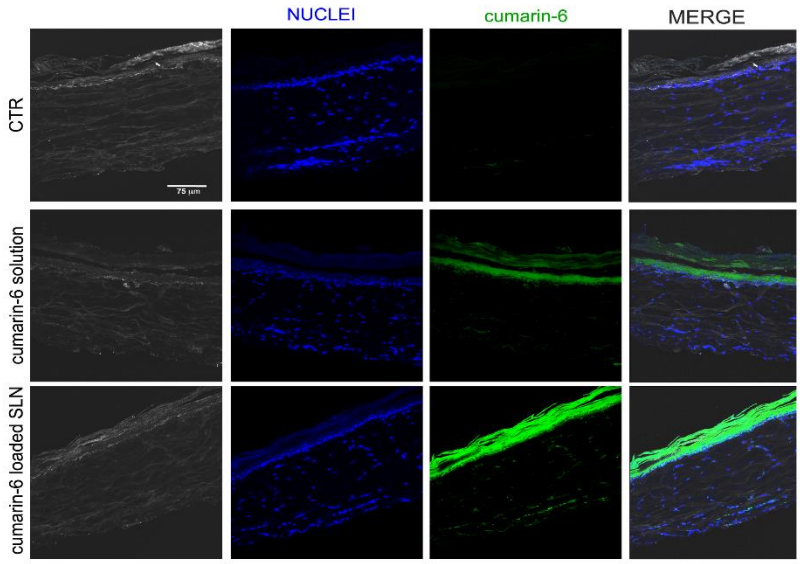

Figure 3: *Confocal imagine of trealose oleate SLNs (CTR), Cumarin-6 solution and SLNs containing cumarin-6.*

4. Conclusions

Trehalose oleate SLNs efficiently encapsulate cyclosporin A and exhibit suitable size for topical administration. The *in vitro* permeation study showed that SLNs increased the amount of cyclosporin A in SC and dermis over control. Localization of SLNs was studied using dye loaded nanoparticles, nanoparticles were found to be concentrated into superficial skin layers. These solid lipid nanoparticles could be effectively used vehicle for the treatment of psoriasis thus avoiding the systemic toxicity of cyclosporin A. However, *in vivo* studies are necessary to evaluate the efficacy and toxicity of this drug delivery system.

References

1. Scheuplein RJ, Blank IH. Permeability of the skin. Physiol Rev. 1971;51(4):702-47.
2. Elias PM, Wakefield JS. Skin barrier function. Nutrition for healthy skin: Springer; 2010. p. 35-48.
3. Noll CR, Noll VM. Protective skin composition. Google Patents; 1998.
4. Cotsarelis G. Epithelial stem cells: a folliculocentric view. Journal of Investigative Dermatology. 2006;126(7):1459-68.
5. Zhang Z, Tsai PC, Ramezanli T, Michniak-Kohn BB. Polymeric nanoparticles-based topical delivery systems for the treatment of dermatological diseases. Wiley Interdisciplinary Reviews: Nanomedicine and Nanobiotechnology. 2013;5(3):205-18.
6. Bowcock A, Krueger J. Getting under the skin: the immunogenetics of psoriasis. 2005. Nat Rev Immunol.5:699-711.
7. Danilenko D. Preclinical models of psoriasis. Veterinary pathology. 2008;45(4):563-75.
8. Bruner CR, Feldman SR, Ventrapragada M, Fleischer Jr AB. A systematic review of adverse effects associated with topical treatments for psoriasis. Dermatology online journal. 2003;9(1).
9. Naldi L, Griffiths C. Traditional therapies in the management of moderate to severe chronic plaque psoriasis: an assessment of the benefits and risks. British Journal of Dermatology. 2005;152(4):597-615.
10. van de Kerkhof P, Vissers WH. Established treatments of psoriasis. Current Drug Targets-Inflammation & Allergy. 2004;3(2):145-56.
11. Colombo M, Cassano N, Bellia G, Vena G. Cyclosporine regimens in plaque psoriasis: an overview with special emphasis on dose, duration, and old and new treatment approaches. The Scientific World Journal. 2013;2013.
12. Berth-Jones J. The use of ciclosporin in psoriasis. Journal of dermatological treatment. 2005;16(5-6):258-77.
13. Choi HK, Flynn GL, Amidon GL. Percutaneous absorption and dermal delivery of cyclosporin A. Journal of pharmaceutical sciences. 1995;84(5):581-3.

14. Duncan J, Wakeel R, Winfield A, Ormerod A, Thomson A. Immunomodulation of psoriasis with a topical cyclosporin A formulation. Acta dermato-venereologica. 1993;73(2):84-7.
15. Gajardo J, Villaseca J. Psoriasis and cyclosporine: an attempt at topical treatment. Revista medica de Chile. 1994;122(12):1404-7.
16. Benson HA, Namjoshi S. Proteins and peptides: strategies for delivery to and across the skin. Journal of pharmaceutical sciences. 2008;97(9):3591-610.
17. Finnin BC, Morgan TM. Transdermal penetration enhancers: applications, limitations, and potential. Journal of pharmaceutical sciences. 1999;88(10):955-8.
18. Jenning V, Gysler A, Schäfer-Korting M, Gohla SH. Vitamin A loaded solid lipid nanoparticles for topical use: occlusive properties and drug targeting to the upper skin. European Journal of Pharmaceutics and Biopharmaceutics. 2000;49(3):211-8.
19. Sivaramakrishnan R, Nakamura C, Mehnert W, Korting H, Kramer K, Schäfer-Korting M. Glucocorticoid entrapment into lipid carriers—characterisation by parelectric spectroscopy and influence on dermal uptake. Journal of Controlled Release. 2004;97(3):493-502.
20. Souto E, Wissing S, Barbosa C, Müller R. Development of a controlled release formulation based on SLN and NLC for topical clotrimazole delivery. International Journal of Pharmaceutics. 2004;278(1):71-7.
21. Müller R, Petersen R, Hommoss A, Pardeike J. Nanostructured lipid carriers (NLC) in cosmetic dermal products. Advanced drug delivery reviews. 2007;59(6):522-30.
22. Richards A, Krakowka S, Dexter L, Schmid H, Wolterbeek A, Waalkens-Berendsen D, et al. Trehalose: a review of properties, history of use and human tolerance, and results of multiple safety studies. Food and Chemical Toxicology. 2002;40(7):871-98.
23. Vassiliou EK, Gonzalez A, Garcia C, Tadros JH, Chakraborty G, Toney JH. Oleic acid and peanut oil high in oleic acid reverse the inhibitory effect of insulin production of the inflammatory cytokine TNF-α both in vitro and in vivo systems. Lipids in Health and Disease. 2009;8(1):25.

24. Parthasarathy S, Khoo JC, Miller E, Barnett J, Witztum JL, Steinberg D. Low density lipoprotein rich in oleic acid is protected against oxidative modification: implications for dietary prevention of atherosclerosis. Proceedings of the National Academy of Sciences. 1990;87(10):3894-8.
25. Gasco M. Solid Lipid Nanospheres from Warm Micro-Emulsions: Improvements in SLN production for more efficient drug delivery. Pharmaceutical Technology Europe. 1997;9:52-8.
26. Provencher SW. CONTIN: a general purpose constrained regularization program for inverting noisy linear algebraic and integral equations. Computer Physics Communications. 1982;27(3):229-42.
27. Wang D-P, Lin C-Y, Chu D-L, Chang L-C. Effect of various physical/chemical properties on the transdermal delivery of cyclosporin through topical application. Drug development and industrial pharmacy. 1997;23(1):99-106.
28. Lopes LB, Collett JH, Bentley MVL. Topical delivery of cyclosporin A: an in vitro study using monoolein as a penetration enhancer. European journal of pharmaceutics and biopharmaceutics. 2005;60(1):25-30.
29. Jain S, Mittal A, K Jain A. Enhanced topical delivery of cyclosporin-A using PLGA nanoparticles as carrier. Current Nanoscience. 2011;7(4):524-30.
30. Escobar-Chavez JJ, Merino-Sanjuán V, López-Cervantes M, Urban-Morlan Z, Pinon-Segundo E, Quintanar-Guerrero D, et al. The tape-stripping technique as a method for drug quantification in skin. Journal of pharmacy & pharmaceutical sciences. 2008;11(1):104-30.
31. Lopes LB, Ferreira DA, de Paula D, Garcia MTJ, Thomazini JA, Fantini MC, et al. Reverse hexagonal phase nanodispersion of monoolein and oleic acid for topical delivery of peptides: in vitro and in vivo skin penetration of cyclosporin A. Pharmaceutical research. 2006;23(6):1332-42.
32. Neises B, Steglich W. Simple method for the esterification of carboxylic acids. Angewandte Chemie International Edition. 1978;17(7):522-4.
33. Yee G, Gmur D, Kennedy M. Liquid-chromatographic determination of cyclosporine in serum with use of a rapid extraction procedure. Clinical chemistry. 1982;28(11):2269-71.

34. Verma D, Fahr A. Synergistic penetration enhancement effect of ethanol and phospholipids on the topical delivery of cyclosporin A. Journal of Controlled Release. 2004;97(1):55-66.
35. Hamel A, Hubler F, Carrupt A, Wenger R, Mutter M. Cyclosporin A prodrugs: design, synthesis and biophysical properties. Chemical Biology & Drug Design. 2004;63(2):147-54.
36. Guterres SS, Alves MP, Pohlmann AR. Polymeric nanoparticles, nanospheres and nanocapsules, for cutaneous applications. Drug target insights. 2007;2:147.
37. Alvarez-Román R, Naik A, Kalia Y, Guy RH, Fessi H. Skin penetration and distribution of polymeric nanoparticles. Journal of Controlled Release. 2004;99(1):53-62.
38. Labouta HI, El-Khordagui LK, Kraus T, Schneider M. Mechanism and determinants of nanoparticle penetration through human skin. Nanoscale. 2011;3(12):4989-99.
39. Barry BW. Novel mechanisms and devices to enable successful transdermal drug delivery. European journal of pharmaceutical sciences. 2001;14(2):101-14.
40. Rolland A, Wagner N, Chatelus A, Shroot B, Schaefer H. Site-specific drug delivery to pilosebaceous structures using polymeric microspheres. Pharmaceutical research. 1993;10(12):1738-44.
41. du Plessis J, Egbaria K, Ramachandran C, Weiner N. Topical delivery of liposomally encapsulated gamma-interferon. Antiviral research. 1992;18(3-4):259-65.

(*) Trombino S, Mellace S, Russo R, Cassano R. Solid Lipid Nanoparticles for Cyclosporin A Topic Release.(Manuscript in submission phase).

SECTION 3

"NATURAL AND SYNTHETIC POLYMERS FOR THE PREPARATION OF BIOMEDICAL MATERIALS"

Part A: Hemostatic Gauze Based on Chitosan and Hydroquinone: Preparation, Characterization and Blood Coagulation Evaluation.

Part B: Application of *in vitro* and *in silico* methods for the accurate and efficient prediction of human pharmacokinetics following transdermal administration.

PART A

"Hemostatic Gauze Based on Chitosan and Hydroquinone: Preparation, Characterization and Blood Coagulation Evaluation"(1)

Abstract

This work concerns on the preparation and performance evaluation of a new chitosan hydroquinone based gauze for hemostatic use. Chitosan and hydroquinone were firstly connected by etherification and then linked to the pre-carboxylate gauze. The functionalized material and the chitosan-hydroquinone ether were characterized by Fourier transform infrared (FT-IR) spectroscopy and differential scanning calorimetry (DSC). FT-IR results showed that an esterification occurred on gauze carboxylic group. The gauze functionalization degree was also evaluated by volumetric analysis. The ether hydroquinone content was obtained by the Folin test. Moreover, the linkage between hydroquinone and chitosan was confirmed by nuclear magnetic resonance (NMR). The hemostatic activity of functionalized gauze was evaluated by dynamic blood clotting assays. Obtained results showed that the prepared material can shorten the blood clotting time and induce the adhesion and activation of platelets. Finally, the new gauze swelling characteristic was evaluated to confirm its high capacity to absorb the blood.

Keywords: *gauze, chitosan, hydroquinone, functionalization, hemostatic.*

1. Introduction

Uncontrolled hemorrhage related to the traumatic event is often the major cause of complications and death, so the use of hemostatic agents may be one of the easiest and most effective methods of treating this phenomenon (2-5). Substantial blood loss predisposes individuals to hypothermia, coagulopathy, acidosis, infection, and multiple organ failure (3-9). Several hemostatic agents have been developed, to control the hemorrhage, and evaluated in animal models. Investigations produced inconsistent and conflicting results regarding the effectiveness of hemostatic agents in controlling hemorrhage, which indicate the need for additional investigation (10-19). In general, the blood coagulation with the use of clamps, compression with plain dressing pads, and suturing of blood vessels is deemed inadequate. Laser coagulation procedures have also shown limited success because of extensive damage to the surrounding tissues. Commercially available dressings are made of materials such as cotton, alginate, and chitosan material (10, 20-22). The cotton simply exerts a pressure action. Instead, chitosan may induce the adhesion of erythrocytes with its amino groups or forming a three-dimensional network structure in blood that captured erythrocytes and then aggregated (23, 24). Also hydroquinone is used to promote the coagulation process. It is involved in the coagulation cascade replacing the reduced vitamin K (KH_2) in the process of activation of the vitamin K-dependent factors. In fact, the hydroquinone represents the biologically active portion of this vitamin. During the carboxylation reaction, part of the vitamin K which is converted from the reduced form to the oxidized (epoxide) is represented by the hydroquinone nucleus (25).

So the hydroquinone, as an analogue of the natural vitamin K, can act as a cofactor of the enzyme γ-glutamyl carboxylase and further favor the process of coagulation. In this context fits our work and has the aim to substitute traditional gauze, impregnated with coagulating agents, with a gauze covalently linking hemostatic agents. In particular, a cotton gauze functionalized with chitosan and hydroquinone was prepared and characterized. The characteristics and blood coagulation properties of this

new hemostatic material, that cut down the well-known free hydroquinone toxicity since it is covalently linked, were investigated (Figure 1) (26).

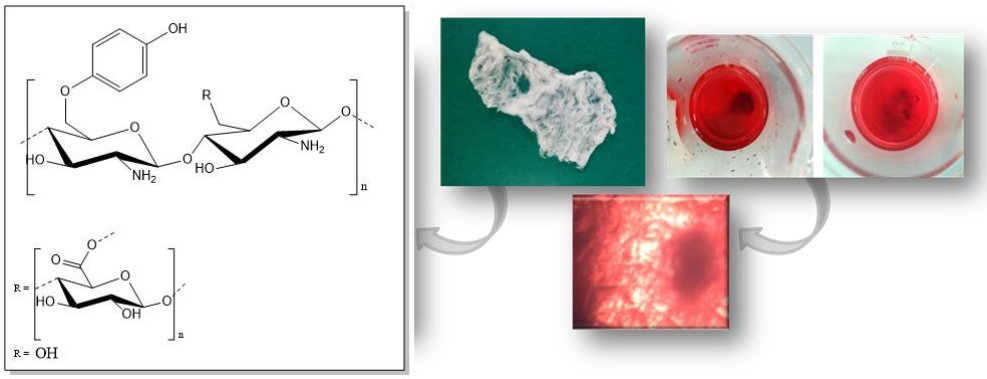

Figure 1. *Schematic representation of hemostatic gauze chitosan-hydroquinone based.*

2. Materials and Methods

2.1 Chemicals

Hydroquinone, chitosan, sodium nitrite ($NaNO_2$), sulfuric acid (H_2SO_4), orthophosphoric acid 85% (H_3PO_4), formic acid 85% (HCOOH), dimethylacetamide (DMAc), lithium chloride (LiCl), dipyperidine - azodicarboxylate (ADDP), tributylphosphine (Bu_3P), hydrochloric acid (HCl), sodium hydroxide (NaOH), sodium carbonate anhydrous (Na_2CO_3), Folin-Ciocalteu reagent, borate buffer (pH 8.5 H_3BO_3 0.1M NaOH 1M) and phosphate saline buffered P-5368 (PBS, pH 7.4 NaCl 0.138 M-KCl 0.0027M) were purchased from Sigma-Aldrich (Sigma Chemical CO, St. Louis, MO). Dichloromethane, acetone, ethyl ether, ethanol, methanol phenolphthalein salt, methyl red, methylene blue were purchased from Carlo Erba (Milan, Italy). Gauze hydrophilic master aid dermatess (100% cotton) was purchased from Pietrasanta Pharma. Type 20 Title 12/8 F.U. Size 10 x 10cm.

2.2 Instrument

The FT-IR spectra were performed using a spectrometer Jasco 4200. ^{1}H-NMR spectra were obtained by the use of a spectrophotometer Burker VM30; the chemical shifts were expressed as δ and referring to the solvent. The UV-VIS spectra have been realized by means of UV-530 spectrophotometer JASCO. The samples were lyophilized using "Freezing-drying" Micro Modulyo, Edwards. The differential scanning calorimetry (DSC) was performed with the PC NETZSCH DSC 200 instrument. Micrographies were obteined by optical microscope Laborlux 12 Pol by Leitz and by Scanning Electron Microscopy (SEM) FEI QUANTA 200, FEG (Field Emission Gun).

2.3 Derivatization of chitosan with hydroquinone

In a three-necked flask fitted with dropping funnel, refrigerant and magnetic stirrer, accurately flamed and under nitrogen stream, sulfuric acid (24 ml) and chitosan (0,6 g) were added. Then, was added hydroquinone (0,5 g) and sodium nitrite (0,0156 g) at room temperature, under magnetic stirring, for 72 hours (27). After that there was the separation of the two phases, aqueous and organic, by means of a separating funnel. The organic phase was dried, the aqueous one was neutralized with sodium hydroxide, frozen, and then lyophilized to recover the solid product. It was characterized by FT-IR, ^{1}H-NMR and DSC.

2.4 Test for the determination of total polyphenols

This test allows to determine the polyphenol content in the sample, in particular the content of hydroquinone that is related to chitosan. The method used for this test is a colorimetric assay based on an experimental procedure recommended by the European Pharmacopea (28).

At first, was prepared a solution (1g/L) in distilled water. Then 2 ml of this solution were transferred into a volumetric flask, containing 10 ml of distilled H_2O, 1 ml of Folin-Ciocalteu reagent and 12 ml of solution at 10.75% of anhydrous sodium carbonate. After 30 minutes the absorbance of the solution was determined by UV-Vis spectrophotometer at a wavelength of 800 nm ($A=1.4\cdot10^{-3}$, $\varepsilon= 0.004$ $mol^{-1}Lcm^{-1}$). A sample of distilled H_2O

was used as white. The hydroquinone content was calculated according to the Lambert-Beer Law.

2.5 Gauze carboxylation

To facilitate the connection between the gauze and the other biologically active substances, it is necessary to accomplish before the gauze carboxylation (29).

In a three-necked flask fitted with dropping funnel, refrigerant and magnetic stirrer, accurately flamed under nitrogen current, the gauze (1 g) and the H_3PO_4 85% (40 ml) were added. After about 1 hour was added sodium nitrite (3 g), shaking vigorously the solution for 5 min. The mixture was left without stirring for about 2 hours. Three addition of sodium nitrite were performed by repeating the same procedure. After 45 min, it was added formic acid (10 ml) to neutralize the excess of sodium nitrite. The product was precipitated with ice ethyl ether (400 ml) and acetone (100 ml).

Subsequently, the obtained gauze was washed with distilled water (100 ml) and with ethanol (100 ml). The product obtained was dried under vacuum and characterized by FT-IR. The gauze after the carboxylation reaction remained intact and white.

2.6 Determination of carboxylic groups content

The carboxylated gauze (0.05 g) was suspended in a mixture formed by a borate buffer (2.5 ml) at pH 8.5 and a methylene blue aqueous solution (2.5 ml, 300 mg/L). Subsequently the suspension was filtered, acidified with1 ml of HCl 0.1 N and distilled water (8 ml) was added (29). The methylene blue content of this solution was determined through a UV-Vis spectrophotometer. The method is based on the binding of the cation of the methylene blue to the carboxylic functions and, therefore, the consequent determination of the decrease of its concentration in the solution. The resulting amount of free unabsorbed methylene blue is calculated and used in the following equation 1 to obtain the content of carboxyl groups:

$$\text{mmol COOH / g dry sample} = \frac{(7.5 - A) \cdot 0.00313}{E} \quad (1)$$

where A is the total amount of free methylene blue in milligrams; E is the weight of the dry sample in grams.

2.7 Derivatization of carboxylated gauze with chitosan-hydroquinone by Mitsunobu reaction

The Mitsunobu reaction allows to obtain esters with high yields starting from a primary or secondary alcohol and a carboxylic acid (30), the carboxylated gauze (0,48 g) was suspended in DMAc (94,2 ml) and LiCl (0,96 g), maintained in a nitrogen flow, and stirred for 30 minutes. Subsequently, were quickly added the ADDP (0,83 g), tributylphosphine (0,806 ml) and the chitosan-hydroquinone (1,40 g). The reaction was conducted at room temperature for 24 hours and under a nitrogen atmosphere. The product obtained was washed with hot methanol (200 ml), then rapidly filtered, dried, and finally characterized by FT-IR. The resulting gauze is white and integrates.

2.8 Determination of the substitution degree (DS)

To calculate the degree of substitution, the functionalized gauze is subjected to basic hydrolysis (29). They were weighed suitable amounts of sample and dissolved in an ethanolic solution of NaOH 0.25M. The mixture is kept under stirring at 100 °C for 24 h. Subsequently, it makes a titration with HCl 0.1N using phenolphthalein as pH indicators for the first equivalence point and the methyl red for the second. The first point is equivalent headline in excess of soda; the second equivalent point indicates the neutralization of the acid salt present. The moles of hydrochloric acid between the first and the second equivalent point corresponding to the moles of free ester. The DS is, therefore, determined by the following equation 2:

$$DS = \frac{\text{MM glucose unit}}{(\text{g sample}/\text{ n free ester}) - \text{MM free ester} - \text{MM } H_2O} \quad (2)$$

where $n_{free\ ester}$ is equal to ($V_{2°\ e.p.}$- $V_{1°\ e.p.}$) * [HCl]; $MM_{glucose\ unit}$ is the molecular mass of glucose unit; g_{sample} the weight of sample; $n_{free\ ester}$ the mol

of free ester; $MM_{free\ ester}$ the molecular mass of free ester and MM_{H2O} the molecular mass of water. The substitution degree was determined by volumetric analysis dispersing an ester derivative in 5 mL of 0.25 M ethanolic sodium hydroxide solution under reflux for 17 h. The dosing, in return of the excess of soda, was realized by titration with HCl 0.1 N (first equivalent point) (31). The moles of chloride acid used between the first and second equivalence correspond to the moles of free esters. The degree of substitution (DS) was determined by the Eq. (1). In this equation MM glucose unit is the molecular mass of a glucose unit; g sample is the weight of the sample; n free ester is the number of moles of free ester; MM free ester is the molecular mass of free ester; and MM H2O is the molecular mass of water.

2.9 Release studies

Chitosan-hydroquinone gauze (0.01215 g), previously washed, was placed in a flask containing 10 mL of PBS. The flask was put in a water bath at 37 °C under stirring. At predetermined time intervals (30min, 1h, 2h), 5 ml of supernatant was removed and the medium was replaced with fresh solution to maintain the same total volume throughout the study. The chitosan-hydroquinone concentration was monitored by the use of UV-Vis spectrophotometry at 260 nm, chitosan-hydroquinone complex wavelength, (ε chi-hydro = 1715 $mol^{-1}Lcm^{-1}$) using PBS as blank.

***2.10 In vitro* whole blood clotting test**

The *in vitro* coagulation test was carried out to evaluate whether the functionalized gauze increase the rate of blood clotting on the blood coagulation activation (32, 33). Pieces of dry material cut into 1cm x 1cm were placed in the glass flasks. Next, 0.25 mL of rat whole blood (containing the anticoagulant citrate dextrose at a 1:6 ratio) was slowly dispensed onto the surface of the dressings.

The blood was collected at the end of the sacrifice during the experiments performed by Prof. Cerra. Prof. Cerra is responsible of a scientific project supervised and approved by the local ethical committee and by Ministery of the Health in accordance with the Guide for the Care and Use of Laboratory

Animals published by the US National Institute of Health (publication No. 85–23, revised 1996) and in accordance with the Italian law (DL 26/14, 2014).

The flasks containing the samples were incubated at 37 ° C. After a predetermined amount of time (30, 60, 90, 120 or 180 s), 20 mL of distilled water were carefully added by dripping water down the inside wall of flasks, preventing disruption of the clotted blood. Red blood cells that were not entrapped in the clot were haemolysed with distilled water and the absorbance of the resultant haemoglobin solution was measured at 540 nm. The absorbance of 0.25 mL of whole blood in 20 mL of distilled water was used as a reference value. The flasks containing the samples were then incubated at 37°C. After a predetermined times intervals (30, 60, 90, 120 and 180 s), 20 mL of distilled water was added along the inside wall of the flasks, by preventing the breakdown of coagulated blood. The red blood cells that have not been trapped in the clot were hemolyzed with the distilled water and the resulting hemoglobin solution was measured in a UV-Vis spectrophotometer at a wavelength of 540 nm. The absorbance of 0.25 mL of whole rat blood in 20 mL of distilled water was used as the reference value. 4 mL of distilled water are used as white (n=6). The pieces of gauze, after blood absorption, were observed by optical microscope and scanning electron microscope (SEM), to highlight the formation of clots.

2.11 Swelling test

The affinity of the derivatized gauze towards the aqueous environment was determined by their swelling degree (% WR) in Na_2HPO_4 (PBS) phosphate buffer. Pieces of dry material (1cm x 1cm) were put in contact with 6 mL of PBS solution at pH 7.4 (to simulate the physiological environment) at the temperatures of 37° C for two hours. Subsequently the wet weight (Wwet) of swollen gauze was measured and then the gauze was freeze-dried and weighed (Wdry). The gauze water content was calculated using the following equation 3:

$$\text{WC } \mathbf{\%} = \frac{\text{Wwet - Wdry}}{\text{Wwet}} \cdot 100 \quad (3)$$

Where WC is the water content of the derivatized gauze, W_{wet} is the weight of the wet gauze (0.188 g) and W_{dry} is the weight of the gauze after lyophilization ($5.74 \cdot 10^{-3}$ g).

2.12 Statistical analysis

All quantitative data were expressed as means ± standard deviations. Differences between means were analysed for statistical significance using the Student's t test. P-values less than 0.05 were considered statistically significant.

3. Results

Chitosan and hydroquinone have been covalently linked by etherification reaction. The obtained ether was characterized by infrared spectrophotometry (FT-IR), which confirmed the successful derivatization. In particular, it was observed the presence of a new band, absent in both the spectra of the starting substances, to 1132 cm^{-1} due to the asymmetric stretching of the C-O-C, and two bands at 3056 cm^{-1} and 3103 cm^{-1} attributable to the stretching of hydroquinone CH. The product achieved was also subjected to differential scanning calorimetry (DSC) evaluation, that revealed the absence of the typical endothermic peaks of chitosan (265 °C) and hydroquinone (172 °C) and the presence of a new peak at 267 ° C. The formation of the ether linkage between the chitosan and the hydroquinone was confirmed, moreover, by means of nuclear magnetic resonance spectroscopy. ^{1}H-NMR ($CDCl_3$) δ (ppm): 6.85-6.80 (m), 4.70-4.21 (m), 3.73-3.10 (m), 2.81-2.71 (m). Finally, through the test for the determination of total polyphenols (TP) was traced, by analysis to the UV-Vis spectrophotometer, the content of hydroquinone linked to chitosan.

This value, calculated after assessment of the absorbance at a wavelength of 800 nm, was equal to 0.15 g of hydroquinone per gram of ether. The ether, adequately characterized, was subsequently used to prepare a functionalized gauze (Fig. 2).

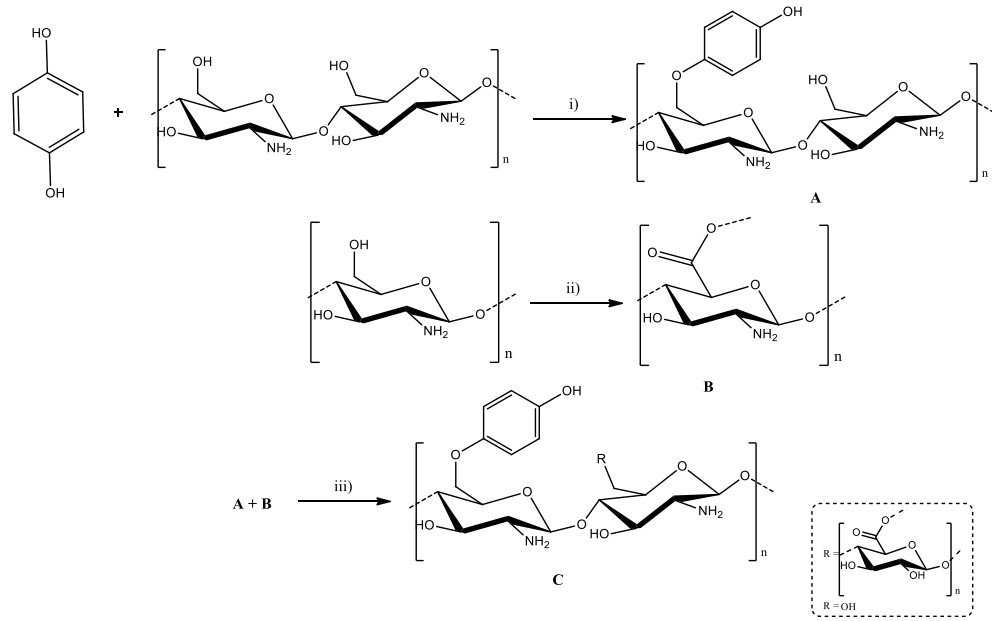

Figure 2. *Scheme of hemostatic gauze preparation. Reaction conditions: i) $NaNO_2$, H_2SO_4; iii) H_3PO_3, $NaNO_2$, HCO_2H; iii) DMA, LiCl, ADDP, Bu_3P.*

Briefly, the gauze was initially carboxylated and characterized. The quantitative analysis of the carboxy groups (27), has revealed a content of 0.469 to 50 mg of gauze. The FT-IR spectrum showed the presence of a new band at 1725 cm^{-1} due to the acid stretching vibration of C=O (Fig. 3 curve b). After carboxylation the gauze was esterified with ether derivative and characterized by FT-IR and DSC. In particular, the FT-IR spectrum of the functionalized gauze (c) was compared with non- derivatized (a) and the carboxylated (b) ones (Fig. 3).

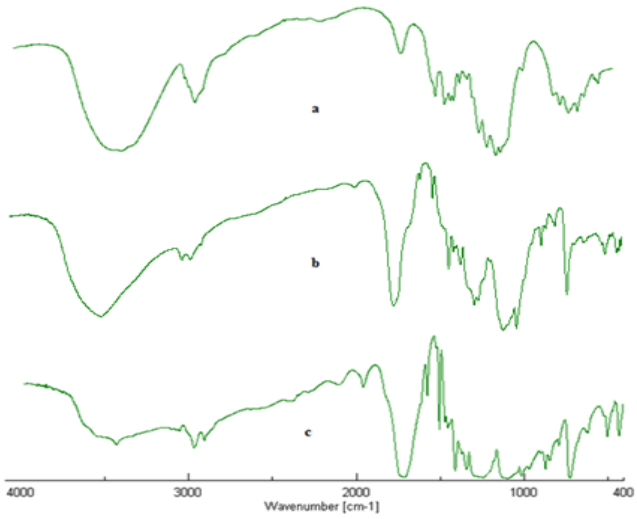

Figure 3. *FT-IR of not derivatized gauze (a); carboxylated gauze (b); functionalized gauze (c).*

From the obtained data it appears the presence of a new band at 1712 cm^{-1} attributable to the vibration of C=O of the ester stretching, and the presence of a vibrations between 3030 cm^{-1} and 3110 cm^{-1} attributable to the stretching of the CH of hydroquinone benzene ring. Furthermore, a quantitative study of the ester groups, for volumetric analysis, was performed by determination of the substitution degree (DS) which is equal to 0.71.

In figure 4 are shown the DSC curves of non derivatized gauze (a), gauze + ether mixture (b), functionalized gauze (c) carboxylated gauze (d) and ether (chi-hydro) (e) respectively. The derivatized gauze not shows an endothermic peak at 249.7 ° C (curve a) which is also present in the curve b gauze + ether mixture which, in addition, show the peak relating to the transition of the ether to 267 ° C, as confirmed by the curve. Relatively to the derivatized gauze, the DSC spectrum reveals the absence of the ether transition peak and a similar trend to that of the non-derivatized gauze and the carboxylated gauze (250.1 °C, curve d) having a transition peak at 246.5 ° C (curve c).

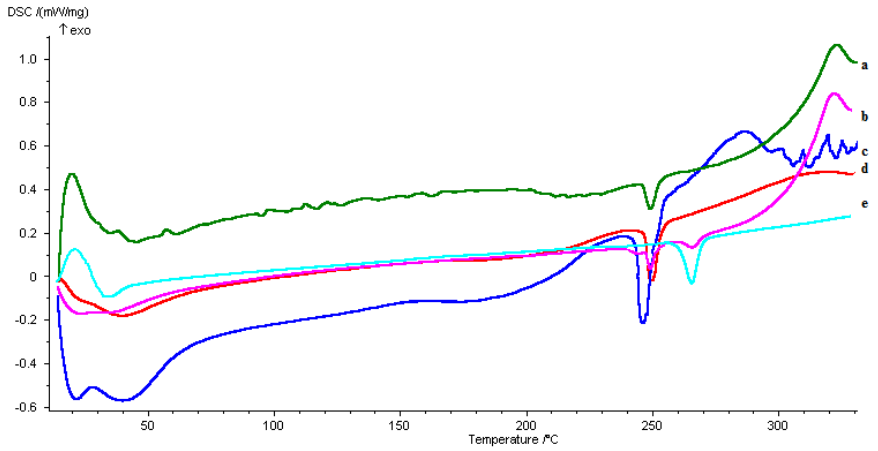

Figure 4. *Curve DSC gauze non derivatized (a); gauze + ether mixture (b), functionalized gauze (c), carboxylated gauze (d) and ether (chi-hydro) (e).*

The purpose of this test was to verify the absence of chitosan-hydroquinone complex release from gauze. At predetermined times intervals the samples were analyzed by UV-Vis spectrophotometer at a wavelength of 260 nm (See chapter 2, Materials and Methods). There was no absorption of the ether chitosan-hydroquinone at this wavelength. Therefore, it is possible to confirm the absence of ether release from gauze.

The blood-clotting test was performed *in vitro* using rat whole blood and the derivatized gauze with chitosan-hydroquinone. This test was conducted to evaluate the effect of functionalized gauze on the activation of blood coagulation. In particular, the rat whole blood was at first dispersed onto pieces of gauze. After a predetermined times the gauze was added with an appropriate volume of distilled water in order to hemolyze the red blood cells that have not been trapped in the clot. The absorbance of the solution was measured by UV-Vis spectrophotometer at a wavelength of 540 nm. The absorbance of 0.25 mL of whole blood in 20 mL of distilled water was used as the reference value. A high absorbance value indicates a slower rate of coagulation.

Derivatized gauze showed a lower absorbance value compared to the reference sample, also the absorbance value of the dressing decreases significantly over time (30-180 s).

In Table 1 are showed the absorbance values of the hemoglobin solutions of the various samples measured in a spectrophotometer.

Sample	Time (sec)	Absorbance
Gauze	*30*	*0.741*
Functionalized gauze+blood	*30*	*0.720*
	60	*0.464*
	90	*0.425*
	120	*0.388*
	180	*0.276*

Table 1. *Absorbance values of hemoglobin solutions of the various samples.*

The pieces of gauze used to carry out the coagulation test were observed at the optical microscope both immediately after the test, both after having been dried for one night at 37 ° C in a stove. The optical micrographs showed in the figure 5 confirm the occurred coagulation at different selected times. In particular, it is possible to observe the interaction between the gauze and blood resulted immediately in a dark-brown or black mass at each evaluated time.

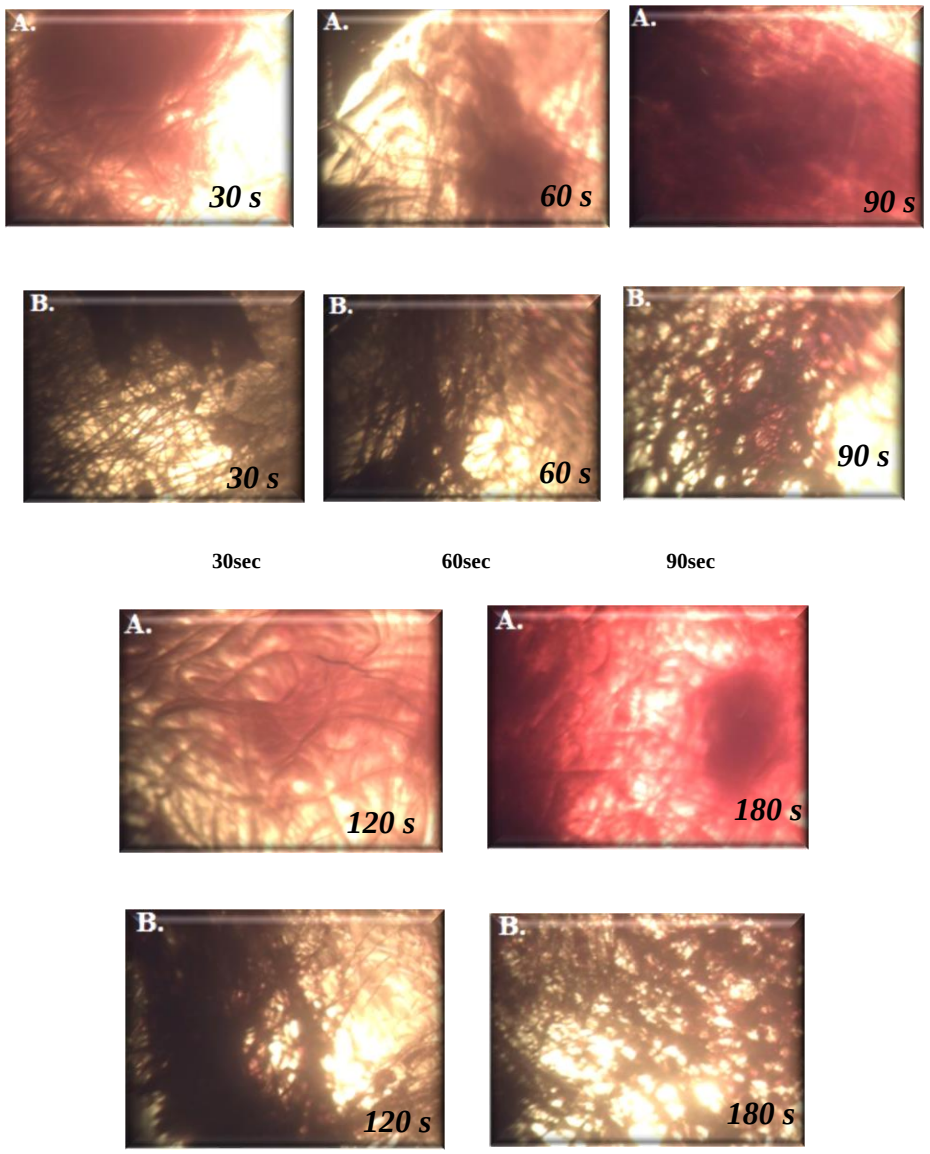

Figure 5. *Optical micrographs of wet (A) and dry (B)gauze.*

The gauze observations, by means of a scanning electron microscope (SEM), after absorption of rat whole blood (180 s), revealed the presence of various red blood cells that adhere strongly on the gauze surface. In particular, red blood cells were bound to each other and formed the aggregated mass (Fig. 6).

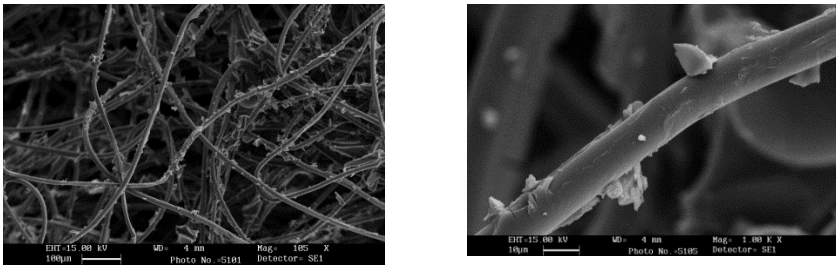

Figure 6. *Scanning electron micrographs of derivatized dry gauze after 180 s exposure to blood.*

The gauze exhibits a considerable content of water equal to 97%. A high swelling degree should correspond to a greater exposure of the coagulants substances (chitosan and hydroquinone) to the blood. The obtained result is in line with the coagulation tests and supports the high capacity of the functionalized gauze to absorb blood and the maintenance, after the coagulation tests, of its original shape favoring the acceleration of coagulation and adhesion of red blood cells and platelets.

4. Discussions

The aim of this work was the synthesis, characterization and performance evaluation of a new hemostatic gauze linking chitosan and hydroquinone. These substances were firstly connected by etherification reaction and then linked to the pre-carboxylate gauze. The functionalized material and the chitosan-hydroquinone ether were characterized by FT-IR spectroscopy and differential DSC. FT-IR results showed that an esterification occurred on gauze carboxylic group. The gauze functionalization degree was also evaluated by volumetric analysis. The ether hydroquinone content was obtained by the Folin test. Moreover, the linkage between hydroquinone and chitosan was confirmed also by nuclear magnetic resonance (NMR). Dynamic blood clotting test showed that this new material can shorten the clotting time. It may be related to platelet aggregation and also to the large amount of plasma absorbed due to the gauze swelling capacity. In addition,

the prepared gauze could cut down the well-known free hydroquinone toxicity, since it is covalently linked, and could decreases the complications connected to the uncontrolled hemorrhage. Actually, various literature data report about various hemostatic agents chitosan based (34) useful for quickly controlling external bleeding when traditional measures such as pressure or simple gauze fail (35). They are available as powder, granules or coated gauze of this material. The granulate formulation is useful specially to stop bleeding in case of deep and difficult wounds. The chitosan-coated gauze allows a more effective application of the hemostatic agent on the origin of hemorrhage. Over the last 10 to 15 years, a number of in vitro and in vivo studies have evaluated the efficacy and safety of these hemostatic products. They were authorized in 2006 by the Food and Drug Administration (FDA) for emergency treatment in case of external bleeding (36, 37). They act independently of the classical coagulation mechanism, work under hypothermia, are effective in patients who take anticoagulants or platelet aggregates and do not cause damage to the surrounding tissue (38). The mechanism of the hepatic effect of chitosan is independent of the classic coagulant waterfall. It has been shown that the hemostatic action of the polymer appears to be related to its cationic nature. Most biological cell surfaces are of anionic nature, so it has been hypothesized that chitosan strongly adheres to tissues at the site of the wound through electrostatic interactions (39). Feng et al. (40) have reported about bioabsorbable, water-soluble hemostatic cellulose based gauze matrix structures, including one or more species of chitosan, etherized cellulose, nonionic surfactant, water-soluble polysaccharide hydrocolloid and/or gum stopping rapidly the bleeding. In addition, Englehart et al. (41) have compared highly porous silica and chitosan-based dressing (TraumaStat) to commercial HemCon in a severe groin injury model in swine. Results showed that TraumaStat was superior to HemCon and gauze dressings in controlling bleeding from a severe groin injury. TraumaStat may be a better hemostatic dressing for control of active hemorrhage than current standards of care. All the described materials are, actually, not comparable to the one prepared in this work that it is made of cellulose, chitosan and hydroquinon covalently linked to have a synergic effect due to the simultaneous presence of chitosan and

hydroquinone, an analogue of the natural vitamin K, that favors the process of coagulation too.

5. Conclusion

This work was aimed at the preparation of a functional gauze linking coagulant substances, useful as a topical haemostatic agent for the treatment of bleeding wounds. The idea of functionalizing the cotton gauze was born from the lack of biomaterials covalently bound with biologically active molecules. So far, in fact, the gauzes have been manufactured and marketed simply impregnated with substances that favor blood clotting. Therefore, a cotton gauze has been derivatized that, despite the chemical treatments suffered during the preparation phase, preserves the structural integrity and the hemostatic activity of the related molecules. In this regard, the coagulant substances, chitosan and hydroquinone, were first linked by a etherification reaction. The ether obtained, characterized by FT-IR, ^{1}H-NMR, DSC and Folin test, was used to derivatize the previously-carboxylated gauze. This last has been, therefore, appropriately characterized by FT-IR, DSC and, through volumetric analysis, the degree of substitution (DS) was evaluated. In addition other studies have been carried out to show that covalently linked gauze molecules are not released, and in vitro tests to evaluate hemostatic activity and water content. The obtained results show that the functionalized gauze has excellent coagulant activity due to its ability to absorb large amounts of blood thus favoring the concentration of blood cells in the hemorrhage site and thus facilitating adhesion of platelets and globules red. This is confirmed by the observations of functionalized gauze, after the coagulation test, at the optical microscope and the electronic scanning microscope, which allowed to highlight the presence of clots on the same.

References

1. Cassano R, Di Gioia ML, Mellace S, Picci N, Trombino S. Hemostatic gauze based on chitosan and hydroquinone: preparation, characterization and blood coagulation evaluation. Journal of Materials Science: Materials in Medicine. 2017;28(12):190.
2. Bellamy RF. The causes of death in conventional land warfare: implications for combat casualty care research. Military medicine. 1491984. p. 55-62.
3. Moore F, Moser K, Read R, Pons P. EPIDEMIOLOGY OF TRAUMA DEATHS: A REASSESSMENT. Journal of Trauma and Acute Care Surgery. 1993;35(1):170.
4. Sauaia A, Moore FA, Moore EE, Haenel JB, Read RA, Lezotte DC. Early predictors of postinjury multiple organ failure. Archives of surgery. 1994;129(1):39-45.
5. Champion HR, Bellamy RF, Roberts CP, Leppaniemi A. A profile of combat injury. Journal of Trauma and Acute Care Surgery. 2003;54(5):S13-S9.
6. Asensio JA, Petrone P, O'Shanahan G, Kuncir EJ. Managing exsanguination: what we know about damage control/bailout is not enough. Proceedings (Baylor University Medical Center). 2003;16(3):294.
7. Mabry RL, Holcomb JB, Baker AM, Cloonan CC, Uhorchak JM, Perkins DE, et al. United States Army Rangers in Somalia: an analysis of combat casualties on an urban battlefield. Journal of Trauma and Acute Care Surgery. 2000;49(3):515-29.
8. Cosgriff N, Moore EE, Sauaia A, Kenny-Moynihan M, Burch JM, Galloway B. Predicting life-threatening coagulopathy in the massively transfused trauma patient: hypothermia and acidoses revisited. Journal of Trauma and Acute Care Surgery. 1997;42(5):857-62.
9. Heckbert SR, Vedder NB, Hoffman W, Winn RK, Hudson LD, Jurkovich GJ, et al. Outcome after hemorrhagic shock in trauma patients. Journal of Trauma and Acute Care Surgery. 1998;45(3):545-9.
10. Alam HB, Burris D, DaCorta JA, Rhee P. Hemorrhage control in the battlefield: role of new hemostatic agents. Military medicine. 2005;170(1):63.

11. MacIntyre AD, Quick JA, Barnes SL. Hemostatic dressings reduce tourniquet time while maintaining hemorrhage control. The American Surgeon. 2011;77(2):162-5.
12. Pusateri AE, Holcomb JB, Kheirabadi BS, Alam HB, Wade CE, Ryan KL. Making sense of the preclinical literature on advanced hemostatic products. Journal of Trauma and Acute Care Surgery. 2006;60(3):674-82.
13. Sondeen JL, Pusateri AE, Coppes VG, Gaddy CCE, Holcomb JB. Comparison of 10 different hemostatic dressings in an aortic injury. Journal of Trauma and Acute Care Surgery. 2003;54(2):280-5.
14. Alam HB, Chen Z, Jaskille A, Querol RILC, Koustova E, Inocencio R, et al. Application of a zeolite hemostatic agent achieves 100% survival in a lethal model of complex groin injury in swine. Journal of Trauma and Acute Care Surgery. 2004;56(5):974-83.
15. Alam HB, Uy GB, Miller D, Koustova E, Hancock T, Inocencio R, et al. Comparative analysis of hemostatic agents in a swine model of lethal groin injury. Journal of Trauma and Acute Care Surgery. 2003;54(6):1077-82.
16. Cox ED, Schreiber MA, McManus J, Wade CE, Holcomb JB. New hemostatic agents in the combat setting. Transfusion. 2009;49(s5).
17. Kozen BG, Kircher SJ, Henao J, Godinez FS, Johnson AS. An alternative hemostatic dressing: comparison of CELOX, HemCon, and QuikClot. Academic Emergency Medicine. 2008;15(1):74-81.
18. Gegel B, Burgert J, Cooley B, MacGregor J, Myers J, Calder S, et al. The effects of BleedArrest, Celox, and TraumaDex on hemorrhage control in a porcine model. Journal of Surgical Research. 2010;164(1):e125-e9.
19. Gegel BT, Burgert JM, Lockhart C, Austin III NCR, Davila CA, Hodges CL, et al. Effects of Celox and TraumaDEX on hemorrhage control in a porcine model. AANA J. 2010;78(2):115-20.
20. Achneck HE, Sileshi B, Jamiolkowski RM, Albala DM, Shapiro ML, Lawson JH. A comprehensive review of topical hemostatic agents: efficacy and recommendations for use. Annals of surgery. 2010;251(2):217-28.
21. Kheirabadi BS, Edens JW, Terrazas IB, Estep JS, Klemcke HG, Dubick MA, et al. Comparison of new hemostatic granules/powders with currently deployed hemostatic products in a lethal model of extremity

arterial hemorrhage in swine. Journal of Trauma and Acute Care Surgery. 2009;66(2):316-28.
22. Kheirabadi BS, Mace JE, Terrazas IB, Fedyk CG, Estep JS, Dubick MA, et al. Safety evaluation of new hemostatic agents, smectite granules, and kaolin-coated gauze in a vascular injury wound model in swine. Journal of Trauma and Acute Care Surgery. 2010;68(2):269-78.
23. Kranokpiraksa P, Pavcnik D, Kakizawa H, Uchida B, Jeromel M, Keller F, et al. Hemostatic efficacy of chitosan-based bandage for closure of percutaneous arterial access sites: An experimental study in heparinized sheep model. Radiology and oncology. 2010;44(2):86-91.
24. Chou T-C, Fu E, Wu C-J, Yeh J-H. Chitosan enhances platelet adhesion and aggregation. Biochemical and Biophysical Research Communications. 2003;302(3):480-3.
25. Brown WH FC, Iverson BL, Anslyn EV Fat-soluble vitamin. In: Organic chemistry2009.
26. Enguita FJ, Leitão AL. Hydroquinone: environmental pollution, toxicity, and microbial answers. BioMed research international. 2013;2013.
27. Gambarotti C, Melone L, Punta C, Shisodia SU. Selective Monoetherification of 1, 4-Hydroquinone Promoted by NaNO2. Current Organic Chemistry. 2013;17(10):1108-13.
28. Blainski A, Lopes GC, De Mello JCP. Application and analysis of the Folin Ciocalteu method for the determination of the total phenolic content from Limonium Brasiliense L. Molecules. 2013;18(6):6852-65.
29. Cassano R, Trombino S, Bloise E, Muzzalupo R, Iemma F, Chidichimo G, et al. New broom fiber (Spartium junceum L.) derivatives: preparation and characterization. Journal of agricultural and food chemistry. 2007;55(23):9489-95.
30. Mitsunobu O, Yamada M. Preparation of esters of carboxylic and phosphoric acid via quaternary phosphonium salts. Bulletin of the Chemical Society of Japan. 1967;40(10):2380-2.
31. Cassano R, Trombino S, Ferrarelli T, Nicoletta FP, Mauro MV, Giraldi C, et al. Hemp fiber (Cannabis sativa L.) derivatives with antibacterial and chelating properties. Cellulose. 2013;20(1):547-57.

32. Chou C-P, Wang Y-C, Chang SJ, Liu P-H, Kuo SM. Evaluation of the effects of chitosan hemostasis dressings on hemorrhage caused by breast biopsy. Breast Care. 2012;7(3):220-4.
33. Kang P-L, Chang SJ, Manousakas I, Lee CW, Yao C-H, Lin F-H, et al. Development and assessment of hemostasis chitosan dressings. Carbohydrate Polymers. 2011;85(3):565-70.
34. Chiara O CM, Chirletti P, Gui D, Pilati P, Seccia M Emostatici Topici nel trauma e in chirurgia d'urgenza.: Edizioni Minerva Medica; 2014. 10-3 p.
35. Brown MA, Daya MR, Worley JA. Experience with chitosan dressings in a civilian EMS system. The Journal of emergency medicine. 2009;37(1):1-7.
36. Dubick MA, Kheirabadi B. New technologies for treating severe bleeding in far-forward combat areas. ARMY INST OF SURGICAL RESEARCH SAN ANTONIO TX, 2010.
37. Seeber P SA. Chemistry of Hemostasis. In: Basics of blood management: (2th ed.) Wiley-Blackwell 2013.
38. Brunton LL CB, Knollmann BC Goodman and Gilman's The Pharmacological Basics of Therapeutics: (12th ed.) The McGraw Hill Companies 2011. 30: 153-76 p.
39. Neveleff DJ, Kraiss LW, Schulman CS. Implementing methods to improve perioperative hemostasis in the surgical and trauma settings. AORN journal. 2010;92(5):S1-S15.
40. Feng V, Hsu D, Yin Y. Bioabsorbable hemostatic gauze. Google Patents; 2006.
41. Englehart MS, Cho SD, Tieu BH, Morris MS, Underwood SJ, Karahan A, et al. A novel highly porous silica and chitosan-based hemostatic dressing is superior to HemCon and gauze sponges. Journal of Trauma and Acute Care Surgery. 2008;65(4):884-92.

PART B

Application of *in vitro* and *in silico* methods for the accurate and efficient prediction of human pharmacokinetics following transdermal administration

Abstract

The aim of this work was to assess the ability of designed dissolvable microneedles (DMN), based on PVA, to enhance and improve the percutaneous delivery of ketoprofen compared with a commercial gel. DMN arrays were characterised with regard to their morphology, mechanical performances, drug content, drug release and stability. In-vitro skin permeation studies were conducted on Franz-type diffusion cells using porcine skin. Results showed that KET-DMN were able to reduce ketoprofen transport lag time and to supply a consistent larger amount of drug compared with the conventional ketoprofen gel. The presented delivery strategy demonstrates potential for enhanced and painless delivery of this drug. In addition, the potential therapeutic outcome of ketoprofen was assessed by using *in silico* modelling. Preliminary data shows that Simcyp® simulation software could be a valuable tool in the screening of promising dermatological formulations. The pharmacokinetic profile of ketoprofen predicted by SKIN-CAD® was shown to be in line with the literature data of human clinical study. These findings set the stage for future human studies of skin medications and biopharmaceuticals for clinical applications.

Keywords: *Ketoprofen, Microneedles, Transdermal, Skin, Dissolvable.*

1. Introduction

Over the last years, transdermal route for drug delivery has proved to offer a wide range of advantages and clinical benefits over the more commonly used dosage forms. Drug delivery directly to the systemic circulation following topical application appears to be a desirable alternative to oral delivery (1). In fact, the skin has a larger surface area, a slow metabolic activity which is especially suitable for drugs that are extensively metabolised by the first pass metabolism and from a clinical perspective it is useful for patients who may not be able to swallow (2). However, the outermost layer of the skin, the stratum corneum, consisting of keratinised epithelial cells in a lipid matrix limits penetration of large drug molecules (i.e. greater than 500 Da) (3). The most common method to overcame this layer is the use of the hypodermic needles. However, the use of this conventional needles is usually associated with emotional trauma, pain and possible needle stick injury (4). Recently, dissolvable microneedles (DMN) have received a great interest as transdermal delivery systems. As the names suggest, DMN are micron-sized needle like structures that breach the stratum corneum barrier and allow drugs access to subcutaneous tissue and systemic circulation. These transdermal systems offers a numerous of advantages including their biocompatible nature and one-step application process which improves patient compliance (5). The encapsulated drug is released into the skin following DMN topical application and their dissolution. However, in order for these processes to be successful, a number of criteria need to be considered in designing the DMN. First, the microneedles must incorporate the drug within a strong biocompatible matrix, without affecting the drug integrity or the strength of the microneedle (6). In addition, in vivo activity of transdermal formulation depends on the bioavailability within the skin at the site of action (7). In this context researchers have given much importance on the assessment of pharmacokinetics of topical formulation, also referred as dermatokinetics. Following a topical application of conventional drug formulation of a topical drug to the skin surface, a few processes occurs in a sequence such as a drug release from the dosage form, its penetration into the skin, permeation through the skin layers and absorption into the systemic circulation in order to reach the target tissues and exhibit the therapeutic responses (8). The

traditional methods for assessing the pharmacokinetics in plasma or urine may not be viable because most of the topically applied drug molecules generally do not produce measurable concentrations in extra cutaneous biological fluids. Regulatory agencies have also been exploring different strategies for the dermatokinetics assessment of topical formulations (9). Several mathematical models have been designed to quantify the drug molecules in the skin layers (10). Dermatokinetics of a drug, hence, determines the efficacy of the treatment. Ketoprofen, a non-steroidal anti-inflammatory drug (NSAID), is among the most commonly administered drugs worldwide. If administered topically, ketoprofen penetrate slowly and in small quantities into the systemic circulation. Hence, its bioavailability and maximal plasma concentration following topical application are generally less than 5% and 15%, respectively (11). On the other hand, ketoprofen has usually a short half-life and several side effects when administered orally, such as gastrointestinal irritation, nausea, dyspepsia and diarrhoea (12). The goal of topical ketoprofen formulations is to minimize systemic adverse effects and improve the compliance. Formulation design can have a dramatic impact on drug penetration into the skin and its permeation depth, consequently affecting the drug absorption rates. Ketoprofen topical products currently available on the market employ permeation enhancers, which may induce skin irritation (13). Therefore, in order to enhance the drug penetration without the need of enhancers, a ketoprofen dissolvable microneedle arrays were prepared in this study and compared to the commercial ketoprofen gel. In addition, the potential therapeutic outcome of ketoprofen was assessed by using *in silico* modelling. Computational models for the prediction of drug plasma levels and bioavailability is increasingly being used for orally administered drugs (14). However, this approach for other administration routes has not been extensively investigated. Preliminary data shows that Simcyp® simulation software appears suitable for prediction of drug plasma levels of oral administration drugs in healthy individuals. Since also the transdermal route can be simulated, this software could be a valuable tool in the screening of promising dermatological formulations (15). Moreover, we used also SkinCad® software, for the *in vitro- in vivo* correlations for topical

preparations, because this software allowing us to make a prediction of clinical study outcome.

2. Materials and method.

2.1. Chemicals

Polyvinyl alcohol 80% hydrolysed (PVA, Mw = 9,000-10,000), ketoprofen, ((RS)-2-(3-benzoylphenyl) propionic acid, Mw = 254.28 M), PBS (Phosphate-buffered saline) and ethanol 96% were sourced from Sigma-Aldrich (Munich, Germany). Silicon moulds and ImmuPatch silicon microneedle arrays were fabricated and provided by the Tyndall National Institute, Cork, Ireland. Ketoprofen 2.5% gel was purchased from a local pharmacy. HPLC-grade acetonitrile and water were purchased from Sigma-Aldrich (Arklow, Ireland). All other chemical reagents were of pharmaceutical grade and used as received.

2.2 Fabrication of Dissolvable Microneedle Arrays

Dissolvable microneedles were fabricated using a micromoulding method at the room temperature (16). The drug solution was prepared by adding 950 µl of 5% w/v PVA aqueous solution into 5mg of ketoprofen previously dissolved in 50 µl of ethanol. PVA was selected for this study as the structural material for the polymer microneedles because it is biocompatible, mechanically strong and highly water soluble (17). Prior to dispensing the drug solution, the silicon moulds with the cavity density of 25 cavities/cm^2 were cleaned with 96% v/v ethanol in a vacuum for 20 minutes, followed by sonication in deionised water for 30 minutes and finally prefilled with fresh deionised water in a vacuum for 2-3 hours. A syringe prefilled with the drug solution was mounted on the Harvard syringe pump and the tubing line with the fuse capillary applicator. The drug solution was then dispensed into the each cavity of the PDMS moulds at a rate of 25 µl/min using the light microscope (Olympus SZ61, PA, USA). A contact angle of 90˚ was maintained between the solution drop and the mould during the whole process. Each cavity was carefully overfilled with the same amount of solution to ensure a strong circular base of resulting DMN and their uniformity. Any moulds not successfully prefilled with water were discarded. The filled moulds were stored in overnight in a vacuum

environment. After 24 hours ketoprofen-loaded DMN (KET-DMN) were removed from the moulds by using an adhesive 3M tape.

2.3 Characterization of Dissolvable Microneedle Arrays

2.3.1. DMN Morphological Properties

Visual characterization of dissolvable microneedles was performed using the light microscope (Olympus SZ61, PA, USA) with an integrated digital camera. The DMN morphological characteristics (i.e. physical integrity, shape and appearance) were analyzed by scoring the individual microneedles on the basis of in house established criteria (Table 1). A score of one represented that there was no microneedle present and four indicated that the microneedle was of the highest standard based on height, shape and point.

Table 1. Criteria for the evaluation of morphological characteristics of dissolvable microneedles (Internal Regulations, School of Pharmacy, UCC, Ireland).

Scoring	Description
1	The presence of only the microneedle base and / or the absence of formation.
2	Incomplete formed microneedle, without top.
3	Fully formed microneedle with irregular shape and / or dull tip.
4	Fully formed microneedle of a proper pyramidal shape and a sharp tip.

2.3.2 DMN Mechanical Performance

TA.XT *plus* Texture Analyser (Stable Micro Systems, Surrey, UK) was used to test the mechanical strength of both KET-DMN and PVA-DMN. Axial fracture force was applied in the microneedle arrays to obtain the DMN failure force. DMN arrays were attached to the moving testing probe of the Texture Analyser using double-sided adhesive tape. The test station pressed DMN array against a flat block of aluminium until the breaking point. Force versus distance curves were acquired. Upon maximum force application, the force suddenly decreased. The point before the sudden force decrease was accepted as the microneedle failure force and confirmed by microscopic evaluation.

2.3.3 Drug Loading Amount

To determine the loading amount of ketoprofen in the microneedle arrays, KET-DMN were placed in an Eppendorf tubes and dissolved in 1ml of the mobile phase for high performance liquid chromatography (HPLC). Sonication which was required for the complete microneedles dissolution, was followed by the solution filtration. The amount of ketoprofen was determined using HPLC as described below (Section 2.6).

2.3.4 DMN Penetration Study

Porcine cadaver ear skin was used as skin model for DMN penetration studies to determine the ability of the microneedles to successfully penetrate the stratum corneum of the skin samples. For this evaluation DMN array 1 × 1 cm was applied onto full-thickness porcine skin *ex vivo* for 5 sec using a vertical in-house made applicator with the force of 10 N. The arrays were left in the skin for either 5 or 15 minutes. After each time-point they were removed and both the skin and the DMN arrays were photographed with a digital camera attached to an inverted light microscope to verify the DMN capacity to pierce the skin and their successful dissolution. Three DMN arrays were used for each time-point.

2.3.5 Short-term Stability Studies

Physical stability of ketoprofen dissolvable microneedles as well as the chemical stability of the drug was assessed for a short period of time. Two time-points (0 and 30 days) and two storage conditions 4°C ± 2°C (low condition) and 40°C ± 2°C, RH 85% ± 5% (accelerated condition) were evaluated. The DMN arrays were placed individually in a hermetically sealed glass vials previously filled with silica gel and cotton wool to avoid humidity. The air was removed by purging the inert gas nitrogen. For the chemical stability a quantitative determination of the drug and its degradation products was analysed using HPLC. For the physical stability DMN appearance, their physical integrity and the percentage reduction in height of microneedles was visually inspected. Results were obtained by evaluating the microneedles on the basis of predetermined criteria described in Section 2.3.1.

2.4. Drug Release Study

In-vitro release profile of ketoprofen from KET-DMN arrays was determined in a medium consisting of PBS:Ethanol, 4:1, at pH 7.4 and 37°C in a water bath. Each array was placed in an Eppendorf tube and immersed in 1ml of release medium. Aliquots were withdrawn at regular time intervals (5 min, 10 min, 15 min, 30 min) and analysed for ketoprofen content using HPLC assay as described in Section 2.6. Release profiles were obtained by plotting time versus percentage of drug released. In addition, two mathematical models were chosen to investigate the ketoprofen release profile from DMN. The ketoprofen release data obtained in the range of 5–30 min were fitted to zero-order kinetics and first-order kinetics to characterise mechanism of drug release (18). The linear regression of the mathematical models was evaluated using squared correlation coefficient (R^2) and used as a criteria for selecting the most appropriate model. Drug release experiments were performed in triplicate, and the mean values and standard deviations (SD) were calculated.

2.5 Skin Permeation Studies

Fresh porcine ears were obtained from a local supplier immediately following the animal's death. After collection, the ears were cleaned and stored at –80°C until the use. Twenty-four hours before the experiment, frozen ear was left for slow thawing at 4°C. The hair, cartilage and subcutaneous fat were carefully removed from the porcine skin and then the skin was washed and visually examined for the integrity. Before use, the thickness of the skin was measured using a varnier caliper (Varnier - Mitutoyo, Japan) and found to be 126 mm. *In-vitro* skin permeation study was performed using static Franz diffusion cells (Perme Gear, Inc., Bethlehem, PA, USA). The skin diffusion area was 3.14 cm^2, and the 15 ml of receptor medium (PBS: ETOH (4:1), pH 7.4) was kept at 37°C and continuously stirred to ensure its homogeneity. Sink conditions in the receptor compartment were maintained considering the saturated solubility of ketoprofen in the medium at 37°C. Following the skin equilibration for 30 min, three DMN arrays were placed on the skin in each Franz cell and again inserted using the custom-made applicator (10 N). Two different experiments were set. In the first study, a ketoprofen solution containing 5

mg of drug was applied onto the skin previously pierced by a silicon ImmuPatch microneedle array, and was used as control. Each ImmuPatch array had 36 microneedles over an area of 1 cm^2, and with the DMN height of 200 μm. In this case the experiment was run for 3 hours. The aim of this first experiment was just to verify if the skin breached with DMN would ensure a better transdermal release of ketoprofen. In the second study, 1mg of ketoprofen 2.5% gel was applied to intact excised porcine skin, to simulate physiological condition, and to be compared with KET-DMN. The purpose of second study was to investigate the behaviour of the commercial gel versus KET-DMN. The second experiment run for 26 hours. The donor compartments were covered with Parafilm (Pechiney Plastic Packaging, Chicago, IL, USA) during the whole experiment to avoid any evaporation and to provide occlusive conditions. In order to determine ketoprofen permeation profile, aliquots (1 ml) were withdrawn from the receptor solution at predetermined time intervals (1, 2, 3, 4, 6, 24 and 26 h) and immediately replaced with equal volumes of the fresh medium to keep the volume constant during the experiment. Cumulative amounts of ketoprofen recovered from the receptor solution over time per area unit were used to calculate the transdermal drug flux (Js, μg/cm^2/h), lag time (Tlag, h), permeability coefficient (Kp, cm/h) and diffusion coefficient (D, cm^2/h). The flux was obtained from the slope of the regression line fitted to the linear portion of the profile, the lag time was determined from the intercept of the plots with the *x*-axis, the permeability coefficient was calculated dividing the flux by the initial concentration and the diffusion coefficient was calculated dividing the square skin thickness by six times the lag time (19) .

2.6 Drug Analyses

The quantification of the drug was performed using a previously developed HPLC method (20)and an Agilent 1200 series HPLC system with a UV/VIS detector (Agilent Technologies, Santa Clara, CA, USA). A reversed phase column (HyperClone C-18, internal pore width 5 μm, 150 mm x 4.6 mm; Phenomenex Ltd, Macclesfield, Cheshire, UK), mobile phase was Water:Acetonitrile (55:45, v/v) at a pH of 2.5, adjusted using phosphoric acid. The flow rate of 1 ml/min and injection volume of 25 μl were employed. Ketoprofen was detected at a wavelength of 233 nm. For the

calibration curve, a series of solutions were prepared from the stock standard solution of ketoprofen (1 mg/ml). The standard curve was found to have linear relationship (r^2 = 0.9999) over the analytical range of 0,19 – 100 μg/ml. For the assessment of the quality and reliability of the obtained results, analytical parameters for validation of the method were considered, according to the ICH guidelines (21). To determine limit of detection (*LoD)* and limit of quantification (*LoQ),* an approach based on the standard deviation of the response and the slope of the representative calibration curve was employed. The *LoD* of a chromatographic method was determined as follows, using Equation. 1:

$$LoD = \frac{3.3\sigma}{S} \quad (1)$$

where σ is the standard deviation of the response (peak area) of the data used to construct the regression line and *S* is the slope of that line. Similarly, the *LoQ* was determined using Equation. 2:

$$LoQ = \frac{10\sigma}{S} \quad (2)$$

Under the stated assay conditions, the retention time of ketoprofen was 5 min. Ketoprofen concentrations were interpolated from the ketoprofen calibration curve using the peak area of the obtained sample chromatogram.

2.7 *In Silico* Modelling

2.7.1 SKIN-CAD® Model Strategy for *in vitro/ in vivo* correlation.

The *in silico* pharmacokinetic-pharmacodynamic (PK-PD) evaluation of transdermal drug delivery was performed using SKIN-CAD® software (Biocom Systems, Inc. Japan - trial version). This software can predict clinical performance using model parameters obtained from *in vitro* skin

permeation studies (22). The simulation provides useful data for designing transdermal and topical drug delivery systems as well as the evaluation of various factors which affect skin permeation and blood concentration of the drug (23). In this work, a study of both ketoprofen skin permeation and its concentration in the blood have been carried out based on a constant delivery model. Mono and bi-layer models have been used with one compartment model to estimate ketoprofen concentration in the blood following topical application in a form of gel or a dissolvable microneedle arrays. The one-compartment model is the simplest pharmacokinetic model which explains the drug transport behaviour with an assumption that the drug concentration equilibrium and distribution occur rapidly. Therefore, it is suitable model to describe the pharmacokinetics of drugs that minimally distribute into the body's tissue (24). Moreover, according to the literature data the one-compartment model is more appropriate for a drug when using transdermal drug delivery (e.g. microneedle arrays) than for oral delivery systems which require longer time for drug dissolution, absorption and distribution (25). Ketoprofen PK parameters for one-compartment model, such as volume of distribution (Vd) and elimination rate constant (Ke), were obtained from literature (26).

When considering ketoprofen delivery from both the dissolvable microneedles and the gel product, the following assumptions are made in this work:

(i) The concentration of ketoprofen in the blood remains low compared to its concentration in the vehicle so the sink conditions are achieved (27).

(ii) Skin binding and metabolism of ketoprofen is assumed to be negligible.

(iii) Ketoprofen molecules that diffuse through the viable skin to the interface between

viable skin and blood microcirculation are taken up by the microcirculation.

(iv) Diffusion through the skin is the rate limiting step in the uptake of ketoprofen. According to Davidson *et al*. the rate at which the drug dissolves into the tissue fluids and the rate at which it is absorbed by the blood is rapid compared to the rate at which it diffuses through the viable skin (28). Moreover, Friend studies confirmed that drug absorption entails diffusion through the primarily lipophilic stratum corneum, and the hydrophilic epidermis: transport between these layers is often the rate-limiting step (29).

The parameters and the physicochemical properties of ketoprofen transdermal delivery used for both gel and dissolvable microneedle arrays are summarized in Table 2.

Table 2. SKIN-CAD® parameters employed for ketoprofen gel and microneedles.

Parameters	Gel	Microneedles
Skin Permeation Model	2-Layer Model	1-Layer Model
Duration for medication (calculation): t_m (hour)	26	26
Application Schedule (Apply - Remove)	0-26	0-26
Surface area of application (cm)	3,14	3
Thickness of Stratum Corneum [cm]	0,002	0,002
Thickness of Whole Skin (In Vitro) [cm]	0,126	0,126
Steady-State Flux Across Intact Skin [mcg/cm2/h]	11,665	2,2039
Time Lag Across Intact Skin [h];	0,6342	0,259812
Steady-State Flux Across Stripped Skin [mcg/cm2/h];	15	----
Time Lag Across Stripped Skin [h]	0,4	------
Distance to Dermal Microcirculation [cm]	0,126	0,126
Diffusion Coefficient in Stratum Corneum [cm2/s]	8,40018E-09	--------
Diffusion Coefficient in Viable Skin [cm2/s]	1,77963E-06	2,82897E-06
Stratum Corneum/Viable Skin Partition Coefficient	1,19519E+01	----------
Skin Surface Concentration [mcg/mL]([mcg/cm3])	3,46992E+03	2,72667E+01
Initial Drug Concentration in Skin [mcg/mL]([mcg/cm3])	0,0000E+00	0,00000E+00
Volume of Distribution, V1 [L]	8,76400E+00*	8,76400E+00*
Elimination Rate Constant, k10 [1/h]	4,95000E-01*	4,95000E-01*

*Data from Geisslinger et al.

2.7.2 Simcyp® Model Strategy for *in vitro* observed /predicted parameters.

The dermal model of Simcyp software (Certara, UK - version 15) is developed just for a prediction of the skin permeability parameters such us partition coefficient, permeability constants and diffusion coefficient, using different methods. As previously described, the drug movement through the skin is characterised by the partition coefficients between layers and permeability constants for each layer. These could be estimated automatically from the physicochemical parameters of the drug molecule including Log*P* (logarithm of the octanol–water partition coefficient), MW (molecular weight), and hydrogen-bond donors (HBDs).

2.8 Statistical analysis

All data presented as the mean values ± SD ($n \geq 3$) were analysed using GraphPad version 5 for Windows (GraphPad Software Inc, La Jolla, CA, USA). The significance of the difference between groups was evaluated by Student's *t*-test or one-way analysis of variance, as appropriate according to the number of groups analysed. Mean differences with $P \leq 0.05$ were considered statistically significant.

3. Results

3.1 Fabrication of Dissolvable Microneedle Arrays

Different methods for microneedle fabrication are described in the literature, including sputtering of dissolved material, extrusion at elevated temperatures (30, 31), spraying (32) , centrifugation, vacuum or combination of these two processes (33-35). For the micromoulding method employed in our work, it is important to consider the physical-chemical characteristics of the drug solution, such as viscosity and surface tension. These properties influence the flow of the drug solution into the cavity of the mould, the wetting of the cavity walls and the removal of the air filling the interior of the mould cavity. Since the cavities of the micron sized moulds are essential, force application (centrifugation and/or vacuum) is necessary to ensure their efficient filling with the drug solution and air removal. In this work, micromoulding method was successfully used to prepare both KET-DMN and PVA-DMN (Figure 1).

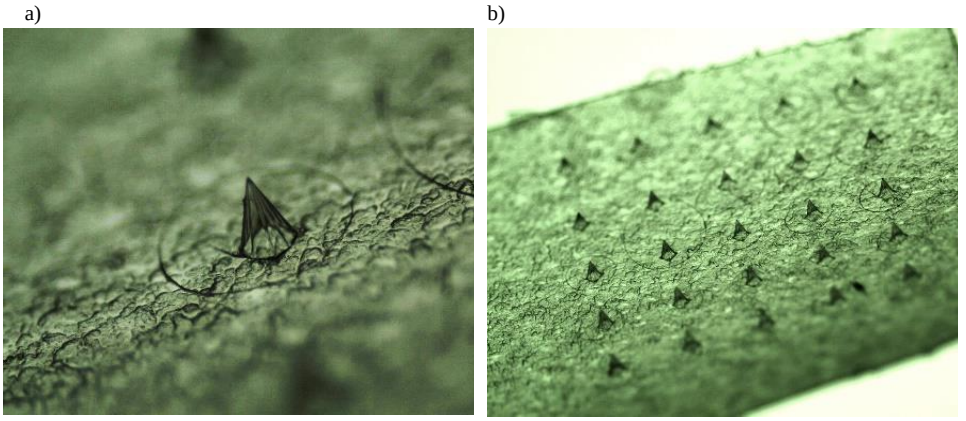

Figure 1: Light microscope images of (a) single needle and (b) DMN arrays containing ketoprofen (KET-DMN).

3.2 Characterization of Dissolvable Microneedle Arrays

3.2.1. DMN Morphological Properties

Both visual inspection of DMN array and single microneedle scoring were assessed to evaluate the effective DMN formation considering their shape and appearance. This analysis was performed using a light microscope with a built-in digital camera, and on the basis of criteria which were previously identified and described in section 2.3.1. The lower limit of acceptability for the samples of dissolvable microneedles are defined based on the European Pharmacopoeia requirements for content uniformity of the drug substance in the transdermal patch (36). Hence, DMN arrays consisting more than 90% of fully formed pyramidal, sharp-tip microneedles with a highest score (score 4) were used for the experiments in this work. The scoring results for three KET-DMN batches are presented on Figure 2.

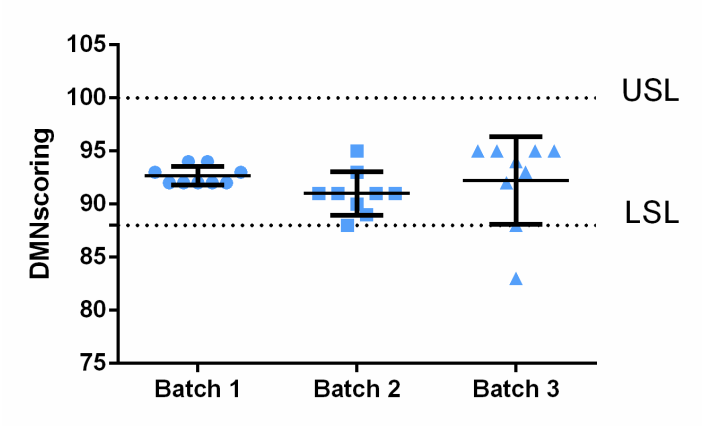

Figure 2: Scoring results estimated from the appearance and morphological characteristics of dissolvable microneedles arrays used in the experimental work. USL upper specification limit, LSL lower specification limit. Means value ± SD, n = 9. ANOVA, $p > 0.5$.

3.2.2 DMN Mechanical Performance

The importance of mechanical strength of microneedles is reflected in their successful and safe application on the skin. In fact, mechanical properties affect the ability of microneedles to withstand the pressure force during the applications (34, 37). The force required for microneedle fracture was determined using a Texture Analyser, as detailed in Section 2.3.2. Figure 3 and 4 show representative graphs in which the axial force applied to the microneedles increased until the ultimate load of the microneedle was reached. The DMN fracture was indicated by a discontinuity in the applied force and confirmed by visual observation of the DMN array after the test.

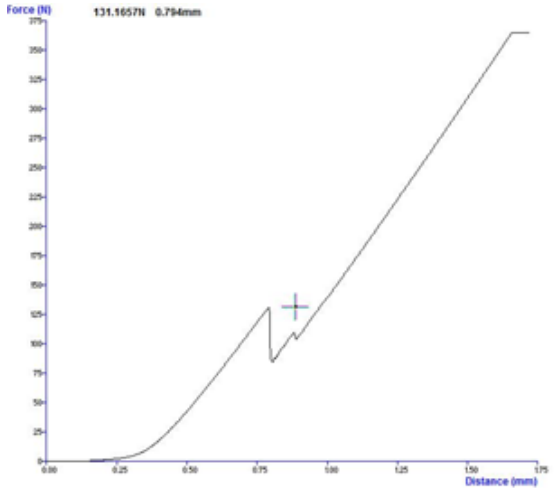

Figure 3: Representative measurement of DMN force during microneedle displacement and fracture under axial load. The discontinuity marks the fracture of KET-DMN.

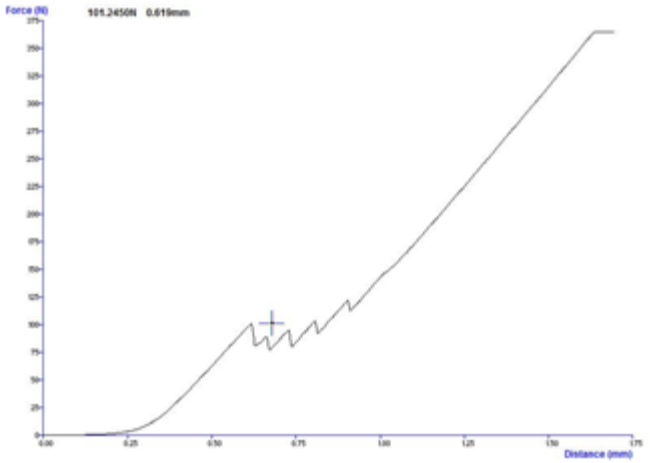

Figure 4: Representative measurement of needle force during microneedle displacement and fracture under axial load. The discontinuity marks the fracture of the PVA-DMN.

The significance of presented failure force measurements is best appreciated when compared to the force required to insert the microneedles into skin. In a separate study (38), insertion force was shown to depend on the interfacial microneedle area of the tip, whereas other geometric parameters of microneedle were found to be less important. Based on this calculation, the

safety factor defined as the ratio of failure force to insertion force is always well above unity in decreasing from 3.8 N to 1.7 N with increasing microneedle length. Measured insertion forces of 0.1–3 N were sufficient to allow manual insertion of DMN array. Comparison of calculated insertion forces to fracture forces showed to be always more than 100 N for both PVA-DMN and KET-DMN demonstrating that fracture forces were always much greater than insertion forces. This suggests that polymer microneedles fabricated in this study have sufficient mechanical strength to be inserted into skin without breaking. This finding is experimentally validated further below in the skin penetration study.

3.2.3 Drug Loading Amount

The amount of ketoprofen loaded in the DMN arrays was calculated based on the amount of ketoprofen quantified by HPLC analysis in each array (actual amount) and the total amount of drug loaded into the DMN (theoretical amount). Considering that an average volume of 10 µl of 5 mg/ml drug solution was used to fabricate one microneedle array, the theoretical amount of ketoprofen per is 50 µg/DMN array. The actual amount revealed from HPLC analyses was found to be 20 µg ± 1,91, hence, the drug loading was 40%.

3.2.4 Skin Penetration Study

It has been widely reported in literature that porcine skin has similar mechanical properties to human skin (39). Therefore, porcine cadaver ear skin was used as skin model for DMN penetration studies to determine the ability of the microneedles to successfully penetrate the stratum corneum. The microneedles arrays were removed from the skin after 5 or 15 minutes and both the skin and the DMN arrays were imaged using a light microscope (Figure 5). It was found that typically all microneedles in the array inserted into the skin effectively dissolve and have the capacity to pierce the skin. In particular, after 5 minutes the microneedles tips had already begun to dissolve indicating onset of rapid dissolution in the skin, while almost complete dissolution was observed after 15 minutes (Figure 6). The results are in accordance with the ultimate aim of our study to design a fast dissolving microneedles that are able to provide a rapid drug release.

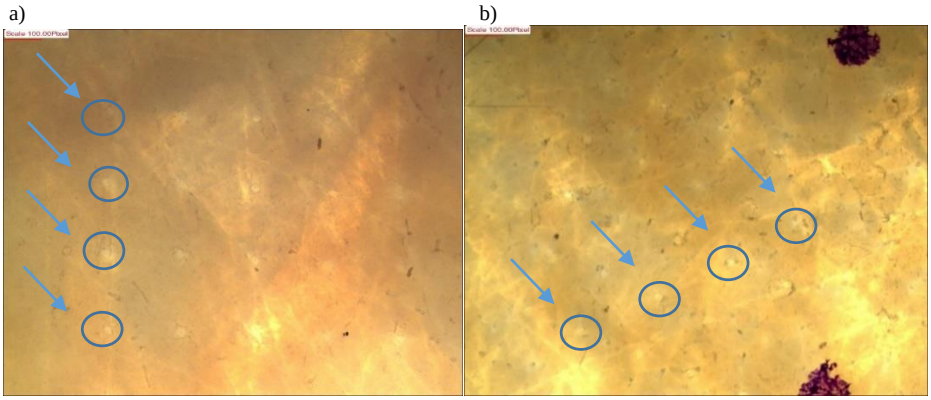

Figure 5: Light microscope images of microneedle penetration performed on porcine ear skin after (a) 5 minutes and (b) 15 minutes.

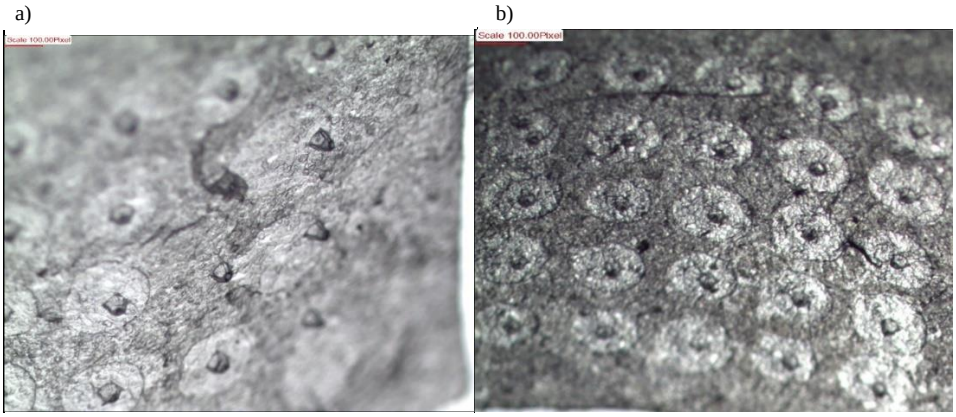

Figure 6: Light microscope images of microneedles arrays after insertion into the skin for (a) 5 minutes and (b) 15 minutes.

3.2.5 Short-term Stability Studies

The material from which dissolvable microneedles are fabricated should be biocompatible, biodegradable and capable of efficient delivery of the desired drug substance. Both natural and synthetic polymers possess these characteristics and, hence, are commonly used for the fabrication of dissolvable microneedles. The stability of microneedles and the

incorporated drug must be considered when the material used for DMN production is sensitive to the environmental conditions, such as humidity and temperature. Therefore, physically stability of the KET-DMN as well as the chemical stability of the ketoprofen were investigated for a short period of time (30 days). For the determination of the physical stability of the dissolvable microneedles, the evaluation of DMN physical integrity, shape and appearance was assessed using a light microscope with a built-in digital camera. Results were obtained by evaluating the microneedles on the basis of predetermined criteria described in Section 2.3.1, and a graphical representation is showed in Figure 7.

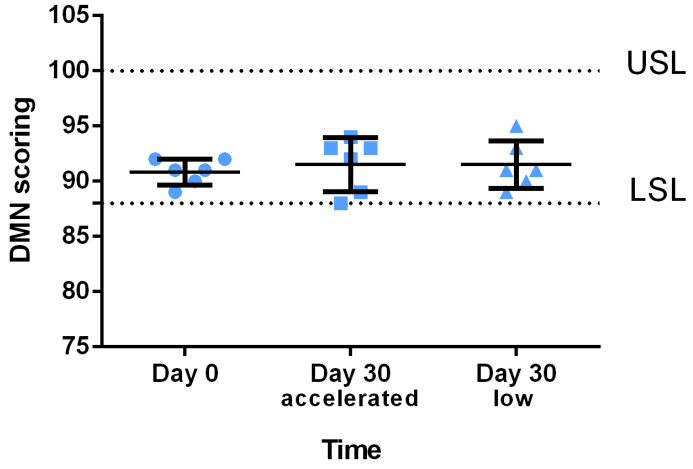

Figure 7: Scoring results estimated from the appearance and morphological characteristics of dissolvable microneedles arrays on day 0 and day 30 under low and accelerated conditions. USL upper specification limit, LSL lower specification limit. Means value ± SD, n = 6. ANOVA, $p > 0.5$.

During the entire period of the short-term stability studies, all microneedles retain the same appearance as at the date of manufacture. No changes were observed in the physical integrity of the microneedles. The different environment conditions did not have a significant impact on DMN physical stability. Following 30 days, microneedles retained their pyramidal shape with sharp tips. There was no statistically significant difference observed between the day 0 and day 30 samples. In addition, the investigated microneedles were dissolved according to the protocol detailed in the

Section 2.3.3. in order to determine the chemical stability of ketoprofen. The drug content was determined by HPLC method, and the results were then compared with the contents of the drug in microneedles arrays on the day of preparation (Figure 8).

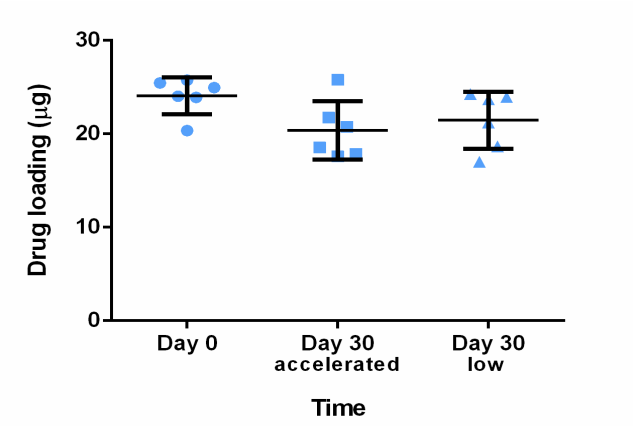

Figure 8: Drug loading of dissolvable microneedles arrays on day 0 and day 30 under low and accelerated conditions. USL upper specification limit, LSL lower specification limit. Means value ± SD, n = 6. ANOVA, $p > 0.05$.

Statistical analysis of the results using one-way ANOVA has shown no statistically significant value between the content of ketoprofen in the KET-DMN at different time-points and storage conditions ($p > 0.05$). Although the amount of ketoprofen remained unchanged it is necessary to examine the presence of degradation products. No degradation peaks (3-acetylbenzophenone and 2-[3-carboxyphenyl] propionic acid) were identified indicating a good chemical stability of the loaded drug during the study period. Even though the primary objective was not the drug protection from chemical degradation, but the achievement of a fast release of the drug improving its therapeutic efficacy, it is clear that the polymer material employed in our work is capable to protect the drug from environmental impact.

3.3 Drug Release Studies

In order to characterise the release profile of ketoprofen from dissolvable microneedles, *in-vitro* release studies were performed. The results showed

that there was an immediate release of the drug after 5 minutes (71,69%), followed by the further ketoprofen release of 81,4% after 15 minutes and complete release after 30 minutes when the microneedles were fully dissolved (Figure 9). Observed release profile is in agreement with our hypothesis that microneedles can be inserted into skin and release encapsulated drug during their rapid dissolution. The rate of release in this scenario is controlled largely by microneedle dissolution rate. By comparing these results with the imaged microneedle dissolution process after insertion into skin for different times it can be concluded that the applied method of drug loading in polymer dissolvable microneedles provided its fast release.

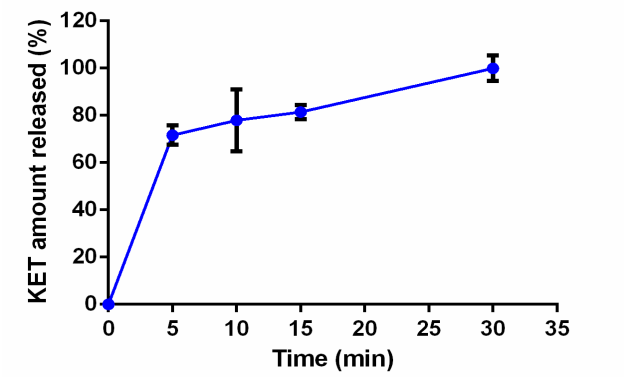

Figure 9: Graphic representation of ketoprofen release profile from dissolvable microneedle arrays, plotting time (min) vs percentage of drug released. Means value ± SD, n = 4.

Furthermore, *in vitro* ketoprofen release studies were also used for determination of the mechanism and kinetics of the drug release process. The pharmaceutical dosage forms following this dissolution profile, such as those containing water-soluble drugs in porous matrices, release the drug in a way that is proportional to the amount of drug remaining in its interior (40). In our case, in fact, it was verified that the release process is directly proportional to the drug concentration, the values of the square of the correlation coefficient (r^2) obtained based on the linear regression confirmed that the kinetic involved in this release is a first order.

3.4 Skin Permeation Studies

The *ex vivo* skin permeation studies were performed in order to determine the mechanism of the drug release and permeation through the skin. For this study a full-thickness porcine skin was used, consisting of stratum corneum, viable epidermis and dermis. Although the lipid composition in SC of porcine skin differs from human tissue, this animal skin model is still considered the most suitable 'natural' membrane for *in vitro* permeation studies (41). In particular, the thickness of the porcine skin is approximate to the thickness of human skin and, most importantly, it exhibits the most similar permeability characteristics compared to other membranes. The vertical static Franz diffusion cells which were used for this study are the most widely accepted for *ex vivo* percutaneous absorption studies. A finite dose approach used in this work is considered more relevant than infinite dose design as it better represents the clinical situation for topical drug products (42). The results from the first set experiment are not shown in this work because we used it simply to prove the concept and build the knowledge about KET-DMN ability to perform an effective transdermal drug delivery. Regarding the second experiment, the percentage of the cumulative amount of ketoprofen permeated through the porcine skin vs time from the ketoprofen gel product and KET-DMN is shown in Figure 10. From the beginning of the exposure, significant difference was observed between the gel and the microneedles, with respect to drug permeation profile. The amount of ketoprofen from DMN arrays and from the gel that permeated through skin was 9,86% and 0,34%, respectively.

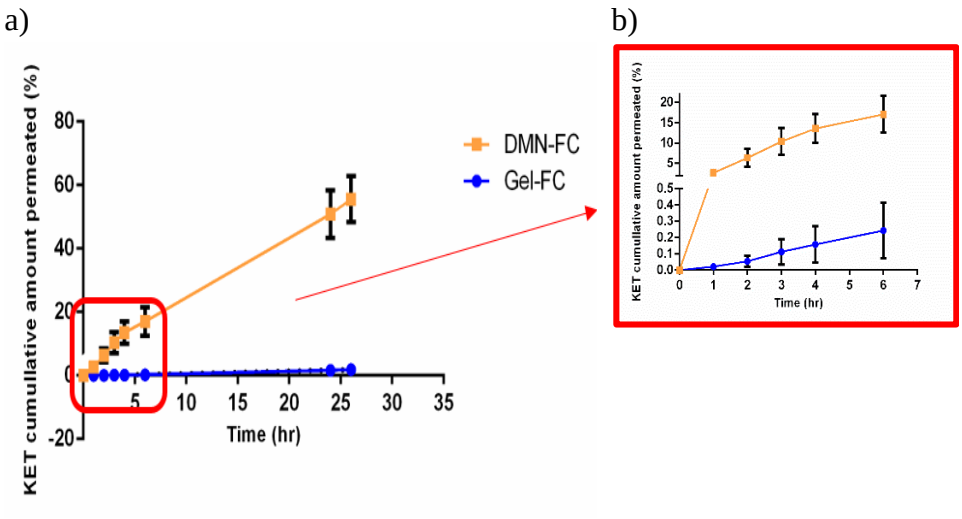

Figure 10: Comparative graphs of *ex vivo* skin permeation profile of ketoprofen from dissolvable microneedle arrays and gel, (a) after 26 h of application, (b) first six hours zoomed in. Means value ± SD, n = 3, T- test, p <0.001, statistically significant difference between the DMN and gel amount at each time point.

In Table 3 are showed the permeability parameters for the commercial ketoprofen gel and KET-DMN. Flux measurement across the skin is perhaps the most useful and insightful *ex vivo* information in development of a topical drug product. Considering that the gel contains a significantly higher drug concentration (2.5% w/w) in comparison to KET-DMN, it is possible to affirm that microneedles significantly improve the ketoprofen transdermal drug delivery for KET-DMN in terms of drug amount and the rate of its delivery. Lag time, permeability coefficient (Kp) and diffusion coefficient (D) were also determined for further characterisation of KET-DMN permeation profile and presented in Table 3.

Table 3. Permeability parameters of ketoprofen from DMN arrays and the gel through porcine skin.

Parameters	**KET-DMN**	**Gel**
Flux (μg/cm^2/h)	2,20 ± 0,02	11,66 ± 0,04
Lag Time (h)	0,259 ± 0,12	0,634 ± 0,19
Kp (cm/h)	1,1*10 $^{-1}$ ± 0,23	4,67*10 $^{-4}$ ± 0,03
D (cm^2/h)	1,018*10^{-2} ± 0,18	1,69*10 $^{-3}$ ± 0,10

Each value represents mean ± S.D. $n \geq 3$. Kp, permeability coefficient, D, diffusion coefficient, DMN, dissolvable microneedle.

Ex vivo permeation studies provide valuable information about the KET-DMN behaviour *in vivo*. The drug permeated indicates the amount of drug available for systemic absorption. This method is commonly used in skin research and normally gives a good correlation with the *in vivo* data (43).

3.5 Drug Analyses

A selective and specific HPLC method was developed, tested and validated for the quantitative determination of ketoprofen in the samples obtained in all stages of experimental work. The development of the method was started on the basis of literature data for the chromatographic conditions of ketoprofen determination (19, 21). The development of an analytical method for precise, accurate, selective and specific qualitative and quantitative determination of the drug was a prerequisite for the overall experimental work. In particular, the detection and quantification limits were calculated to be 0.04 μg/ml and 0.12 μg/ml, respectively.

3.6 *In Silico* Models

In recent years, promoted approaches by many regulatory bodies strongly encourage scientists investigating the chemicals and drugs safety to replace animal models with the alternatives. Modelling and simulation based on the mathematical models are already a well-established, parallel tool which allows for specific endpoint prediction and control.

3.6.1 SKIN-CAD® for *in vitro/ in vivo* correlation.

The FDA Guidance on IVIVC provides general methods and guidelines for the establishment of IVIVC. The number of studies reported in the area of

establishing IVIVC for non-oral dosage forms are very occasional and further research is necessary in the development of more meaningful dissolution and permeation methods (44). Using SKIN-CAD® software it was possible to predict human blood concentration - time profile for ketoprofen following its transdermal application (Figure 11). Furthermore, all the relevant PK parameters were obtained including maximum serum concentration (Cmax), area under the curve (AUC) and the time to reach the maximum blood concentration (Tmax) (Table 4). The simulation results of the ketoprofen pharmacokinetic profile are in agreement with the literature data of human clinical study for ketoprofen gel (45). At the moment no clinical data regarding ketoprofen dissolvable microneedle arrays are available for comparison. Moreover, the results predict that the percentage of ketoprofen that reaches systemic concentration would be considerably higher when the drug is administered using microneedles, hence, the delivery system can significantly affect the drug profiles *in vivo*. Higher Cmax values for ketoprofen gel product than for KET-DMN can be explained by approximately 400-fold higher initial concentration of the drug in the gel.

Table 4 Gel and KET-DMN PK values.

	GEL	**KET-DMN**
Cmax	8,44	1,52
AUC	$1,97 *10^{+2}$	$3.6*10^{+1}$
Tmax	6h	5h

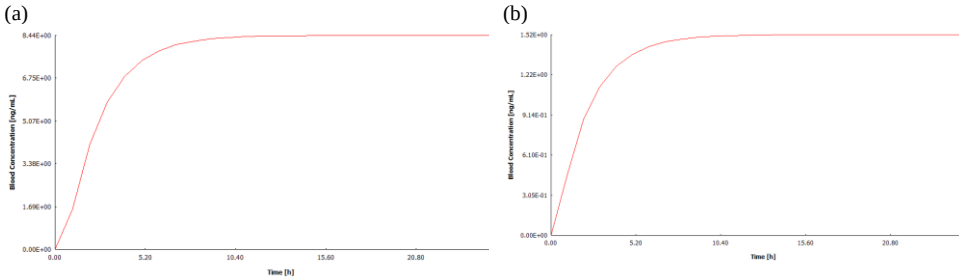

Figure 11. SKIN-CAD® graphical prediction of human blood concentration - time profile for (a) Gel and (b) KET-DMN array.

A very valuable prediction that SKIN-CAD® also provides is the drug distribution in the different skin layers following topical application (Figure 12). These two graphs highlight the different behaviour between the gel and the microneedle arrays in terms of the drug permeation. In particular, for the gel, the stratum corneum is the main limitation barrier and that affects both the amount of ketoprofen permeated and the drug distribution in the skin over time (Fig 12a). In general, topically applied drugs are poorly absorbed because only a small fraction crosses the stratum corneum. Most of the drug remains on the skin surface, or it is subject to loss from a multitude of factors (exfoliation, sweating, wash-off, rub-off, adsorption onto clothing, and chemical or photochemical degradation) (46). However, with microneedle arrays the distribution profile of ketoprofen in the skin is completely different (Fig 12b). Microneedles are capable of enhancing the transport of drug across the skin compared with the other transdermal delivery systems and approaches. As explained before, the enhanced drug penetration observed is due to the disruption of stratum corneum (47).

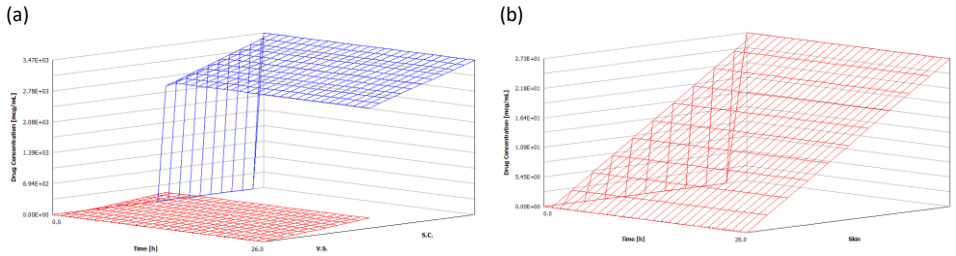

Figure 12. SKIN-CAD® graphical prediction of ketoprofen skin distribution for (a) Gel and (b) Microneedles arrays.

The skin permeability profile obtained from SKIN-CAD® is presented in Figure 13. This profile complies perfectly with the results observed from the *ex vivo* permeation studies for both gel and microneedle arrays for the first six hours of the experiment. However, there is an altered amount predicted for the last two time points (i.e. 24h and 26h). This difference can be explained by the fact that two input parameters used (i.e. the flux and the lag time) were calculated from the linear part of the curve (1-4 hours). Moreover, integrity of the skin can be compromised during the experiment affecting the results, which has been already reported in the literature (48).

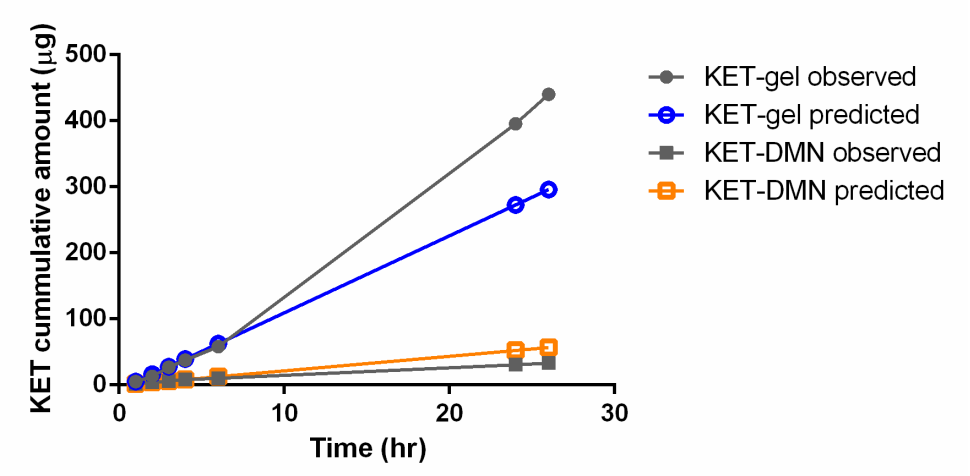

Figure 13: Comparative graphs of *ex vivo* skin permeation profile of ketoprofen from dissolvable microneedle arrays and gel predicted vs observed after 26 h of application.

3.6.2 Simcyp® for *in vitro* observed /predicted parameters

The MPML MechDermA model of Simcyp® software was not able to predict the observed parameters reasonably well using only physicochemical properties of the drug (Table 5). Only the predicted permeability coefficient was close to the observed one. Various publically available and extensively tested models were incorporated in the Simcyp® simulator and are available for use (49). Still, further validation of the dermal model is needed to improve confidence in such modelling strategy.

Table 5. Permeability parameters of ketoprofen from DMN arrays and the gel through porcine skin.

Parameters	**Observed**	**Predicted Simcyp®**
Kp (cm/h)	$1{,}1*10^{-1}$	$1{,}6*10^{-1}$
D (cm^2/h)	$1{,}018*10^{-2}$	$1{,}60*10^{-3}$
Kpvesc	11,95	4,23

Kp, permeability coefficient, D, diffusion coefficient, Kpvesc partition coefficient viable epidermis-stratum corneum.

4. Discussion

Conventional transdermal patches provide delivery only for the small subset of drugs that can cross skin at useful rates (50). On the other hand limitation of conventional hypodermic polymer formulations is that they often require surgical implantation or needle injection (51). This limits the ability of such systems to be self-administered and generally requires the time and expense of trained clinical personnel. Thus, the possibility of dissolvable microneedle-based delivery method could provide a significant advance that captures the ease of use afforded by a patch and the versatile properties of biocompatible polymers. Microneedles can be painlessly inserted into the skin in a minimally invasive manner that lends itself to self-administration by patients (52). We identified a biodegradable polymer PVA as a material for the fabrication of microneedles for self-administration of drug from a minimally invasive array. A sensitive fabrication method was employed to secure drug stability, sufficient mechanical strength of DMN for insertion into skin, and their rapid dissolution. Furthermore, PVA is highly water soluble, biocompatible FDA approved pharmaceutical excipient, which has a high tensile strength (53). Micromoulding fabrication method faithfully reproduces microneedle structures in an economical manner suitable for scale up to mass production. The use of polymer microneedles described in this study may provide advantages that overcome limitations of silicon and metal. Many polymer materials are inexpensive, mechanically strong, and enjoy a long-standing safety record in medical devices (54). Moreover, the biodegradable polymers used here further alleviate issues of safety, because broken microneedles left embedded in the skin can safely degrade and disappear. Safe disposal of polymer microneedles is also facilitated by the ability to burn, dissolve in a solvent, or mechanically destroy needles to prevent intentional or accidental re-use; destruction of used needles in developing countries is a high priority of the U.S. Centre for Disease Control and Prevention, the World Health Organization, and other international agencies (55). After Following the dissolvable microneedle arrays preparation, studies to determine the ability to pierce the skin were also conducted, revealing that the microneedles could pierce the stratum corneum, the main barrier for efficient transdermal drug delivery. KET-DMN showed evidence of dissolution within the skin after 5 minutes

suggesting that the drug was able to diffuse within the skin after a very short time. In addition, we assessed the efficacy profiles of drug loaded into the microneedles as well as the behaviour of the KET-DMN under storage at various conditions to assess their robustness over time. KET- DMN arrays were shown to encapsulate ketoprofen without loss of drug activity and to exhibit good stability after storage up to 30 days. Based on literature, microneedle research is currently focused on using the DMN arrays to administer vaccines. Vaccines for influenza and herpes simplex virus (HSP) have been incorporated into polymeric microneedles (56). Degradation of materials may lead to a reduction of the height of the microneedle, and thus to a reduction of the content of the incorporated drug and/or the inability to its delivery to the desired depth in the appropriate layer of the skin (57). Therefore, the confirmed stability of our KET- DMN is essential for the efficacy and safety delivery of the drug. Further studies were conducted to evaluate the transdermal release of the drug. Drug release kinetics was controlled over times. Previous studies using microneedles made of other materials have demonstrated an improved delivery of proteins, DNA, vaccines and other compounds both *in vitro* and *in vivo* (58). KET-DMN not only was able to enhance skin permeability of ketoprofen providing an improvement in the drug amount released as compared to the commercial ketoprofen gel, but also provided better penetration parameters, thus justifying its use as a drug delivery systems of choice for transdermal route. Another aim of this study was to perform a correlation study by *in silico* models, such as SKIN-CAD® that allow a prediction of clinical study outcome. This software provided the possibility of replacing animal models for dermal absorption with the *in silico* model for skin absorption and simulating the dermatokinetics outcome. This is, hence, a reasonable model for evaluating and optimizing the design of transdermal drug delivery systems showing the influence of formulation on drug release and absorption. SKIN-CAD® can also be useful for studying the effects of various factors on skin permeation and blood concentration profiles allowing users to proceed from *in vitro* studies to clinical trial by PK-PD simulation at preclinical stage. In addition, in a clinical study, participants identified many potential benefits of the microneedle delivery system, including reduced pain, less tissue damage and risk of transmitting infections

compared with conventional injections, as well as potential for self-administration. The public (100%) and professional (74%) participants were positive overall about microneedle technology (4).

5. Conclusion

Ketoprofen loaded dissolvable microneedle arrays have been successfully fabricated and characterized. A major obstacle to transdermal ketoprofen delivery has been overcome by the approach applied in this study. KET-DMN were able to reduce ketoprofen transport lag time and to supply a consistent larger amount of drug compared with the conventional ketoprofen gel. The presented delivery strategy demonstrates potential for enhanced and painless delivery of ketoprofen. *In silico* results show that SKIN-CAD® simulation was in agreement with the in vitro experimental results. The pharmacokinetic profile of ketoprofen predicted by SKIN-CAD® was shown to be in line with the literature data of human clinical study. Overall, dissolving microneedles may be useful as a method for patients to self-administer drugs without the pain or hazards of hypodermic needles.

The author wish to thank the Biocom systems, Japan for providing the trial version of SKIN-CAD.

References

1. Tanner T, Marks R. Delivering drugs by the transdermal route: review and comment. Skin Research and Technology. 2008;14(3):249-60.
2. Cheung K, Das DB. Microneedles for drug delivery: trends and progress. Drug delivery. 2016;23(7):2338-54.
3. Lee I, Lin WM, Shu JC, Tsai SW, Chen CH, Tsai MT. Formulation of two-layer dissolving polymeric microneedle patches for insulin transdermal delivery in diabetic mice. Journal of Biomedical Materials Research Part A. 2017;105(1):84-93.
4. Birchall JC, Clemo R, Anstey A, John DN. Microneedles in clinical practice–an exploratory study into the opinions of healthcare professionals and the public. Pharmaceutical research. 2011;28(1):95-106.
5. Wang QL, Zhu DD, Liu XB, Chen BZ, Guo XD. Microneedles with Controlled Bubble Sizes and Drug Distributions for Efficient Transdermal Drug Delivery. Scientific Reports. 2016;6.
6. Lee JW, Park J-H, Prausnitz MR. Dissolving microneedles for transdermal drug delivery. Biomaterials. 2008;29(13):2113-24.
7. Bronaugh RL, Collier SW, Macpherson SE, Kraeling M. Influence of metabolism in skin on dosimetry after topical exposure. Environmental health perspectives. 1994;102(Suppl 11):71.
8. Nair A, Jacob S, Al-Dhubiab B, Attimarad M, Harsha S. Basic considerations in the dermatokinetics of topical formulations. Brazilian Journal of Pharmaceutical Sciences. 2013;49(3):423-34.
9. Topical dermatologic corticosteroids: in vivo bioequivalence., (1995).
10. Shashi P, Anroop N, Vipin S, Neelam S. Skin kinetics and dermal clearance. International Research Journal of Pharmacy. 2012;3(8):14-5.
11. Heyneman CA, Lawless-Liday C, Wall GC. Oral versus topical NSAIDs in rheumatic diseases. Drugs. 2000;60(3):555-74.
12. Peura DA, Goldkind L. Balancing the gastrointestinal benefits and risks of nonselective NSAIDs. Arthritis research & therapy. 2005;7(4):S7.
13. Wu P-C, Chang J-S, Huang Y-B, Chai C-Y, Tsai Y-H. Evaluation of percutaneous absorption and skin irritation of ketoprofen through rat skin:

in vitro and in vivo study. International journal of pharmaceutics. 2001;222(2):225-35.
14. Dokoumetzidis A, Kalantzi L, Fotaki N. Predictive models for oral drug absorption: from in silico methods to integrated dynamical models. Expert opinion on drug metabolism & toxicology. 2007;3(4):491-505.
15. Jamei M, Marciniak S, Feng K, Barnett A, Tucker G, Rostami-Hodjegan A. The Simcyp® population-based ADME simulator. Expert opinion on drug metabolism & toxicology. 2009;5(2):211-23.
16. McGrath MG, Vrdoljak A, O'Mahony C, Oliveira JC, Moore AC, Crean AM. Determination of parameters for successful spray coating of silicon microneedle arrays. International journal of pharmaceutics. 2011;415(1):140-9.
17. Thomas LV, Arun U, Remya S, Nair PD. A biodegradable and biocompatible PVA–citric acid polyester with potential applications as matrix for vascular tissue engineering. Journal of Materials Science: Materials in Medicine. 2009;20(1):259.
18. Costa P, Lobo JMS. Modeling and comparison of dissolution profiles. European journal of pharmaceutical sciences. 2001;13(2):123-33.
19. Vučen SR, Vuleta G, Crean AM, Moore AC, Ignjatović N, Uskoković D. Improved percutaneous delivery of ketoprofen using combined application of nanocarriers and silicon microneedles. Journal of Pharmacy and Pharmacology. 2013;65(10):1451-62.
20. Ceschel G, Maffei P, Borgia SL. Correlation between the transdermal permeation of ketoprofen and its solubility in mixtures of a pH 6.5 phosphate buffer and various solvents. Drug delivery. 2002;9(1):39-45.
21. Guideline IHT. Validation of analytical procedures: text and methodology. Q2 (R1). 2005;1.
22. SKIN-CAD - Transdermal drug delivery 2017 [cited 2017]. Available from: http://www.fqs.pl/chemistry_materials_life_science/products/skin_cad.
23. Simulator for Skin Pharmacokinetics SKIN-CAD® Version 6.1 2017 [cited 2017]. Available from: http://www.biocom.co.jp/en/skin-cad/.
24. Van Ginneken C, Russel F. Saturable pharmacokinetics in the renal excretion of drugs. Clinical pharmacokinetics. 1989;16(1):38-54.

25. Al-Qallaf B, Das DB, Davidson A. Transdermal drug delivery by coated microneedles: Geometry effects on drug concentration in blood. Asia-Pacific Journal of Chemical Engineering. 2009;4(6):845-57.
26. Geisslinger G, Menzel S, Wissel K, Brune K. Pharmacokinetics of ketoprofen enantiomers after different doses of the racemate. British journal of clinical pharmacology. 1995;40(1):73-5.
27. Mori D, Kawamata H, Tojo K. Drug concentration–time profile in the plasma following the dissolution-type transdermal delivery. Journal of chemical engineering of Japan. 2003;36(1):45-8.
28. Davidson A, Al-Qallaf B, Das DB. Transdermal drug delivery by coated microneedles: geometry effects on effective skin thickness and drug permeability. Chemical Engineering Research and Design. 2008;86(11):1196-206.
29. Friend D. Transdermal delivery of contraceptives. Critical reviews in therapeutic drug carrier systems. 1989;7(2):149-86.
30. Miyano T, Tobinaga Y, Kanno T, Matsuzaki Y, Takeda H, Wakui M, et al. Sugar micro needles as transdermic drug delivery system. Biomedical Microdevices. 2005;7(3):185-8.
31. Kolli CS, Banga AK. Characterization of solid maltose microneedles and their use for transdermal delivery. Pharmaceutical research. 2008;25(1):104-13.
32. McGrath MG, Vucen S, Vrdoljak A, Kelly A, O'Mahony C, Crean AM, et al. Production of dissolvable microneedles using an atomised spray process: effect of microneedle composition on skin penetration. European Journal of Pharmaceutics and Biopharmaceutics. 2014;86(2):200-11.
33. Chu LY, Choi SO, Prausnitz MR. Fabrication of dissolving polymer microneedles for controlled drug encapsulation and delivery: bubble and pedestal microneedle designs. Journal of pharmaceutical sciences. 2010;99(10):4228-38.
34. Park J-H, Allen MG, Prausnitz MR. Biodegradable polymer microneedles: fabrication, mechanics and transdermal drug delivery. Journal of Controlled Release. 2005;104(1):51-66.
35. Wang P-C, Wester BA, Rajaraman S, Paik S-J, Kim S-H, Allen MG, editors. Hollow polymer microneedle array fabricated by photolithography process combined with micromolding technique. Engineering in Medicine

and Biology Society, 2009 EMBC 2009 Annual International Conference of the IEEE; 2009: IEEE.
36. Commission B, Council G, Commission G. British pharmacopoeia. Her Majesty's Stationery Office; 2001.
37. Brett PN, Parker T, Harrison AJ, Thomas TA, Carr A. Simulation of resistance forces acting on surgical needles. Proceedings of the Institution of Mechanical Engineers, Part H: Journal of Engineering in Medicine. 1997;211(4):335-47.
38. Davis SP, Landis BJ, Adams ZH, Allen MG, Prausnitz MR. Insertion of microneedles into skin: measurement and prediction of insertion force and needle fracture force. Journal of biomechanics. 2004;37(8):1155-63.
39. Kochhar JS, Quek TC, Soon WJ, Choi J, Zou S, Kang L. Effect of microneedle geometry and supporting substrate on microneedle array penetration into skin. Journal of pharmaceutical sciences. 2013;102(11):4100-8.
40. Dash S, Murthy PN, Nath L, Chowdhury P. Kinetic modeling on drug release from controlled drug delivery systems. Acta Pol Pharm. 2010;67(3):217-23.
41. Schmook FP, Meingassner JG, Billich A. Comparison of human skin or epidermis models with human and animal skin in in-vitro percutaneous absorption. International journal of pharmaceutics. 2001;215(1):51-6.
42. Chang R-K, Raw A, Lionberger R, Yu L. Generic development of topical dermatologic products: formulation development, process development, and testing of topical dermatologic products. The AAPS journal. 2013;15(1):41-52.
43. Wissing S, Müller R. Solid lipid nanoparticles as carrier for sunscreens: in vitro release and in vivo skin penetration. Journal of Controlled Release. 2002;81(3):225-33.
44. Emami J. In vitro–in vivo correlation: from theory to applications. J Pharm Pharm Sci. 2006;9(2):169-89.
45. Flouvat B, Roux A, Delhotal-Landes B. Pharmacokinetics of ketoprofen in man after repeated percutaneous administration. Arzneimittel-Forschung. 1989;39(7):812-5.

46. Barry BW. Novel mechanisms and devices to enable successful transdermal drug delivery. European journal of pharmaceutical sciences. 2001;14(2):101-14.
47. Bariya SH, Gohel MC, Mehta TA, Sharma OP. Microneedles: an emerging transdermal drug delivery system. Journal of Pharmacy and Pharmacology. 2012;64(1):11-29.
48. Buist HE, van de Sandt JJ, van Burgsteden JA, de Heer C. Effects of single and repeated exposure to biocidal active substances on the barrier function of the skin in vitro. Regulatory Toxicology and Pharmacology. 2005;43(1):76-84.
49. Polak S, Ghobadi C, Mishra H, Ahamadi M, Patel N, Jamei M, et al. Prediction of concentration–time profile and its inter-individual variability following the dermal drug absorption. Journal of pharmaceutical sciences. 2012;101(7):2584-95.
50. Prausnitz MR, Mitragotri S, Langer R. Current status and future potential of transdermal drug delivery. Nature reviews Drug discovery. 2004;3(2):115-24.
51. Rosen H, Abribat T. The rise and rise of drug delivery. Nature Reviews Drug Discovery. 2005;4(5):381-5.
52. Park J-H, Allen MG, Prausnitz MR. Polymer microneedles for controlled-release drug delivery. Pharmaceutical research. 2006;23(5):1008-19.
53. Mansour HM, Sohn M, Al-Ghananeem A, DeLuca PP. Materials for pharmaceutical dosage forms: molecular pharmaceutics and controlled release drug delivery aspects. International journal of molecular sciences. 2010;11(9):3298-322.
54. Braybrook JH. Biocompatiblity: Assessment of medical devices and materials. Biocompatiblity: Assessment of Medical Devices and Materials, by Julian H Braybrook (Editor), pp 246 ISBN 0-471-96597-9 Wiley-VCH, December 1996. 1996:246.
55. Simonsen L, Kane A, Lloyd J, Zaffran M, Kane M. Unsafe injections in the developing world and transmission of bloodborne pathogens: a review. 1999.
56. Moga KA, Bickford LR, Geil RD, Dunn SS, Pandya AA, Wang Y, et al. Rapidly–dissolvable microneedle patches via a highly scalable and

reproducible soft lithography approach. Advanced Materials. 2013;25(36):5060-6.
57. Donnelly RF, Morrow DI, Singh TR, Migalska K, McCarron PA, O'Mahony C, et al. Processing difficulties and instability of carbohydrate microneedle arrays. Drug development and industrial pharmacy. 2009;35(10):1242-54.
58. Prausnitz MR. Microneedles for transdermal drug delivery. Advanced drug delivery reviews. 2004;56(5):581-7.

Acknowledgements

I would like to express my sincere gratitude to my supervisor Dr Roberta Cassano for the continuous support during my PhD study and related research, for her patience and knowledge. Deepest thanks to Prof. Sonia Trombino for her guidance and motivation, she helped me in all the time of research. My thanks also go to Prof. Nevio Picci who provided me the opportunity to give access to the laboratory and research facilities. I owe a special thanks to my colleagues in Italy and in UCC School of Pharmacy for the stimulating discussions, for the time spent working together and for all the fun we have had. I could not have imagined having a better visiting period experience. Really thanks guys!!!

A very profound end special gratitude goes out to Dr Sonja Vucen, my advisor and mentor during the visiting period in Cork, for her unfailing support, assistance and encouragement, but also for the hard work done together which boosted me to widen my research from various perspectives.

Last but not the least, I would like to thank my goddaughter Clarice for the joy that she gives me every moment spent together, and also immense thanks to my family and relatives for supporting and encouraging me always during my life!!!

"Appreciation is the purest vibration that exists today on the planet."
(Abraham-Hicks)